

ผลของการปรับปรุงตัวรองรับอะลูมินา ไทเทเนียและซิลิกาด้วยเกลือลิเทียมต่อคุณลักษณะและสมบัติการ  
เป็นตัวเร่งของตัวเร่งปฏิกิริยาโคบอลต์บนตัวรองรับ



นางสาว อรพินท์ โชคไพศาล

ศูนย์วิทยทรัพยากร  
จุฬาลงกรณ์มหาวิทยาลัย

วิทยานิพนธ์นี้เป็นส่วนหนึ่งของการศึกษาตามหลักสูตรปริญญาวิศวกรรมศาสตรมหาบัณฑิต

สาขาวิชาวิศวกรรมเคมี ภาควิชาวิศวกรรมเคมี

คณะวิศวกรรมศาสตร์ จุฬาลงกรณ์มหาวิทยาลัย

ปีการศึกษา 2551

ลิขสิทธิ์ของจุฬาลงกรณ์มหาวิทยาลัย

EFFECT OF GALLIUM-MODIFIED  $\text{Al}_2\text{O}_3$   $\text{TiO}_2$  AND  $\text{SiO}_2$  SUPPORTS  
ON CHARACTERISTICS AND CATALYTIC PROPERTIES OF  
SUPPORTED COBALT CATALYSTS



Miss Orapin Chokpaisan

ศูนย์วิทยทรัพยากร  
จุฬาลงกรณ์มหาวิทยาลัย

A Thesis Submitted in Partial Fulfillment of the Requirements  
for the Degree of Master of Engineering Program in Chemical Engineering  
Department of Chemical Engineering  
Faculty of Engineering  
Chulalongkorn University  
Academic Year 2008  
Copyright of Chulalongkorn University

Thesis Title            EFFECT OF GALLIUM-MODIFIED  $\text{Al}_2\text{O}_3$ ,  $\text{TiO}_2$  AND  $\text{SiO}_2$   
SUPPORTS ON CHARACTERISTICS AND CATALYTIC  
PROPERTIES OF SUPPORTED COBALT CATALYSTS

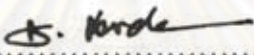
By                            Miss Orapin Chokpaisan

Field of Study            Chemical Engineering

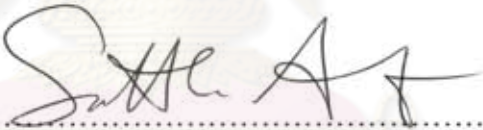
Advisor                    Assistant Professor Bunjerd Jongsomjit, Ph.D

---

Accepted by the Faculty of Engineering, Chulalongkorn University in Partial  
Fulfillment of the Requirements for the Master's Degree

  
.....Dean of the Faculty of Engineering  
(Associate Professor Boonsom Lerthirunwong, Dr.Ing.)

THESIS COMMITTEE

  
..... Chairman  
(Professor Suttichai Assabumrungrat, Ph.D.)

  
..... Advisor  
(Assistant Professor Bunjerd Jongsomjit, Ph.D.)

  
..... Examiner  
(Assistant Professor Joongjai Panpranot, Ph.D.)

  
.....External Examiner  
(Assistant Professor Okorn Mekasuwandamrong, Ph.D.)

อรพินท์ โชคไพศาล : ผลของการปรับปรุงตัวรองรับอะลูมินา ไททาเนียและซิลิกาด้วย  
 แกลเลียมต่อคุณลักษณะและสมบัติการเป็นตัวเร่งของตัวเร่งปฏิกิริยาโคบอลต์บนตัวรองรับ  
 (EFFECT OF GALLIUM-MODIFIED  $Al_2O_3$ ,  $TiO_2$  AND  $SiO_2$  SUPPORTS  
 ON CHARACTERISTICS AND CATALYTIC PROPERTIES OF  
 SUPPORTED COBALT CATALYSTS) อ. ที่ปรึกษาวิทยานิพนธ์หลัก : ผศ. ดร.  
 บรรเจิด จงสมจิตร, 109 หน้า

วิทยานิพนธ์นี้ศึกษาผลของการปรับปรุงตัวรองรับอะลูมินา ไททาเนียและซิลิกาด้วย  
 แกลเลียมต่อคุณลักษณะและสมบัติการเป็นตัวเร่งของตัวเร่งปฏิกิริยาโคบอลต์บนตัวรองรับสำหรับ  
 ปฏิกิริยาคาร์บอนมอนอกไซด์ไฮโดรจีเนชัน โดยเตรียมตัวเร่งปฏิกิริยาด้วยวิธีเคลือบฝังตัวรองรับ  
 ด้วยแกลเลียมในอัตราส่วน 0.2 และ 1 เปอร์เซ็นต์โดยน้ำหนัก หลังจากนั้นนำไปเคลือบฝังอีกครั้ง  
 ด้วยโคบอลต์ด้วยอัตราส่วน 20 เปอร์เซ็นต์โดยน้ำหนัก ปฏิกิริยาไฮโดรจีเนชันของคาร์บอนมอนอกไซด์  
 ไฮโดร (มีอัตราส่วนของไฮโดรเจนต่อคาร์บอนมอนอกไซด์=10/1) ถูกใช้เพื่อทดสอบความว่องไวของ  
 ตัวเร่งปฏิกิริยาและการเลือกเกิดของผลิตภัณฑ์ ผลการศึกษาแสดงให้เห็นว่าตัวเร่งปฏิกิริยาโคบอลต์  
 บนตัวรองรับอะลูมินามีความว่องไวมากกว่าตัวเร่งปฏิกิริยาโคบอลต์บนตัวรองรับซิลิกา ทั้งนี้ความ  
 ว่องไวของตัวเร่งปฏิกิริยาขึ้นอยู่กับความเป็นกรดของตัวเร่งปฏิกิริยา เมื่อมีการการปรับปรุงตัว  
 รองรับอะลูมินาด้วยแกลเลียมทำให้ความว่องไวของตัวเร่งปฏิกิริยาเพิ่มขึ้น ในทางตรงข้ามการ  
 ปรับปรุงตัวรองรับซิลิกาด้วยแกลเลียมส่งผลให้ความว่องไวของตัวเร่งปฏิกิริยาลดลง นอกจากนี้การ  
 ปรับปรุงตัวรองรับด้วยแกลเลียมส่งผลกระทบต่อสมบัติการเป็นตัวเร่งของตัวเร่งปฏิกิริยาโดย  
 ความสามารถในการรีดิวซ์ของโคบอลต์เพิ่มขึ้นเมื่อปรับปรุงแกลเลียมบนตัวรองรับอะลูมินาและจะ  
 ลดลงเมื่อปรับปรุงแกลเลียมบนตัวรองรับซิลิกา อย่างไรก็ตามการปรับปรุงตัวรองรับอะลูมินาและซิลิกา  
 ด้วยแกลเลียมลดการเสื่อมสภาพของตัวเร่งปฏิกิริยา สำหรับตัวเร่งปฏิกิริยาโคบอลต์บนตัว  
 รองรับไททาเนีย พบว่ามีการเสื่อมสภาพของตัวเร่งปฏิกิริยาอย่างรวดเร็วซึ่งเกิดจากซัลเฟอร์ที่อยู่บน  
 พื้นผิวของตัวรองรับไททาเนีย

ภาควิชา.....วิศวกรรมเคมี..... ลายมือชื่อนิสิต.....อรพินท์ โชคไพศาล.....

สาขาวิชา.....วิศวกรรมเคมี..... ลายมือชื่อ อ.ที่ปรึกษาวิทยานิพนธ์หลัก.....

ปีการศึกษา.....2551.....

##5070512921: MAJOR CHEMICAL ENGINEERING

KEY WORDS: GA MODIFICATION/ COBALT CATALYST/ CARBON MONOXIDE HYDROGENATION

ORAPIN CHOKPAISAN: EFFECT OF GALLIUM-MODIFIED  $\text{Al}_2\text{O}_3$ ,  $\text{TiO}_2$  AND  $\text{SiO}_2$  SUPPORTS ON CHARACTERISTICS AND CATALYTIC PROPERTIES OF SUPPORTED COBALT CATALYSTS. ADVISOR: ASST. PROF. BUNJERD JONGSOMJIT, Ph.D., 109 pp.

The study focused on effect of Ga-modified  $\text{Al}_2\text{O}_3$ ,  $\text{TiO}_2$  and  $\text{SiO}_2$  supports on characteristics and catalytic properties of supported cobalt catalyst during CO hydrogenation. Ga was first impregnated onto the supports to produce Ga-modified supports containing 0.2 and 1 wt% of Ga in the final catalyst. Then, Co catalysts having 20 wt% of Co were prepared from those supports by the incipient wetness impregnation method. CO hydrogenation ( $\text{H}_2/\text{CO} = 10/1$ ) was also performed to determine the overall activity and selectivity. It revealed that the activities of  $\text{Co}/\text{Al}_2\text{O}_3$  catalysts were higher than those of the  $\text{Co}/\text{SiO}_2$  catalysts. However, activity depended on acid sites of catalyst. Ga modification on  $\text{Al}_2\text{O}_3$  supports resulted in increased activities. On contrary, addition of Ga onto  $\text{SiO}_2$  decreased activities. It was found that Ga modification had a significant impact on the catalyst properties. The reduced Co metal atoms determined by the  $\text{H}_2$  chemisorption increased with Ga modification on  $\text{Al}_2\text{O}_3$ , but decreased with Ga modification on  $\text{SiO}_2$ . However, Ga modification on  $\text{Al}_2\text{O}_3$  and  $\text{SiO}_2$  supports decrease the catalyst deactivation. For the  $\text{TiO}_2$ -supported Co catalyst, it was found that the activity decreased dramatically. This was probably due to the catalysts had sulphur on the surface as impurities

Department : .....Chemical Engineering.... Student's Signature... อธิษฐาน ไชยกุล

Field of Study : ...Chemical Engineering.... Advisor's Signature... [Signature]

Academic Year : .....2008.....

## ACKNOWLEDGEMENTS

The author would like to express her greatest gratitude and appreciation to her advisor, Asst. Prof. Dr, Bunjerd Jongsomjit for his invaluable guidance, providing value suggestions and his kind supervision throughout this study. In addition, she is also grateful to Professor Dr. Sutichai Assabumrungrat, as the chairman, Assistant Professor Joongjai Panpranot and Assistant Professor Okorn Mekasuwandamrong as the members of the thesis committee. The author would like to thank the Thailand Research Fund (TFR) according to the RMU50-B. Jongsomjit project for the financial support of this research.

Many thanks for kind suggestions and useful help to Mr. Pongsathorn Wongwaiwattanakul, Miss Supawan Supawanitchmongkol, Miss Sirirat Rojanapipatkul, and many friends in the petrochemical laboratory who always provide the encouragement and co-operate along the thesis study.

Most of all, the author would like to express her highest gratitude to her parents who always pay attention to her all the times for suggestions, support and encouragement.

ศูนย์วิทยทรัพยากร  
จุฬาลงกรณ์มหาวิทยาลัย

# CONTENTS

	<b>Page</b>
ABSTRACT (IN THAI).....	iv
ABSTRACT (IN ENGLISH).....	v
ACKNOWLEDGMENTS.....	vi
CONTENTS.....	vii
LIST OF TABLES.....	x
LIST OF FIGURES.....	xi
CHAPTER	
I INTRODUCTION.....	1
II LITERATURE REVIEWS.....	4
2.1 Co-support compound formation.....	4
2.2 Gallium- modified supports.....	7
III THEORY.....	9
3.1 Fischer-Tropsch synthesis (FTS) .....	9
3.1.1 The surface carbide mechanism.....	12
3.1.2 The hydroxycarbene mechanism.....	14
3.1.3 The CO insertion mechanism.....	15
3.2 Aluminium.....	17
3.2.1 Properties of alumina .....	17
3.2.1.1 Properties of $\gamma$ - $\text{Al}_2\text{O}_3$ .....	20
3.3 Silicon dioxide.....	22
3.3.1 General feature of silica.....	22
3.4 Titanium (IV) oxide .....	25
3.5 Cobalt.....	28
3.5.1 General.....	28
3.5.2 Physical properties.....	28
3.6 Cobalt aluminate and cobalt oxide.....	31
3.6.1 Cobalt aluminate ( $\text{CoAl}_2\text{O}_4$ ).....	31
3.6.2 Cobalt Oxides.....	32
3.7 Cobalt-based catalysts.....	33
3.8 Cobalt-support compound formation (Co-SCF).....	34

CHAPTER	<b>Page</b>
3.8.1 Co-Aluminate Formation.....	34
3.9 Gallium.....	34
IV EXPERIMENTAL.....	36
4.1 Catalyst preparation.....	36
4.1.1 Chemicals.....	36
4.1.2 Preparation of Ga-modified Al <sub>2</sub> O <sub>3</sub> , SiO <sub>2</sub> and TiO <sub>2</sub> .....	37
4.1.3 Preparation of Co catalyst.....	37
4.2 Catalyst characterization.....	37
4.2.1 X-ray diffraction (XRD).....	37
4.2.2 N <sub>2</sub> physisorption .....	37
4.2.3 NH <sub>3</sub> -Temperature Programmed Desorption (TPD).....	38
4.2.4 Scanning electron microscopy and energy dispersive X-ray spectroscopy (SEM/EDX).....	39
4.2.5 Transmission electron microscopy (TEM).....	39
4.2.6 Temperature-programmed reduction (TPR).....	40
4.2.7 Hydrogen chemisorption.....	40
4.2.8 X-ray photoelectron spectroscopy (XPS).....	40
4.3 Reaction study in CO hydrogenation.....	41
4.3.1 Materials.....	41
4.3.2 Apparatus.....	41
4.3.3 Procedures.....	43
Research methodology.....	46
V RESULTS AND DISCUSSION .....	49
5.1 Characteristics of Ga-modified Al <sub>2</sub> O <sub>3</sub> and SiO <sub>2</sub> -supported Co catalyst.....	49
5.2 Reduction behavior of Ga-modified Al <sub>2</sub> O <sub>3</sub> and SiO <sub>2</sub> -supported Co catalyst.....	68



	<b>Page</b>
CHAPTER	
5.3 Catalytic activity for CO-hydrogenation over Ga-modified Al <sub>2</sub> O <sub>3</sub> and SiO <sub>2</sub> -supported Co catalyst.....	69
VI CONCLUSIONS AND RECOMMENDATIONS.....	72
6.1 Conclusions.....	72
6.2 Recommendations.....	73
REFERENCES.....	74
APPENDICES.....	78
APPENDIX A: EFFECT OF GA-MODIFIED TiO <sub>2</sub> SUPPORT ON CHARACTERISTICS AND CATALYST PROPERTIES OF SUPPORTED COBALT CATALYST.....	79
APPENDIX B: CALCULATION FOR CATALYST PREPARATION.....	90
APPENDIX C: CALCULATION OF THE CRYSTALLITE SIZE.....	93
APPENDIX D: CALCULATION OF THE ACIDITY.....	97
APPENDIX E: CALCULATION FOR TOTAL H <sub>2</sub> CHEMISORPTION.....	99
APPENDIX F: CALIBRATION CURVES.....	100
APPENDIX G: CALCULATION OF CO CONVERSION, REACTIONIC RATE AND SELECTIVITY.....	107
APPENDIX H: LIST OF PUBLICATIONS.....	108
VITA .....	109

## LIST OF TABLES

Table	Page
3.1 Physical properties of silica .....	22
3.2 Crystallographic properties of anatase, brookite, and rutile.....	27
3.3 Physical properties of cobalt .....	30
3.4 Chemical properties of gallium.....	35
4.1 Chemicals used in the preparation of catalysts.....	36
4.2 Operating condition for gas chromatograph.....	43
5.1 Crystallite size of $\text{Co}_3\text{O}_4$ from XRD of Ga-modified and unmodified $\text{Al}_2\text{O}_3$ and $\text{SiO}_2$ supported cobalt catalysts.....	51
5.2 BET surface area, pore volume and pore size of Ga-modified and unmodified $\text{Al}_2\text{O}_3$ and $\text{SiO}_2$ supported cobalt catalysts.....	52
5.3 XPS data of Ga-modified and unmodified $\text{Al}_2\text{O}_3$ and $\text{SiO}_2$ supported cobalt Catalysts.....	64
5.4 Acidity of Ga-modified and unmodified $\text{Al}_2\text{O}_3$ and $\text{SiO}_2$ supported cobalt catalysts.....	66
5.5 Results of $\text{H}_2$ chemisorption of Ga-modified and unmodified $\text{Al}_2\text{O}_3$ and $\text{SiO}_2$ supported cobalt catalysts.....	67
5.6 Reaction study of Ga-modified and unmodified $\text{Al}_2\text{O}_3$ and $\text{SiO}_2$ supported cobalt catalysts.....	70
A.1 The average crystallite sizes of Ga-modified $\text{TiO}_2$ supported cobalt Catalysts.....	80
A.2 BET surface area, pore size and pore volume of Ga-modified $\text{TiO}_2$ supported cobalt catalysts.....	80
A.3 XPS data of Ga-modified $\text{TiO}_2$ supported cobalt catalysts.....	86
A.4 Reaction study of Ga-modified and unmodified $\text{TiO}_2$ supported cobalt catalysts.....	89
F.1 Conditions use in Shimadzu modal GC-8A and GC-14B.....	101

## LIST OF FIGURES

	<b>Page</b>
3.1 Desorption of water from alumina surface.....	19
3.2 Lewis acid and Lewis basic sites on alumina.....	19
3.3 Assignment of the OH stretchings of transitional aluminas.....	21
3.4 Crystal structure of TiO <sub>2</sub> .....	26
3.5 Structure of cobalt aluminate.....	32
4.1 Flow diagram of CO hydrogenation system.....	45
5.1 XRD patterns for the Ga-modified and unmodified Al <sub>2</sub> O <sub>3</sub> and SiO <sub>2</sub> supported cobalt catalysts.....	50
5.2 A typical spectrum of the Co/Al <sub>2</sub> O <sub>3</sub> -1%Ga from EDX analysis.....	53
5.3 A typical spectrum of the Co/SiO <sub>2</sub> -1%Ga from EDX analysis.....	54
5.4 SEM micrograph and EDX mapping of the calcined Co/Al <sub>2</sub> O <sub>3</sub> -1%Ga catalysts..	56
5.5 SEM micrograph and EDX mapping of the calcined Co/SiO <sub>2</sub> -1%Ga catalysts...	57
5.6 TEM micrograph of Co supported on Ga-modified and unmodified Al <sub>2</sub> O <sub>3</sub> supported cobalt catalysts.....	59
5.7 TEM micrograph of Co supported on Ga-modified and unmodified SiO <sub>2</sub> supported cobalt catalysts.....	60
5.8 The deconvolution of XPS spectra of Ga-modified and unmodified Al <sub>2</sub> O <sub>3</sub> supported cobalt catalysts.....	62
5.9 The deconvolution of XPS spectra of Ga-modified and unmodified SiO <sub>2</sub> supported cobalt catalysts.....	63
5.10 NH <sub>3</sub> -TPD profiles of Ga-modified and unmodified Al <sub>2</sub> O <sub>3</sub> and SiO <sub>2</sub> supported cobalt catalysts.....	65
5.11 TPR profile of Ga-modified and unmodified Al <sub>2</sub> O <sub>3</sub> and SiO <sub>2</sub> supported cobalt catalysts.....	68
A.1 XRD patterns of Ga-modified and unmodified TiO <sub>2</sub> supported cobalt catalysts..	79
A.2 A typical spectrum of the Co/TiO <sub>2</sub> -1%Ga from EDX analysis.....	81
A.3 SEM micrograph and EDX mapping of the calcined Co/TiO <sub>2</sub> -1%Ga catalysts...	82
A.4 TEM micrograph of Co supported on Ga-modified and unmodified TiO <sub>2</sub> supported cobalt catalysts.....	83

	<b>Page</b>
A.5 The deconvolution of XPS spectra of Ga-modified and unmodified TiO <sub>2</sub> supported cobalt catalysts.....	85
A.6 NH <sub>3</sub> -TPD profiles of Ga-modified TiO <sub>2</sub> supported cobalt catalysts.....	87
A.7 TPR profile of Ga-modified and unmodified TiO <sub>2</sub> supported cobalt catalysts....	88
C.1 The measured peak of $\gamma$ -Al <sub>2</sub> O <sub>3</sub> to calculate the crystallite size.....	95
C.2 The plot indicating the value of line broadening due to the equipment. The data were obtained by using $\alpha$ -alumina as standard.....	96
F.1 The calibration curve of methane.....	102
F.2 The calibration curve of ethylene.....	102
F.3 The calibration curve of ethane.....	103
F.4 The calibration curve of propane.....	103
F.5 The calibration curve of propylene.....	104
F.6 The calibration curve of butane.....	104
F.7 The calibration curve of butylene.....	105
F.8 The chromatograms of catalyst sample from thermal conductivity detector, gas chromatography Shimadzu model 8A (Molecular sieve 5A column).....	106
F.9 The chromatograms of catalyst sample from flame ionization detector, gas chromatography Shimadzu model 14B (VZ10 column).....	106

# CHAPTER I

## INTRODUCTION

Cobalt-based catalysts are applied most widely for hydrogenation reactions in a variety of systems. It has been known that supported cobalt (Co) catalysts are preferred for Fischer–Tropsch (FT) synthesis because of their high activities during FT synthesis based on natural gas, high selectivity to linear long chain hydrocarbons and also low activities for the competitive water–gas shift (WGS) reaction (E. Iglesia, 1997). To increase the catalytic activity, cobalt is usually supported on a high surface area support in order to obtain a high metal dispersion. Various supports for cobalt have been used, such as silica (J. Panpranot *et al.*, 2002), alumina (B. Jongsomjit *et al.*, 2003; T. K. Das *et al.*, 2002; Y. Zhang *et al.*, 1999], titania (J. Li *et al.*, 2002) and zeolites (X. Li *et al.*, 2003). It has been shown that the reducibility of the cobalt catalysts and, in general, the dispersion of the metal phase formed depend on the support used (M. Kraum and M. Baerns, 1999), the cobalt precursor used (M. Kraum and M. Baerns, 1999; S. Sun *et al.*, 2000), the metal loading (R. Riva *et al.*, 2000), the preparation method, thermal treatment and the reduction process (Y. Zhang *et al.*, 1999). Besides, modification of the supports would also have influence for the significant change in the characteristics and reaction behaviors of the catalysts.

The effects of variety of promoters and modification of the support can increase the reducibility of Co, preserve the activity by preventing the formation of coke, exhibit cluster and ligand effects, act as a source of hydrogen spillover, and enhance the dispersion. Many promoters such as Ru (Panpranot *et al.*, 2002; J. Li *et al.*, 2002; Y. Zhang *et al.*, 1999), Zr (Rohr *et al.*, 2000; B. Jongsomjit *et al.*, 2003), La (J. Haddad *et al.*, 1996), B (Li and N.J. Coville, 1999), Pt (D. Schanke *et al.*, 1995) and Re (T.K. Das *et al.*, 2002) have been investigated for Co catalysts. The focus of this study was to investigate the impact of Ga modification on different supports for cobalt catalysts. It has been known that Ga containing catalyst has been reported to have catalytic activity in catalytic combustion, CO oxidation and NO<sub>x</sub> selective reduction (K. Shimizu *et al.*, 1997).

The addition of gallium or indium oxide on alumina is known to enhance the low temperature performance for NO reduction by hydrocarbons in lean conditions, as shown by Maunula *et al.*, 1999. Haneda *et al.*, 2001. have also shown the good catalytic performance of Ga<sub>2</sub>O<sub>3</sub>-Al<sub>2</sub>O<sub>3</sub> catalysts prepared by sol-gel method for the selective reduction of NO with propylene in the presence of oxygen. Similarly, Shimizu *et al.*, 1997 reported that the Ga<sub>2</sub>O<sub>3</sub>/  $\gamma$  - Al<sub>2</sub>O<sub>3</sub> catalyst prepared by impregnation of  $\gamma$  -Al<sub>2</sub>O<sub>3</sub> (JRC ALO4) with a gallium nitrate solution showed a high activity for selective catalytic reduction (SCR) of NO with methane. Petre *et al.*, 2001 have shown that depositing Ga<sub>2</sub>O<sub>3</sub> on acidic supports leads to a decrease in the acidic character of the resulting catalysts in comparison with the gallium-free supports. However, less is known about the effect of Ga modification on the supported cobalt catalysts.

In this present study, it was focused on the effect of Ga modified Al<sub>2</sub>O<sub>3</sub>, SiO<sub>2</sub> and TiO<sub>2</sub> of cobalt catalysts. Experimentally, the Co was supported on Al<sub>2</sub>O<sub>3</sub>, SiO<sub>2</sub> and TiO<sub>2</sub> with and the Ga modification prepared by the incipient wetness impregnation. Then, the catalyst samples were characterized using BET surface area, X-ray diffraction (XRD), temperature-programmed reduction (TPR), H<sub>2</sub>-chemisorptions, scanning electron microscopy (SEM), energy dispersive X-ray spectroscopy (EDX), and transmission electron microscopy (TEM). The reaction study on carbon monoxide (CO) hydrogenation under methanation was performed in order to evaluate the catalytic activity and selectivity of products.

The study was scoped as follows:

1. Preparation of Ga-modified different supports ( $\gamma$ -Al<sub>2</sub>O<sub>3</sub>, TiO<sub>2</sub> and SiO<sub>2</sub>) containing 0.2 and 1 wt% of Ga<sub>2</sub>O<sub>3</sub> in the final catalyst by impregnation method.
2. Preparation of modified Ga-based supported Co catalyst (20 wt%Co) using the incipient wetness impregnation method.

3. Characterization of the catalyst using BET surface area, X-ray diffraction (XRD), temperature-programmed reduction (TPR), H<sub>2</sub>-chemisorptions, scanning electron microscopy (SEM), energy dispersive X-ray spectroscopy (EDX), X-Ray photoelectron spectroscopic (XPS), ammonia temperature-programmed desorption (NH<sub>3</sub>-TPD) and transmission electron microscopy (TEM).
4. Reaction study of the catalyst samples in carbon monoxide (CO) hydrogenation at 220°C and 1 atm and a H<sub>2</sub>/CO ratio of 10 under methanation condition.



ศูนย์วิจัยทรัพยากร  
จุฬาลงกรณ์มหาวิทยาลัย

## CHAPTER II

### LITERATURE REVIEWS

There are several studies of alumina, silica, titania and Ga-modified supported catalysts. Many researchers have found better knowledge about this supports especially supported cobalt catalyst in Co hydrogenation. These reports are very useful and will use to develop works for the future.

#### 2.1 Co-support compound formation

Supported cobalt catalysts are important for the Fischer–Tropsch synthesis of high molecular weight, paraffinic waxes which can be hydrocracked to produce lubricants and diesel fuels. The type and structure of the support influence the dispersion, particle size and reducibility, and thereby the activity for Co-supported catalysts. R. Riva *et al.*, 2000 studied the interaction of cobalt with two different kinds of support: silica and titania and their effect on the dispersion and reducibility by XPS, TPR, TPO, XRD and TEM. They also showed that the interaction is much stronger in the case of titania. The different reactivity of cobalt with silica and titania explains why reducing and reoxidizing treatments have opposite effects on the dispersion of cobalt depending on whether it is supported on SiO<sub>2</sub> or TiO<sub>2</sub>. The low reactivity of cobalt with silica favours sintering effects. Conversely, due to the high reactivity of cobalt with titania, the coverage of TiO<sub>2</sub> by cobalt tends to increase after the same treatments and M. Voß *et al.*, 2002 investigated the structural, chemical and electronic properties of Co and Co/Mn catalysts supported on Al<sub>2</sub>O<sub>3</sub>, SiO<sub>2</sub> and TiO<sub>2</sub> by a combination of different methods such as TEM, XRD, XPS, TPR and TPO. They reported that temperature-programmed reduction and oxidation reveal the formation of various oxides in dependence on temperature. In case of the alumina- and titania-supported cobalt catalysts, the formation of high-temperature compounds CoAl<sub>2</sub>O<sub>4</sub> and CoTiO<sub>3</sub>, respectively. Moreover, these compounds are not reducible under the applied conditions, the degrees of reduction are only 18-20% (Co/Al<sub>2</sub>O<sub>3</sub>) and 77% (Co/TiO<sub>2</sub>).



Beside the supported, the promoter is one important focus in the development of this process is the improvement of the catalyst activity by increasing the number of active Co metal sites that are stable under reaction conditions. S. Ali *et al.*, 1995 investigated the influence of Zr promotion of 20 wt% Co/SiO<sub>2</sub> on Fischer-Tropsch synthesis using catalysts prepared in different ways and having different loadings of Zr (up to 8.5 wt%). The Zr-promoted exhibited higher overall rates of FTS compared to unpromoted Co/SiO<sub>2</sub>. The sequentially impregnated Co/Zr/SiO<sub>2</sub> catalysts appeared to be the most active. However, the co-impregnation method of preparation appeared to result in higher cobalt dispersion. While Zr promotion did not appear to promote or inhibit H<sub>2</sub> activation, hydrogen spillover may have been partly responsible for enhancing the activity of the sequentially impregnated Zr/Co/SiO<sub>2</sub> catalysts. Zr also possibly created an active interface with Co that increased catalyst activity by facilitating Co dissociation. Although high levels of promotion tended to increase the selectivity for higher hydrocarbon, Zr appears to be primarily an excellent rate promoter for Co/SiO<sub>2</sub>. Similarly, A. Feller *et al.*, 1999 studied the addition of zirconium oxide chloride to the catalyst formulation of Co/SiO<sub>2</sub>. It leads to a higher reducibility of cobalt, due to the formation of a cobalt zirconium species, which can be reduced at lower temperatures than cobalt silicate. Furthermore, the metal particle size of cobalt is increased, but the size of cobalt clusters is reduced. The Co-Zr/SiO<sub>2</sub> catalysts were tested for their activity in the Fischer-Tropsch synthesis. The steady-state activity increased with increasing zirconium loading, which was attributed to the resistance against reoxidation of the larger cobalt particles and thus to the larger amount of surface cobalt metal present at steady-state in the zirconium promote catalysts. With increasing zirconium content the number of surface metal atoms at steady-state conditions increases, leading to a higher extent of secondary reactions, but the size of the cobalt clusters decreases, leading to a decrease in the extent of secondary reactions. With increasing zirconium content the extent of secondary hydrogenation of olefins (e.g., ethene) passes a minimum, and the C<sub>5+</sub>-selectivity passes a maximum due to readsorption of small, reactive organic product compounds, which can be incorporated in larger product compounds. Double bond isomerization increases with increasing zirconium content. This might be attributed to the catalytic activity of zirconia.

G. Jacobs *et al.*, 2002 investigated the effect of support, loading and promoter on the reducibility of cobalt catalysts. They have reported that significant support interactions on the reduction of cobalt oxide species were observed in the order  $\text{Al}_2\text{O}_3 > \text{TiO}_2 > \text{SiO}_2$ . Addition of Ru and Pt exhibited a similar catalytic effect by decreasing the reduction temperature of cobalt oxide species, and for Co species where a significant surface interaction with the support was present, while Re impacted mainly the reduction of Co species interaction with the support. They also suggested that, for catalysts prepared with a noble metal promoter and reduced at the same temperature, the increase in the number of active sites was due mainly to improvements in the percentage reduction rather than the actual dispersion (cluster size). Increasing the cobalt loading, and therefore the average Co cluster size, was found to exhibit improved reducibility by decreasing interactions with the support.

and B.H. Davis *et al.*, 2002 studied the effect of the addition of small amounts of boron, ruthenium and rhenium on the Fischer–Tropsch (F–T) catalyst activity and selectivity of a 10wt.% Co/TiO<sub>2</sub> catalyst has been investigated in a continuously stirred tank reactor (CSTR). A wide range of synthesis gas conversions has been obtained by varying space velocities over the catalysts. The addition of a small amount of boron (0.05 wt.%) onto Co/TiO<sub>2</sub> does not change the activity of the catalyst at lower space times and slightly increases synthesis gas conversion at higher space times. The product selectivity is not significantly influenced by boron addition for all space velocities investigated. Ruthenium addition (0.20 wt.%) onto Co/TiO<sub>2</sub> and CoB/TiO<sub>2</sub> catalysts improves the catalyst activity and selectivity. At a space time of 0.5 h-g cat./NL, synthesis gas conversion increases from 50–54 to 68–71% range and methane selectivity decreases from 9.5 to 5.5% (molar carbon basis) for the promoted catalyst. Among the five promoted and non-promoted catalysts, the rhenium promoted Co/TiO<sub>2</sub> catalyst (0.34 wt.% Re) exhibited the highest synthesis gas conversion, and at a space time of 0.5 h-g cat./NL, synthesis gas conversion was 73.4%. In comparison with the results obtained in a fixed bed reactor, the catalysts displayed a higher F–T catalytic activity in the CSTR.

## 2.2 Gallium-modified supports

Gallia containing catalyst has been reported to have catalytic activity in catalytic combustion, CO oxidation and  $\text{NO}_x$  selective reduction. A. L. Petre *et al.*, 2002 investigated the effect of boria, gallia and indium loadings on the surface acidities of  $\text{Al}_2\text{O}_3\text{-M}_2\text{O}_3$  ( $\text{M}=\text{B}, \text{Ga}, \text{In}$ ) systems as determined by the chemisorption of acidic and basic probe molecules (sulfur dioxide and ammonia). Each sample was prepared by a conventional impregnation method and calcined at 873 K in dry air for 3 hours. They were found that the addition of  $\text{B}_2\text{O}_3$  on alumina increased the number of acid sites, while no real basicity could be evidenced. In the case of  $\text{Al}_2\text{O}_3\text{-Ga}_2\text{O}_3$ , they were also found that the addition of  $\text{Ga}_2\text{O}_3$  on alumina caused a decrease in the acidity of alumina and did not affect markedly the basicity, while depositing indium oxide on alumina decreased both the acidity and basicity. Moreover, alumina-supported  $\text{Ga}_2\text{O}_3$  and  $\text{In}_2\text{O}_3$  samples displayed a well-preserved amphoteric character. F. Domínguez *et al.*, 2005 studied the effect of gallia (gallium oxide,  $\text{Ga}_2\text{O}_3$ ) on the catalytic behavior for benzene hydrogenation reactions of platinum supported on alumina. Gallia/alumina supported 0.5% Pt catalysts with different gallia content (0, 1, 10 and 100 wt% of gallia), varying from pure alumina to pure gallia, were prepared. They were suggested that the increase of gallia content in the alumina reduced the surface area, the dispersion and the activity. Moreover, the addition of gallia to the alumina did not provide enough acidity to generate isomerization products. It was not possible to determine neither the effect on the activity of the gallium species reduced at high temperatures nor eliminate diffusional control at reaction temperature of 250°C and T. Mathew *et al.*, 2005 synthesized  $\text{Ga}_2\text{O}_3\text{-Al}_2\text{O}_3$  mixed oxides by sol-gel method on catalytic performances for steam reforming of dimethyl ether (DME). They suggested that  $\text{Ga}_2\text{O}_3$  significantly affected the catalytic performance with respect to the DME conversion and  $\text{H}_2$  yield. In addition, the catalytic activity increased with the gallium concentration in  $\text{Ga}_2\text{O}_3\text{-Al}_2\text{O}_3$  mixed oxides. It was very interesting that without the aid of an additional transition metal component,  $\text{Ga}_2\text{O}_3$  and  $\text{Ga}_2\text{O}_3\text{-Al}_2\text{O}_3$  mixed oxide system exhibited good activity in the reforming reaction.

M. Takahashi *et al.*, 2006 synthesized  $\text{Ga}_2\text{O}_3\text{-Al}_2\text{O}_3$  solid solutions with aluminum isopropoxide and gallium acetylacetonate as precursor using glycothermal method. They were found that the reaction with a higher  $\text{Al}/(\text{Ga}+\text{Al})$  charged ratio yielded the glycol derivative of boehmite as a by-product and increasing in the Al content in the solid solution increased the surface area and the thermal stability of the solid solution. The oxides system exhibited extremely high catalytic activity for selective catalytic reduction of  $\text{NO}_x$  with methane as a reducing agent. Moreover, the solid solution showed high durability under steaming conditions. In the solid solution,  $\text{Ga}^{3+}$  and  $\text{Al}^{3+}$  ions selectively occupied tetrahedral and octahedral sites of the spinel structure, respectively. From the characteristic, they concluded that tetrahedral  $\text{Ga}^{3+}$  ions were the active sites for this reaction. In the other words, tetrahedral  $\text{Ga}^{3+}$  ions with  $\text{Al}^{3+}$  ions in the next-nearest-neighbor (NNN) sites were the active sites for this reaction. M. Takahashi *et al.*, 2007 also investigated the effect of organic media used in synthesized  $\text{Ga}_2\text{O}_3\text{-Al}_2\text{O}_3$  solid by solvothermal method on catalytic performances for selective catalytic reduction of  $\text{NO}_x$  with methane. In the solvothermal synthesized, the crystal structure of mixed oxides was controlled by the initial formation of  $\text{Ga}_2\text{O}_3$  nuclei. When diethylenetriamine was used for prepared, the resulting catalyst extremely high activities for this reaction and had lower densities of acid sites than those prepared in other solvents.

## CHAPTER III

### THEORY

#### 3.1 Fischer-Tropsch synthesis (FTS)

Fischer-Tropsch synthesis (FTS) that discovered by Fischer and Tropsch over 80 years ago, as an alternate process, can convert the synthesis gas ( $H_2/CO$ ) derived from carbon sources such as coal, peat, biomass and natural gas, into hydrocarbons and oxygenates. During the past decades, FTS has been developed continuously by many researchers, although the rise and fall in research intensity on this process has been highly related to the demands for liquid fuels and relative economics. This synthesis is basically the reductive polymerization (oligomerization) of carbon monoxide by hydrogen to form organic products containing mainly hydrocarbons and some oxygenated products in lesser amounts.

By manipulation of the reaction conditions, the process may be designed to produce heavier saturated hydrocarbons or lower olefins or oxygenated hydrocarbons as we shall see in the following discussion.

Metals that have significant activity for Fischer-Tropsch synthesis include iron, cobalt, nickel and ruthenium. Iron has proved so far to be the best. It is superior to cobalt with respect to conversion rate, selectivity and flexibility. Nickel has disadvantage of producing appreciable amounts of methane. Ruthenium enhance the formation of high molecular weight alkanes and catalyzes polymerization to polymethane. Other group VIII metals are of low activity. Copper does not catalyze Fisher-Tropsch synthesis.

The catalyst is usually prepared by fusion or precipitation over a silica, alumina or kieselguhr support. Small amounts of promoters such as alkaly metal or copper salts are included in the catalytic mix. Copper is believe to facilitate the reduction of the catalyst, alkali metal salt, particularly  $K_2O_2$  enhance activity and

olefins selectivity. The support increased the surface area of the catalyst metal thus extremely increasing in dispersion.

Sulfur compounds generally poison the catalyst and they must be removed from the synthesis gas feed stream. However, partial sulfur poisoning may have favorable effects. Thus, it has been found that deliberate slight sulfur poisoning of the iron/manganese catalyst enhances selectivity to short chain olefins.

Three main types of reactors are currently in use in the Fischer-Tropsch processes: Fixed-bed, fluidized-bed and slurry bed reactors. Fixed-bed reactors are usually tubular, each tube having 50 mm ID and 12 m length. A single reactor may contain as many as 2000 such tubes. Fluidized-bed reactors provide for better heat transfer and continuous regeneration of the catalyst. The catalyst used in fluidized-bed reactors must have high physical stability. SASOL (in South Africa), uses fluidized-bed reactors 46 m high, 230 cm in diameter with reaction temperature of 320-360°C and pressure. In the slurry-bed reactors the feed gas is bubbled through a suspension of finely divided catalyst particles. It has the advantage of good temperature control thus providing greater flexibility of reaction conditions.

Each type of reactor is better suited for certain product composition. Fixed-bed reactors, for example, produce high boiling straight-chain hydrocarbons consisting, typically, of 33% gasoline hydrocarbons (C<sub>5</sub>-C<sub>11</sub>), 17% diesel and 40% heavy paraffins and higher waxes. The gasoline fraction is of low octane value and requires further treatment (isomerization or blending) before use. Fluidized-bed reactors are the best when lighter hydrocarbons are desired. A typical product composition is 72% lower molecular weight gasoline-range hydrocarbons rich in olefins and 14% oxygenated hydrocarbons. However, the product is low in diesel. Thus two or more different reactors may be operated in parallel to provide an integrated fuel plant.

The demands on selectivity of Fischer-Tropsch reactions are ever-increasing. In the earlier days of the process the concern was to improve selectivity with respect to better gasoline grade and/or diesel oil chemicals. With the realization of feasible

route of converting synthesis gas to industrial intermediates, more stringent conditions are being imposed on the reaction parameters to make the process more selective.

Selectivity improvement is sought with respect to product properties such as chain length, chain branching, olefin content, alcohol content and methane content. Reaction conditions that particularly eliminate or minimize carbon deposition are desirable. In order to achieve and improve product selectivity the optimization of the following reaction parameters has been investigated: reaction temperature and pressure,  $H_2/CO$  ratio, conversion, space velocity, amount and type of promoters, nature of the catalyst, size of catalyst particles and mode of its deposition, type of support, and type of reactor.

We have already seen examples of how the choice of the metal catalyst and support affects the product distribution. The effect of the choice of the reactor type on the nature of the reaction products has also been demonstrated.

Selectivity to olefins may be enhanced by addition of promoters such as  $K_2O$ , Ti, Mn or V. Selectivity of greater than 70% to  $C_2-C_4$  olefins at high conversion rate has been achieved.

The search for selectivity to lower olefins by controlling the chain growth and inhibiting hydrogenation has been followed in three directions:

- (a) The use of highly dispersed catalyst either by improving the method of deposition or using special dispersing supports.
- (b) The use of bimetallic catalyst eg. With Mn/Fe ratio of 9:1 at 330 °C up to 90% olefin selectivity has been achieved. However, the activity of the catalyst and its life-time are low.
- (c) The use of shape-selective catalyst.

Since the Fischer-Tropsch process was originally intended for the production of hydrocarbons, little attention was paid in the early phases of the

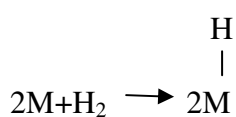
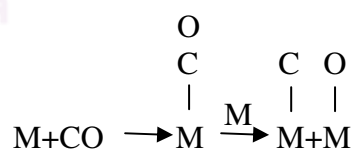
application of the process to the oxygenated products obtained as co-products. With the search for more economical sources of the oxygenated hydrocarbons, the possibility of tuning the Fischer-Tropsch process for the production such as oxygenates has been investigated. It has been found that with a nitrated iron catalyst, selectivity for alcohols may exceed 80%. A Rh/Hg/SiO<sub>2</sub> catalyst system gave 75% selectivity with respect to ethanol. The major side products are olefins.

The Fischer-Tropsch process may be defined as being the hydrogenative oligomerization of CO over heterogeneous catalyst to produce alkanes, alkenes oxygenated hydrocarbons and water. A complete mechanism must account for the formation of all products observed. The first attempt at elucidating the mechanism of the process was made by the inventors of the process themselves, Fischer and Tropsch.

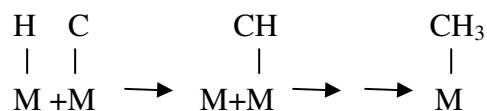
### 3.1.1 The surface carbide mechanism

Fischer and Tropsch apparently were trying to explain the formation of alkanes and alkenes rather than introduce a mechanism for whole line of the products that could be formed from the process. They observed that hydrocarbon formation occurred with heterogeneous metal catalysts (Ni, Fe, Co, Ru) that tend to absorb CO dissociatively to form surface carbide species. Their mechanism consists of the following steps:

#### (i) Initiation:

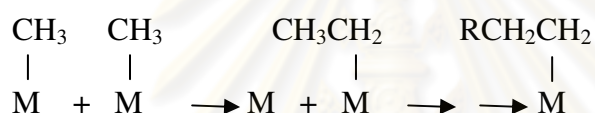




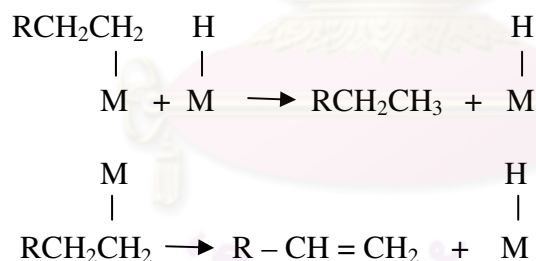


Note: M-X means species X chemisorbed on the metal surface atom M. The hyphen has no implication with respect to the strength of the M-X interaction or the order of the bond. More recently it has been suggested, based spectroscopic evidence, that in order to for an absorbed CO to undergo dissociation it must be bonded side-on to the metal, not end-on.

**(ii) Propagation:**

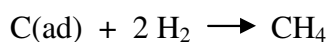


**(iii) Termination:**



The carbide mechanism has survived the several decades since its introduction. Several items of evidence arising from recent investigation support this mechanism e.g.

(a) In the hydrogenation of CO over clean Ni surface it has been observed that CO<sub>2</sub> evolution proceeds that CH<sub>4</sub> thus



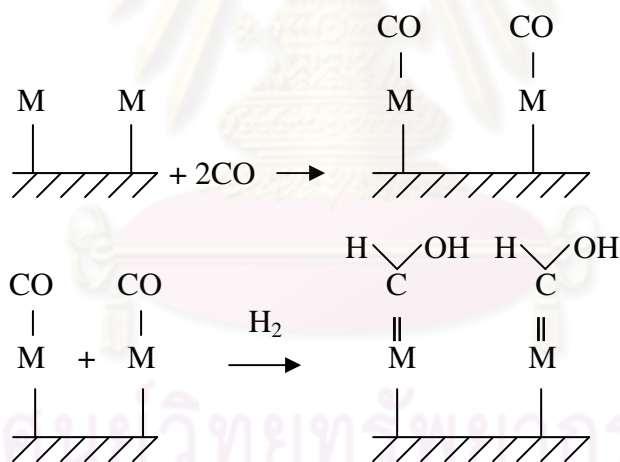
(b) Decomposition of diazomethane ( $\text{CH}_2\text{N}_2$ ) at  $200^\circ\text{C}$  in the presence of  $\text{H}_2$  over Co, Fe and Ru catalysts gives linear alkanes and olefins with distribution similar to that obtained from  $\text{CO}/\text{H}_2$  reaction over the same catalyst.

(c) Distribution of  $^{13}\text{C}$  in  $\text{CH}_2=\text{CH}$  formed when  $^{13}\text{CO}$ ,  $\text{H}_2$ - and  $^{12}\text{CH}_2\text{N}_2$  were reacted under Fischer-Tropsch conditions is consistent with the distribution predicted based on the carbided mechanism and inconsistent with other proposed mechanism.

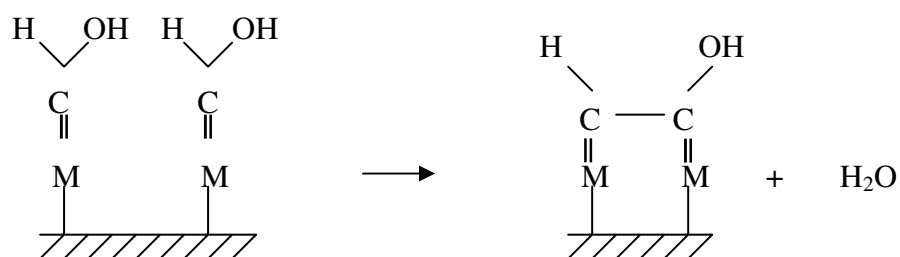
However, a drawback of this mechanism is that it does not explain the formation of oxygenated products.

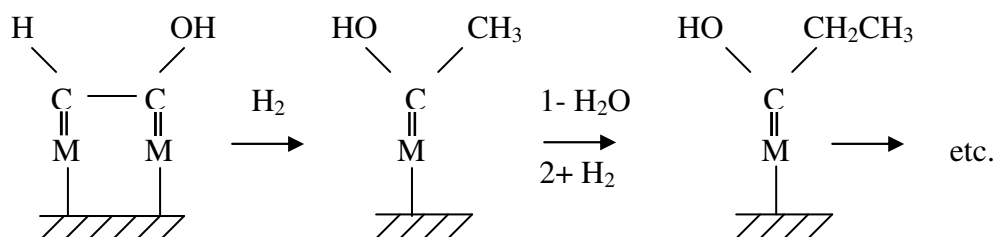
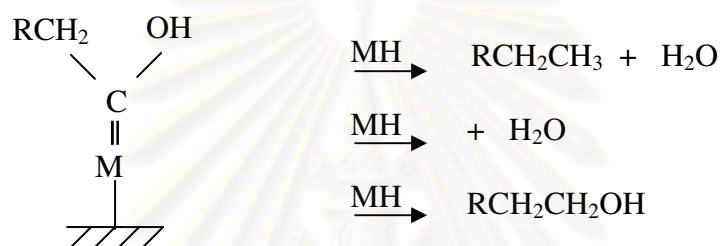
### 3.1.2 The hydroxycarbene mechanism

#### (i) Initiation:



#### (ii) Propagation:

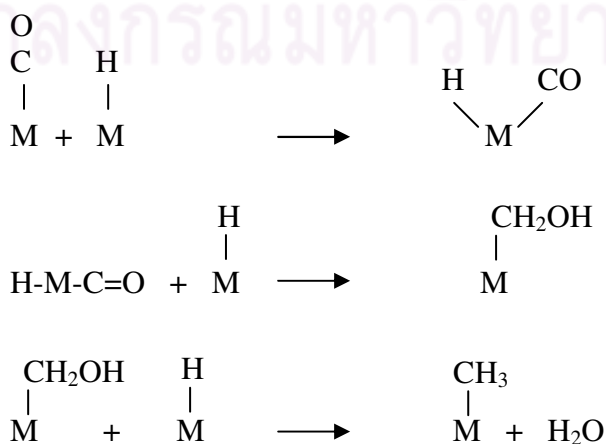


**(iii) Termination:**

This mechanism explains the formation of alkanes, and olefins as well as oxygenated hydrocarbons. However, it precludes the dissociation of CO, which is not consistent with many experimental observations.

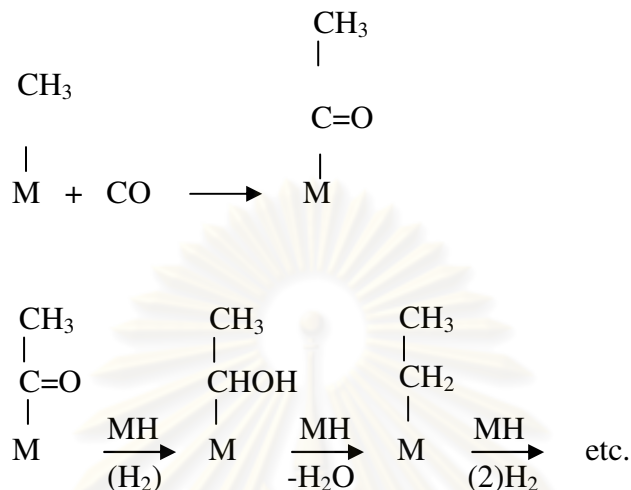
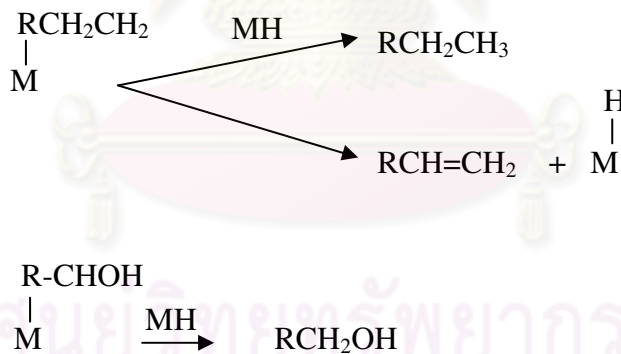
**3.1.3 The CO insertion mechanism.****(i) initiation :**

The initiation of active species is similar to that of the carbide mechanism although the mechanism of its formation is different



**(ii) Propagation:**

propagation proceeds via CO insertion rather than  $-\text{CH}_2-$  insertion.

**(iii) Termination:**

Normally, catalysts used for FTS are group VIII metals. By nature, the hydrogenation activity increases in order of  $\text{Fe} < \text{Co} < \text{Ni} < \text{Ru}$ . Ru is the most active. Ni forms predominantly methane, while Co yields much higher ratios of paraffins to olefins and much less oxygenated products such as alcohols and aldehydes than Fe does.

The current main goal in FTS is to obtain high molecular weight, straight chain hydrocarbons. However, methane and other light hydrocarbons are always

present as less desirable products from the synthesis. According to the Anderson-Schulz-Flory (ASF) product distribution, typically 10 to 20% of products from the synthesis are usually light hydrocarbon ( $C_1$ - $C_4$ ). These light alkanes have low boiling points and exist in the gas phase at room temperature, which is inconvenient for transportation. Many attempts have been made to minimize these by-products and increase the yield of long chain liquid hydrocarbons by improving chain growth probability. It would be more efficient to be able to convert these less desirable products into more useful forms, rather than re-reforming them into syngas and recycling them (Farrauto and Bartholomew, 1997). Depending upon the type of catalyst used, promoters, reaction conditions (pressure, temperature and  $H_2/CO$  ratios), and type of reactors, the distribution of the molecular weight of the hydrocarbon products can be noticeably varied.

## 3.2 Aluminium

### 3.2.1 Properties of alumina

Alumina which is  $Al_2O_3$  in general form is a polymorphic material. Alumina can be easily synthesized small particles and obtained desirous surface area and pore distribution. Commercial alumina have surface area between 100-600  $m^2/g$ . High porosity solid cause high intra surface area, good metal dispersion and increasable effective of catalytic. There are many forms of alumina ( $\alpha$ -,  $\gamma$ -,  $\delta$ -,  $\eta$ -,  $\kappa$ -,  $\chi$ -,  $\theta$ -,  $\rho$ -, and  $\iota$ -  $Al_2O_3$ ) but the  $\alpha$ -  $Al_2O_3$  is the only stable form. The thermodynamically stable phase is alpha alumina ( $\alpha$ -  $Al_2O_3$ , corundum) where all Al ions are equivalent in octahedral coordination in a hep oxide array.  $\alpha$ -  $Al_2O_3$  (corundum) powders are applied in catalysis as supports, for example, of silver catalysts for ethylene oxidation to ethylene oxide, just because they have low Lewis acidity, low catalytic activity, and conversely, they are mechanically and thermally very strong. All other alumina polymorphs are metastable. (Evans 1993).

The other forms are frequently termed 'transition' aluminas. These transition aluminas are frequently termed 'activated' or 'active' aluminas.  $\rho$ - $Al_2O_3$  is

amorphous but the other forms have reasonably well-defined X-ray diffraction patterns. The activated aluminas use as an adsorbent. Even though the surface of an activated alumina has a strong affinity for water, it makes very effective as a desiccant. Activated alumina can be used for removing water from a very wide range of compounds including acetylene, benzene, alkanes, alkenes and other hydrocarbons, air, ammonia, argon, chlorinated hydrocarbons, chlorine, natural gas and petroleum fuels, oxygen, sulfur dioxide and transformer oils (Evans 1993).

Activated alumina can dry a gas to a water content lower than that achievable with any other commercially available desiccant. In addition to water removal, activated alumina can be used selectively to adsorb certain other chemical species from gaseous or liquid streams. Polar molecules such as fluorides or chlorides are readily adsorbed and so activated alumina is used in petroleum refining to adsorb HCl from reformed hydrogen and organic fluorides from hydrocarbons produced by the HF-alkylation process (Evans 1993).

Activated aluminas find widespread application as both catalysts in their own right and as catalyst substrates. The more significant applications are summarized as the claus catalyst for the removal of the hydrogen sulfide in natural gas processing, petroleum refining and coal treatment, as alcohol dehydration to give olefins or ethers, as hydrotreating to remove oxygen, sulfur, nitrogen and metal (V and Ni) impurities from petroleum feedstocks and to increase the H/C ratio, as reforming catalysts: Pt and Re catalysts on a  $\gamma$ - $\text{Al}_2\text{O}_3$  substrate are used to raise the octane-number of petrol, as automotive exhaust catalysts (Evans 1993).

Activated alumina has a surface with both Lewis and Bronsted acidic and basic sites. Acidity is derived from the  $\text{Al}^{3+}$  ions and  $\text{H}_2\text{O}$  molecules coordinated to cationic sites, while basicity is due to basic hydroxide groups and  $\text{O}^{2-}$  anion vacancies (Evans 1993).

If alumina contact to humidity, surface are adsorped water molecules and when alumina were dried at 100 °C to 150 °C, water molecules are desorbed but

remain hydroxyl group (-OH) cause acidity of alumina are weak Bronsted acid. (Figure 3.1) Calcination temperatures below 300 °C, the acid strength and concentration of alumina are low and at 500 °C reduce Bronsted acid sites. (Wittayakhun *et al.* 2004)

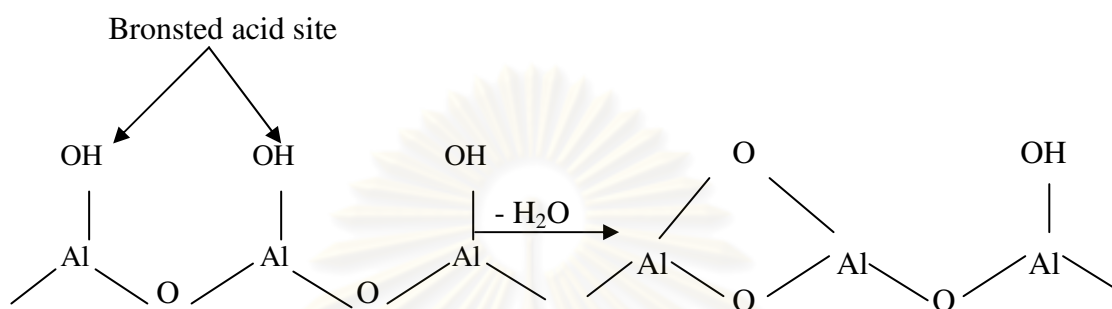


**Figure 3.1** Desorption of water from alumina surface (Wittayakhun *et al.* 2004).

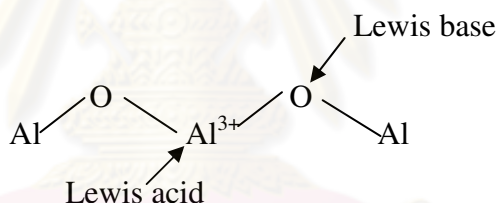


**Figure 3.2** Lewis acid and Lewis basic sites on alumina (Wittayakhun *et al.* 2004).

As shown in Figure 3.2, further increasing temperatures above 600 °C, adjacent -OH combine and more emit H<sub>2</sub>O and contribute to Al<sup>3+</sup> are Lewis acid sites and O<sup>2-</sup> are Lewis basic sites. Hardness of surface bring about no reaction between Lewis acid and Lewis base which both sites have high activity in various reaction such as Dehydration of alcohol and isomerization of alkene. The decline in acidity for calcination temperatures above 800 °C can be attributed to the collapse in surface area as the alumina is converted to its alpha form (Wittayakhun *et al.* 2004).

### 3.2.1.1 Properties of $\gamma$ - $\text{Al}_2\text{O}_3$

$\gamma$ -  $\text{Al}_2\text{O}_3$  which is the most used form of alumina in industry and any field of technologies is mostly obtained by decomposition of the boehmite oxyhydroxide  $\gamma$ - $\text{AlOOH}$  (giving medium surface area lamellar powders,  $\sim 100 \text{ m}^2/\text{g}$ ) or of a poorly crystallized hydrous oxyhydroxide called “pseudoboehmite” at 327 to 527 °C, giving high surface area materials ( $\sim 500 \text{ m}^2/\text{g}$ ). However, the details of its structure are still matter of controversy. It has a cubic structure described by Lippens (Fierro *et al.*2006) and de Boer (Fierro *et al.*2006) to be a defective spinel, although it can be tetragonally distorted. Being the stoichiometry of the “normal” spinel  $\text{MgAl}_2\text{O}_4$  (with Al ions virtually in octahedral coordination and Mg ions in tetrahedral coordination) the presence of all trivalent cations in  $\gamma$ -  $\text{Al}_2\text{O}_3$  implies the presence of vacancies in usually occupied tetrahedral or octahedral coordination sites. Soled proposed that the cation charge can be balanced, more than by vacancies, by hydroxyl ions at the surface. In fact,  $\gamma$ -  $\text{Al}_2\text{O}_3$  is always hydroxylated; dehydroxylation occurring only at a temperature where conversion to other alumina forms is obtained. XRD studies using the Rietveld method, performed by Zhou (Fierro *et al.*2006) and Snyder (Fierro *et al.*2006), suggested that  $\text{Al}^{3+}$  cations can be in positions different from those of spinels, that is, in trigonal coordination. The possibility of a structure of  $\gamma$ -  $\text{Al}_2\text{O}_3$ , as “hydrogen-spinel” has been proposed based on IR spectroscopy. Calculations based on the composition  $\text{HAl}_5\text{O}_4$  have been performed but found that this structure is very unstable. Sohlberg et al. (Fierro *et al.*2006) arrived to a structure very similar to that proposed by Zhou (Fierro *et al.*2006) and Snyder (Fierro *et al.*2006), based on spinel but with occupation of extraspinel sites. On the contrary, Digne et al. (Fierro *et al.*2006) and Krokidis et al. (Fierro *et al.*2006) proposed a structure based on ccp oxide lattice but different from that of a spinel, with 25% of Al ions in tetrahedral interstice and no structural vacancies. According to these authors, this structure, although unstable with respect to corundum, is more stable than that of the spinel based structures.  $\gamma$ -  $\text{Al}_2\text{O}_3$  is also active as an acidic catalyst. As for example it is very active in the dehydration of alcohols to olefins and to ether as well as both in double bond isomerization and in skeletal isomerization of olefins.



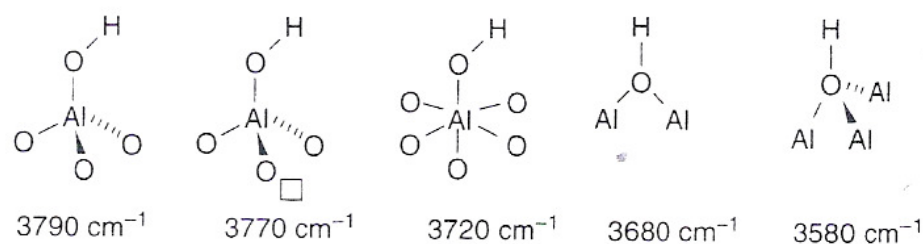


**Figure 3.3** Assignment of the OH stretchings of transitional aluminas, following Busca *et al.*, based on the comparison with the spectra of nondefective and partially defective spinel aluminates and ferrites. The square represents a vacancy in a normally occupied position of stoichiometric spinels (Fierro *et al.*2006).

In Figure 3.3 the assignments of the five main  $\nu\text{OH}$  bands of the surface hydroxyl groups of transitional aluminas proposed by Busca *et al.* (Fierro *et al.*2006) The catalytic activity of transitional aluminas are undoubtedly mostly related to the Lewis acidity of a small number of low coordination surface aluminum ions, as well as to high ionicity of the surface Al-O bond. The alumina's Lewis sites have been well characterized by adsorption of probes such as pyridine, carbon monoxide, and several bases followed by IR, ammonia and amines followed by calorimetric, triphenylphosphine followed by  $^{31}\text{P}$  NMR, to be the strongest among metal oxides, only weaker than those of Al halides. Volumetric, TPD and calorimetric experiment allowed also to determine the amount of such very strong Lewis sites present on transitional alumina surfaces, which however depend on the dehydroxylation degree (depending on the activation temperature) and the peculiar phase and preparation (Fierro *et al.*2006).

### 3.3 Silicon dioxide (Patnaik, 2002)

#### 3.3.1 General feature of silica

**Table 3.1** Physical properties of silica

Other names	Silica
Molecular formula	SiO <sub>2</sub>
Molar mass	60.1 g/mol
Appearance	white or colourless solid (when pure)
Density and phase	2.6 g/cm <sup>3</sup> , solid
Solubility in water	insoluble
Melting point	1610 °C
Boiling point	2230 °C

In its many forms, silica has been used in all stages of civilization, from the ancient flints of the Stone Age to the modern silica laboratory ware. Because of its many uses, and of the many varied forms in which it occurs, silica has been called by more names than any other mineral. Many of the older names of flint are now so obsolete that repetition is needless, but many of the present-day names for quartz gems are unknown save to a few jewellers. Then, too, the exact research of the modern laboratory has shown several distinct crystallographic varieties of silica; some of which are closely connected with the temperatures experienced in their life-history.

The many different names, and their different connotations, which are now in use for silica minerals, call for a classification and arrangement in a more ample, yet more concise manner than is to be found in the usual discussion of the varieties of silica. This article is written with the hope of making a scientific classification of

these names, so that the use of the different terms will no longer be a cause for tedious searching for definitions.

These varieties are named in the order formed with descending temperatures. Recrystallization changes occur at the temperatures noted when ample time is allowed for the action, often in the laboratory only in the presence of catalysts. Besides the changes at these critical temperatures, there are probably similar changes from unstable forms towards quartz at atmospheric temperatures, especially after long time intervals. With fairly rapid cooling or heating intermediate forms may not occur in their stable zone, but a direct change from one to another without the intermediate product may take place. Most of the recrystallization changes noted are found to occur at both ascending and descending temperatures.

(A) SILICA GLASS - amorphous, a true non-crystalline glass, stable below the melting point and above the "gc" temperature. Quartz Glass, Fused Silica, Fused Quartz, are other names for this supercooled liquid. In most forms at atmospheric temperatures there are traces of cristobalite.

(B) CRISTOBALITE - isometric, or pseudo-isometric, "gc" range is at 1710° where Cristobalite changes to glass as temperatures rise, or glass to cristobalite as they fall. Cristobalite, an alternate spelling. Beta Cristobalite, also called High Cristobalite, is the high temperature product, forming in the "gc" range in cooling. It is isometric, and in cooling recrystallizes to Alpha Cristobalite, or Low Cristobalite, at 200-275°, providing cooling through the "ct" and "tq" ranges has been too rapid for recrystallization. It is tetragonal.

(C) TRIDYMITE - hexagonal, bipyramidal. "ct" range is at 1470°, where cristobalite changes to tridymite on cooling. Glass may crystallize as tridymite at 1670° if the cooling was too rapid through the "gc" range. Beta Second Tridymite, or Upper High Tridymite, is the high temperature product, forming in the "ct" range in cooling, and which recrystallizes to Beta First Tridymite, also called Lower High Tridymite, at

163° if cooling was too rapid for the "tq" transformation. This in turn alters to Alpha Tridymite, or Low Tridymite, at 117°, which is the usual tridymite of nature.

- Asmanite - a meteoric tridymite, related to the above series.
- Vestan - a doubtful silica mineral, probably to be ascribed to tridymite.
- Granuline - a doubtful pulverescent mineral which seems allied to tridymite on optical grounds.

(D) QUARTZ - hexagonal, forms from tridymite in the "tq" range at 870° in cooling. Glass may change to crystalline quartz at about 1400° providing cooling was too rapid for the "gc", "gt" and "ct" transformations. Beta Quartz, or High Quartz, is the high temperature product, forming at the "tq" point. It is hemihedral. On cooling it recrystallizes to Alpha Quartz, also called Low Quartz, at 573°, yielding the stable low temperature mineral. It is tetartohedral, showing polarity along the c axis and is divisible into Right Hand Quartz and Left Hand Quartz

(E) CHALCEDONY - a cryptocrystalline, or very finely fibrous mineral, which has not been successfully located in the thermal equilibrium diagram. Heating to 725-850° usually results in an alteration to tridymite, which thereafter acts as normal tridymite. Chalcedony is usually found as a deposit from solutions, and may be a mixture of glass and quartz, or more probably an intermediate product in the dehydration of the opal colloid. Various subdivisions of chalcedony have been made on optical grounds.

- Chalcedony - biaxial, positive, elongation positive.
- Chalcedonite - biaxial, negative.
- Lussatite - biaxial, positive, parallel, elongation.
- Quartzine - biaxial, positive, negative elongation  
pseudochalcedonite, Lutecite.
- Jenzschite - differently soluble, but of same S. G. as chalcedony.

- Melanophlogite - possibly impure chalcedony.  
 Sulfuricin - probably a chalcedony rich in sulphur.

(F) COLLOIDAL SILICA - is usually hydrous, and is commonly described under opal. Silicon occurs in nature combined with oxygen in various forms of silica and silicates. Silicates have complex structures consisting of  $\text{SiO}_4$  tetrahedral structural units incorporated to a number of metals. Silicon is never found in nature in free elemental form. Among all elements silicon forms the third largest number of compounds after hydrogen and carbon. There are well over 1000 natural silicates including clay, mica, feldspar, granite, asbestos, and hornblende. Such natural silicates have structural units containing orthosilicates,  $\text{SiO}_4^{4-}$ , pyrosilicates  $\text{Si}_2\text{O}_7^{6-}$ , and other complex structural units, such as,  $(\text{SiO}_3)_n^{2n-}$  that have hexagonal rings arranged in chains or pyroxene  $(\text{SiO}_3^{2-})_n$  and amphiboles,  $(\text{Si}_4\text{O}_{11})_n^{6-}$  in infinite chains. Such natural silicates include common minerals such as tremolite,  $\text{Ca}_2\text{Mg}_5(\text{OH})_2\text{Si}_8\text{O}_{22}$ ; diopside,  $\text{CaMg}(\text{SiO}_3)_2$ ; kaolin,  $\text{H}_8\text{Al}_4\text{Si}_4\text{O}_{18}$ ; montmorillonite,  $\text{H}_2\text{Al}_2\text{Si}_4\text{O}_{12}$ ; talc,  $\text{Mg}_3[(\text{OH})_2\text{SiO}_{10}]$ ; muscovite (a colorless form of mica),  $\text{H}_2\text{KAl}_3(\text{SiO}_4)_3$ ; hemimorphite,  $\text{Zn}_4(\text{OH})_2\text{Si}_2\text{O}_7 \cdot \text{H}_2\text{O}$ ; beryl,  $\text{Be}_3\text{Al}_2\text{Si}_6\text{O}_{18}$ ; zircon,  $\text{ZrSiO}_4$ ; benitoite,  $\text{BaTiSi}_3\text{O}_9$ ; feldspars,  $\text{KAlSi}_3\text{O}_8$ ; zeolites,  $\text{Na}_2\text{O} \cdot 2\text{Al}_2\text{O}_3 \cdot 5\text{SiO}_2 \cdot 5\text{H}_2\text{O}$ ; nephrite,  $\text{Ca}(\text{Mg},\text{Fe})_3(\text{SiO}_3)_4$ ; enstatite,  $(\text{MgSiO}_3)_n$ ; serpentine,  $\text{H}_4\text{Mg}_3\text{Si}_2\text{O}_{10}$ ; jadeite,  $\text{NaAl}(\text{SiO}_3)_2$ ; topaz,  $\text{Al}_2\text{SiO}_4\text{F}_2$ ; and tourmaline,  $(\text{H},\text{Li},\text{K},\text{Na})\text{Al}_3(\text{BOH})_2\text{SiO}_{19}$ . silica, the other most important class of silicon compounds, exists as sand, quartz, flint, amethyst, agate, opal, jasper, and rock crystal.

### 3.4 Titanium (IV) oxide

Titanium (IV) oxide occurs naturally in three crystalline forms: anatase, which tends to be more stable at low temperature, brookite, which is usually found only in minerals, and rutile, which tends to be more stable at higher temperatures and thus is sometimes found in igneous rock. These crystals are substantially pure titanium (IV) oxide but usually amounts of impurities, e.g., iron, chromium, or vanadium, which

darken them. A summary of the crystallographic properties of the three varieties is given in Table 3.2.

Although anatase and rutile are both tetragonal, they are not isomorphous (Figure 3.4). Anatase occurs usually in near-regular octahedral, and rutile forms slender prismatic crystal, which are frequently twinned. Rutile is the thermally stable form and is one of the two most important ores of titanium.

The three allotropic forms of titanium (IV) oxide have been prepared artificially but only rutile, the thermally stable form, has been obtained in the form of transparent large single crystal. The transformation from anatase to rutile is accompanied by the evolution of ca. 12.6 KJ/mol (3.01 kcal/mol), but the rate of transformation is greatly affected by temperature and by the presence of other substance which may either catalyze or inhibit the reaction. The lowest temperature at which conversion of anatase to rutile takes place at a measurable rate is ca. 700°C, but this is not a transition temperature. The change is not reversible;  $\Delta G$  for the change from anatase to rutile is always negative.

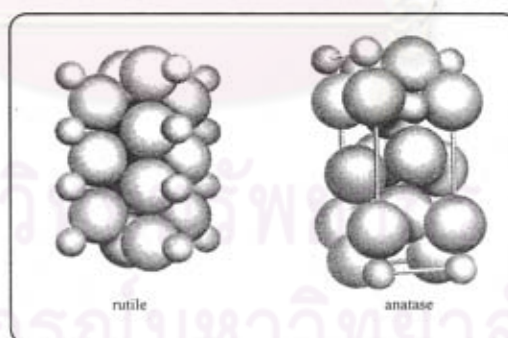


**Figure 3.4** Crystal structure of  $\text{TiO}_2$ . (Fujishima *et al.*,1999)

Brookite has been produced by heating amorphous titanium (IV) oxide, prepared from alkyl titanates of sodium titanate with sodium or potassium hydroxide in an autoclave at 200 to 600°C for several days. The important commercial forms of

titanium (IV) oxide are anatase and rutile, and these can readily be distinguished by X-ray diffraction spectrometry.

Since both anatase and rutile are tetragonal, they are both anisotropic, and their physical properties, e.g. refractive index, vary according to the direction relative to the crystal axes. In most applications of these substances, the distinction between crystallographic directions is lost because of the random orientation of large numbers of small particles, and it is mean value of the property that is significant.

**Table 3.2** Crystallographic properties of anatase, brookite, and rutile.

Properties	Anatase	Brookite	Rutile
Crystal structure	Tetragonal	Orthorhombic	Tetragonal
Optical	Uniaxial, negative	Biaxial, positive	Uniaxial, negative
Density, g/cm <sup>3</sup>	3.9	4.0	4.23
Harness, Mohs scale	5 <sup>1/2</sup> – 6	5 <sup>1/2</sup> – 6	7 – 7 <sup>1/2</sup>
Unit cell	D <sub>4h</sub> <sup>19</sup> .4TiO <sub>2</sub>	D <sub>2h</sub> <sup>15</sup> .8TiO <sub>2</sub>	D <sub>4h</sub> <sup>12</sup> .3TiO <sub>2</sub>
Dimension, nm			
a	0.3758	0.9166	0.4584
b		0.5436	
c	0.9514	0.5135	2.953

Measurement of physical properties, in which the crystallographic directions are taken into account, may be made of both natural and synthetic rutile, natural anatase crystals, and natural brookite crystals. Measurements of the refractive index of titanium (IV) oxide must be made by using a crystal that is suitably orientated with respect to the crystallographic axis as a prism in a spectrometer. Crystals of suitable size of all three modifications occur naturally and have been studied. However, rutile is the only form that can be obtained in large artificial crystals from melts. The refractive index of rutile is 2.75. The dielectric constant of rutile varies with direction

in the crystal and with any variation from the stoichiometric formula,  $\text{TiO}_2$ ; an average value for rutile in powder form is 114. The dielectric constant of anatase powder is 48.

Titanium (IV) oxide is thermally stable (mp  $1855^\circ\text{C}$ ) and very resistant to chemical attack. When it is heated strongly under vacuum, there is a slight loss of oxygen corresponding to a change in composition to  $\text{TiO}_{1.97}$ . The product is dark blue but reverts to the original white color when it is heated in air.

### **3.5 Cobalt** (Young 1960; Othmer, 1991)

#### **3.5.1 General**

Cobalt, a transition series metallic element having atomic number 27, is similar to silver in appearance.

Cobalt and cobalt compounds have expanded from use colorants in glasses and ground coat frits for pottery to drying agents in paints and lacquers, animal and human nutrients, electroplating materials, high temperature alloys, hard facing alloys, high speed tools, magnetic alloys, alloys used for prosthetics, and used in radiology. Cobalt is also as a catalyst for hydrocarbon refining from crude oil for the synthesis of heating fuel.

#### **3.5.2 Physical Properties**

The electronic structure of cobalt is  $[\text{Ar}] 3d^7 4s^2$ . At room temperature the crystalline structure of the  $\alpha$  (or  $\epsilon$ ) form, is close-packed hexagonal (cph) and lattice parameters are  $a = 0.2501$  nm and  $c = 0.4066$  nm. Above approximately  $417^\circ\text{C}$ , a face-centered cubic (fcc) allotrope, the  $\gamma$  (or  $\beta$ ) form, having a lattice parameter  $a = 0.3544$  nm, becomes the stable crystalline form. Physical properties of cobalt are listed in Table 3.3.



The scale formed on unalloyed cobalt during exposure to air or oxygen at high temperature is double-layered. In the range of 300 to 900°C, the scale consists of a thin layer of mixed cobalt oxide,  $\text{Co}_3\text{O}_4$ , on the outside and cobalt (II) oxide,  $\text{CoO}$ , layer next to metal. Cobalt (III) oxide,  $\text{Co}_2\text{O}_3$ , may be formed at temperatures below 300 °C. Above 900°C,  $\text{Co}_3\text{O}_4$  decomposes and both layers, although of different appearance, are composed of  $\text{CoO}$  only. Scales formed below 600°C and above 750°C appear to be stable to cracking on cooling, whereas those produced at 600-750°C crack and flake off the surface.

Cobalt forms numerous compounds and complexes of industrial importance. Cobalt, atomic weight 58.933, is one of the three members of the first transition series of Group 9 (VIII B). There are thirteen known isotopes, but only three are significant:  $^{59}\text{Co}$  is the only stable and naturally occurring isotope;  $^{60}\text{Co}$  has a half-life of 5.3 years and is a common source of  $\gamma$ -radioactivity; and  $^{57}\text{Co}$  has a 270-d half-life and provides the  $\gamma$ -source for Mössbauer spectroscopy.

Cobalt exists in the +2 or +3 valence states for the major of its compounds and complexes. A multitude of complexes of the cobalt (III) ion exists, but few stable simple salts are known. Octahedral stereochemistries are the most common for cobalt (II) ion as well as for cobalt (III). Cobalt (II) forms numerous simple compounds and complexes, most of which are octahedral or tetrahedral in nature; cobalt (II) forms more tetrahedral complex than other transition-metal ions. Because of the small stability difference between octahedral and tetrahedral complexes of cobalt (II), both can be found in equilibrium for a number of complexes. Typically, octahedral cobalt (II) salts and complexes are pink to brownish red; most of the tetrahedral  $\text{Co}$  (II) species are blue.

**Table 3.3** Physical properties of cobalt (Othmer, 1991)

Property	Value
atomic number	27
atomic weight	58.93
transformation temperature, °C	417
heat of transformation, J/g <sup>a</sup>	251
melting point, °C	1493
latent heat of fusion, $\Delta H_{\text{fus}}$ J/g <sup>a</sup>	395
boiling point, °C	3100
latent heat of vaporization at bp, $\Delta H_{\text{vap}}$ kJ/g <sup>a</sup>	6276
specific heat, J/(g <sup>o</sup> C) <sup>a</sup>	
15-100°C	0.442
molten metal	0.560
coefficient of thermalexpansion, °C <sup>-1</sup>	
cph at room temperature	12.5
fcc at 417°C	14.2
thermal conductivity at 25 °C, W/(m·K)	69.16
thermal neutron absorption, Bohr atom	34.8
resistivity, at 20 °C <sup>b</sup> , 10 <sup>-8</sup> Ω·m	6.24
Curie temperature, °C	1121
saturation induction, 4πI <sub>s</sub> , T <sup>c</sup>	1.870
permeability, μ	
initial	68
max	245
residual induction, T <sup>c</sup>	0.490
coercive force, A/m	708
Young's modulus, Gpac	211

**Table 3.3** Physical properties of cobalt (cont.)

Property	Value		
Hardness <sup>f</sup> , diamond pyramid, of %Co	99.9	99.98 <sup>e</sup>	
At 20 °C	225	253	
At 300 °C	141	145	
At 600 °C	62	43	
At 900 °C	22	17	
strength of 99.99 %cobalt, MPa <sup>g</sup>	as cast	annealed	sintered
tensile	237	588	679
tensile yield	138	193	302
compressive	841	808	
compressive yield	291	387	

<sup>a</sup>To convert J to cal, divided by 4.184.

<sup>b</sup>conductivity = 27.6 % of International Annealed Copper Standard.

<sup>c</sup>To convert T to gauss, multiply by 10<sup>4</sup>.

<sup>d</sup>To convert GPa to psi , multiply by 145,000.

<sup>e</sup>Zone refined.

<sup>f</sup>Vickers.

<sup>g</sup>To convert MPa to psi , multiply by 145.

### 3.6 Cobalt aluminate and cobalt oxide

#### 3.6.1 Cobalt aluminate (CoAl<sub>2</sub>O<sub>4</sub>)

CoAl<sub>2</sub>O<sub>4</sub> is a binary oxide consisting of cobalt oxides and aluminum oxides that crystallize in spinel structure. The unit cell of spinels is represented by formula of AB<sub>2</sub>O<sub>4</sub>. the Co<sup>2+</sup> ions occupy the tetrahedrally coordinated A site and Al<sup>3+</sup> ions occupy the octahedrally coordinated B site. The structure of cobalt aluminate is shown in Figure 3.5

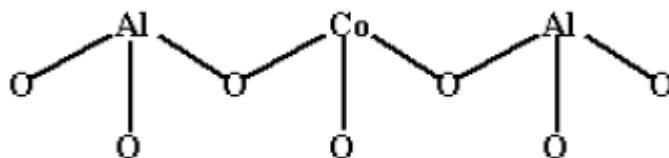


**Figure 3.5** Structure of cobalt aluminate

Spinel-type structures are usually synthesized at high temperature from a mixture at solid state of the two oxide components. In this spinel-type structure, the metal aluminates seem to be a good option because of their properties such as greater thermal stability, high resistance to acids and alkalis, hydrophobicity, low surface acidity, high melting points and surface area, lower temperature sinterability, increase hardness, ductility, better diffusion, etc (Edelstein, 1999). These properties make it interesting materials as catalysts and carriers for active metals to substitute the more traditional systems.  $\text{CoAl}_2\text{O}_4$  has received special interest due to their technological applications as inorganic ceramic blue pigment (Cho and Kakihana, 1999; Mimani, 2001; Zayat and Lavy, 2000; Bacon and Roberts, 1953).  $\text{CoAl}_2\text{O}_4$  is also of great interest in the field of heterogeneous catalysis while it has been used for catalytic application (Chokkaram *et al.*, 1997; Arian *et al.*, 1998). Recently,  $\text{CoAl}_2\text{O}_4$  has been prepared by several methods, such as co-precipitated method, sol-gel method, hydrothermal method, polymerized complex methods and solvothermal method

### 3.6.2 Cobalt Oxides

Cobalt has three well-known oxides:

Cobalt (II) oxide,  $\text{CoO}$ , is an olive green, cubic crystalline material. Cobalt (II) oxide is the final product formed when the carbonate or the other oxides are calcined to a sufficiently high temperature, preferably in a neutral or slightly reducing atmosphere. Pure cobalt (II) oxide is a difficult substance to prepare, since it readily takes up oxygen even at room temperature to re-form a higher oxide. Above about  $850^\circ\text{C}$ , cobalt (II) oxide form is the stable oxide. The product of commerce is usually

dark gray and contains 75-78 wt % cobalt. Cobalt (II) oxide is soluble in water, ammonia solution, and organic solvents, but dissolves in strong mineral acids. It is used in glass decorating and coloring and is a precursor for the production of cobalt chemical.

Cobalt (III) oxide,  $\text{Co}_2\text{O}_3$ , is formed when cobalt compounds are heated at a low temperature in the presence of an excess of air. Some authorities hold that cobalt (III) oxide exists only in the hydrate form. The lower hydrate may be made as a black powder by oxidizing neutral cobalt solutions with substances like sodium hypochlorite.  $\text{Co}_2\text{O}_3 \cdot \text{H}_2\text{O}$  is completely converted to  $\text{Co}_3\text{O}_4$  at temperatures above  $265^\circ\text{C}$ .  $\text{Co}_3\text{O}_4$  will absorb oxygen in a sufficient quantity to correspond to the higher oxide  $\text{Co}_2\text{O}_3$ .

Cobalt oxide,  $\text{Co}_3\text{O}_4$ , is formed when cobalt compounds, such as the carbonate or the hydrated sesquioxide, are heated in air at temperatures above approximately  $265^\circ\text{C}$  and not exceeding  $800^\circ\text{C}$ .

### 3.7 Co-based Catalysts

Supported cobalt (CO) catalysts are the preferred catalysts for the synthesis of heavy hydrocarbons from natural gas based syngas ( $\text{CO}$  and  $\text{H}_2$ ) because of their high Fischer-Tropsch (FT) activity, high selectivity for linear hydrocarbons and low activity for the water-gas shift reaction. It is known that reduced cobalt metal, rather than its oxides or carbides, is the most active phase for CO hydrogenation in such catalysts. Investigations have been done to determine the nature of cobalt species on various supports such as alumina, silica, titania, magnesia, carbon, and zeolites. The influence of various types of cobalt precursors used was also investigated. It was found that the use of organic precursors such as CO (III) acetyl acetate resulting in an increase of CO conversion compared to that of cobalt nitrate. (Kraum and Baerns, 1999)

### 3.8 Cobalt-Support Compound Formation (Co-SCF)

Compound formation between cobalt metal and the support can occur under pretreatment and/or reaction conditions, leading to catalyst deactivation. The compound formation of cobalt metal with support materials, however, is difficult to predict because of the lack of sufficient thermodynamic data. Co-support compound formation can be detected evidentially.

#### 3.8.1 Co-Aluminate Formation

Interaction of cobalt with its alumina support has been observed by many authors using various techniques including TPR, XRD, EXAFS, and XPS (ESCA). The migration of cobalt ions into alumina lattice sites of octahedral or tetrahedral symmetry is limited to the first few layers of the support under normal calcination conditions. The reaction of Co with  $\gamma$ -Al<sub>2</sub>O<sub>3</sub> can form a surface spinel in Co/ $\gamma$ -Al<sub>2</sub>O<sub>3</sub> catalysts. The surface spinel structure can not be observed by X-ray diffraction because it does not have long range, three dimensional order. It has been suggested that cobalt ions occupying surface octahedral site of  $\gamma$ -Al<sub>2</sub>O<sub>3</sub> are reducible while cobalt ions occupying tetrahedral sites are non-reducible, at least at temperatures  $\leq$  900°C. At lower calcination temperatures, filling of the octahedral sites is more favorable. Filling of the tetrahedral site of  $\gamma$ -Al<sub>2</sub>O<sub>3</sub> may be enhanced by an increase in calcination temperature.

### 3.9 Gallium

Gallium (chemical symbol Ga, atomic number 31) is a rare, soft, silvery metal. It is a brittle solid at low temperatures, but it liquefies slightly above room temperature and melts in the hand. It is one of only a few materials that expands when freezing (like water), and its liquid form has a higher density than the solid form (like water). Gallium occurs in trace amounts in bauxite (an aluminum ore) and zinc ores.

Gallium is most commonly used in the form of the compound gallium(III) arsenide, which is a semiconductor useful for integrated circuits, light-emitting diodes (LEDs), and laser diodes. The nitride and phosphide of gallium are also valuable semiconductor materials, and gallium itself is used as a dopant in semiconductors. In addition, this metal is a component in low-melting temperature alloys, and its alloy with indium and tin is used in medical thermometers to replace mercury. Also, gallium can wet (coat) glass to create brilliant mirrors.

**Table 3.4** Chemical properties of gallium.

Atomic number	31
Atomic mass	69.72 g.mol <sup>-1</sup>
Electronegativity according to Pauling	unknown
Density	5.1 g.cm <sup>-3</sup> at 20°C
Melting point	29.8 °C
Boiling point	2204 °C
Vanderwaals radius	0.161 nm
Ionic radius	0.083 nm (+3)
Isotopes	6
Electronic shell	[ Ar ] 3d <sup>10</sup> 4s <sup>2</sup> 4p <sup>1</sup>
Energy of first ionisation	578.6 kJ.mol <sup>-1</sup>
Energy of second ionisation	1978.8 kJ.mol <sup>-1</sup>
Energy of third ionisation	2389 kJ.mol <sup>-1</sup>
Energy of fourth ionisation	2962.3 kJ.mol <sup>-1</sup>
Standard potential	- 0.52 V

## CHAPTER IV

### EXPERIMENTAL

This chapter consists of experimental systems and procedures used in this work which is divided into three parts including catalyst preparation, catalyst characterization and reaction study in CO hydrogenation.

The first part (section 4.1) is described catalyst preparation such as Ga-modified  $\text{Al}_2\text{O}_3$ ,  $\text{SiO}_2$  and  $\text{TiO}_2$  and Preparation of Co catalyst. The second part (section 4.2) is explained catalyst characterization by various techniques including of BET surface area, TPR, XRD, SEM/EDX, TEM, XPS,  $\text{NH}_3$ -TPD and  $\text{H}_2$  Chemisorption. Finally, the last part (section 4.3) is illustrated catalyst activity measurement in CO hydrogenation.

#### 4.1 Catalyst preparation

##### 4.1.1 Chemicals

The details of chemicals used in this experiment are shown in Table 4.1

**Table 4.1** Chemicals used in the preparation of catalysts.

Chemical	Supplier
Cobalt (II) nitrate hexahydrate 98% ( $\text{Co}(\text{NO}_3)_2 \cdot 6\text{H}_2\text{O}$ )	Aldrich
Aluminum oxide	Fluka
Silicon dioxide 99.5% ( $\text{SiO}_2$ ), nanopowder, 15 nm,	Aldrich
$\text{TiO}_2$ (JRC-TIO1, anatase)	Catalysis Society of Japan
Gallium (III) nitrate hydrate 99.9%	Aldrich



#### 4.1.2 Preparation of Ga-modified Al<sub>2</sub>O<sub>3</sub>, SiO<sub>2</sub> and TiO<sub>2</sub>

The Ga-modified supports were prepared by the impregnation method. There were three kinds of the supports used [(i) Al<sub>2</sub>O<sub>3</sub> from Fluka, (ii) SiO<sub>2</sub> (99.5%), nanopowder, 15 nm from Aldrich and TiO<sub>2</sub>(JRC-TIO1, anatase) (Catalysis Society of Japan)]. First, Zr was impregnated into the support using a solution of Gallium (III) nitrate hydrate(99.9% from Aldrich) to produce Ga-modified supports having 0.2 and 1 wt% of Ga<sub>2</sub>O<sub>3</sub>. Second, the Ga-modified supports were dried at 110 °C for 20 h and calcined at 500 °C for 4 h prior to impregnation of cobalt.

#### 4.1.3 Preparation of Co catalyst

Cobalt nitrate [Co(NO<sub>3</sub>)<sub>2</sub>.6H<sub>2</sub>O] was dissolved in deionized water and impregnated into the support as mentioned above to give a final catalyst with 20 wt% cobalt. The catalyst precursor was dried at 110 °C for 20 h and calcined in air at 500°C for 4 h.

### 4.2 Catalyst Characterization

#### 4.2.1 X-Ray Diffraction (XRD)

XRD were performed to determine the bulk crystalline phases of catalyst. It was conducted using a SIEMENS D-5000 X-ray diffractometer connected with a computer with Diffract ZT version 3.3 program for fully control of the XRD analyzer. The experiments were carried out by using CuK<sub>α</sub> ( $\lambda = 1.54439 \text{ \AA}$ ) radiation with Ni filter in the range  $2\theta = 20\text{-}80^\circ$  resolution 0.04.

#### 4.2.2 N<sub>2</sub> Physisorption

BET surface area, pore volume and pore diameter were measured by N<sub>2</sub> adsorption–desorption isotherm at liquid nitrogen temperature (-196 °C) using a

Micromeritics ASAP 2020. The surface area and pore distribution were calculated according to Brunauer-Emmett-Teller (BET) and Barret-Joyner-Halenda (BJH) methods, consecutively.

The reaction apparatus of BET surface area measurement consisted of two feed lines for helium and nitrogen. The flow rate of the gas was adjusted by means of fine-metering valve on the gas chromatograph. The sample cell made from pyrex glass. The mixture gases of helium and nitrogen flowed through the system at the nitrogen relative of 0.3. The catalyst sample (ca. 0.2 to 0.5 g) was placed in the sample cell, which was then heated up to 160 °C and held at this temperature for 2 h. After the catalyst sample was cooled down to room temperature, nitrogen uptakes were measure as follows.

Step (1) Adsorption step: The sample that set in the sample cell was dipped into liquid nitrogen. Nitrogen gas that flowed through the system was adsorbed on the surface of the sample until equilibrium was reached.

Step (2) Desorption step: The sample cell with nitrogen gas-adsorption catalyst sample dipped into the water at room temperature. The adsorbed nitrogen gas was desorbed from the surface of the sample. This step was completed when the indicator line was in the position of base line.

Step (3) Calibration step: 1 ml of nitrogen gas at atmospheric pressure was injected through the calibration port of the gas chromatograph and the area was measured. The area was the calibration peak.

#### **4.2.3 NH<sub>3</sub>-Temperature Programmed Desorption (TPD)**

Temperature programmed desorption (TPD) of NH<sub>3</sub> was performed in a Micromeritic ChemiSorb 2750 automated system attached with ChemiSoft TPx software. The amount of NH<sub>3</sub> adsorbed on the surface was determined by temperature

programmed desorption. The thermal conductivity detector was used to measure the amount of  $\text{NH}_3$

Approximately 0.2 grams of sample was placed in a quartz tube in a temperature-controlled oven. Helium gas with flow rate at 15 ml/min was released to flow through sample. The sample was heated from room temperature to  $200^\circ\text{C}$  with a heating rate of  $10^\circ\text{C}/\text{min}$  and held for 1 hour. Then, the sample was cooled down to  $40^\circ\text{C}$ . In the next step, 15 vol% ammonium gas with flow rate at 20 ml/min flowed through sample instead of helium, and hold for 30 minutes. Adsorption of 15 vol% ammonium on the catalyst surface occurred in this step. Consequently, helium gas at the same flowed through our sample instead of ammonium and also holds for another hour. In the final step which was the desorption step; sample was heated from  $40^\circ\text{C}$  to  $650^\circ\text{C}$  with a heating rate of  $10^\circ\text{C}/\text{min}$ . The signal from this step was recorded every second and reported on a microcomputer.

#### **4.2.4 Scanning electron microscopy (SEM) and Energy dispersive X-ray spectroscopy (EDX)**

SEM and EDX were used to determine the catalyst morphologies and elemental distribution throughout the catalyst granules, respectively. The SEM of JEOL mode JSM-5410LV was applied using the secondary electron mode at 15 kV. EDX was performed using Link Isis series 300 program.

#### **4.2.5 Transmission Electron Microscope (TEM)**

The morphology and size of the catalysts were determined using a JEOL-TEM 200CX transmission electron spectroscopy operated at 160 kV at the Scientific and Technological Research Equipment Center (STREC), Chulalongkorn University.

#### 4.2.6 Temperature programmed reduction (TPR)

TPR was used to determine the reduction behaviors of the samples using a Micromeritics Chemisorb 2750.

1. The catalyst sample 0.1 g used in the sample cell.
2. Prior to operation, the catalysts were heated up to 200 °C in flowing nitrogen and held at this temperature for 1 h.
3. After the catalyst sample was cooled down to room temperature, the carrier gas was 5% H<sub>2</sub> in Ar (30 CC/min) were ramping from 35 to 800 °C at 10 °C/min.
4. A cold trap was placed before the detector to remove water produced during the reaction.
5. A thermal conductivity detector (TCD) was used to determine the amount of hydrogen consumption during TPR.

#### 4.2.7 Hydrogen Chemisorption

Static H<sub>2</sub> chemisorption at 100 °C on the reduce catalysts was used to determine the number of reduce surface cobalt metal atoms and overall cobalt dispersion. The total hydrogen chemisorption was calculated from the number of injection of a known volume. H<sub>2</sub> chemisorption was carried out following the procedure described by Reuel and Bartholomew, 1984 using a Micromeritics Pulse Chemisorb 2750. Prior to chemisorption, the catalysts will be reduced at 350 °C for 3 hours after ramping up at a rate of 1 °C/min.

#### 4.2.8 X-ray photoelectron spectroscopy (XPS)

XPS was used to examine the binding energy and the surface composition of the catalysts by using an AMICUS spectrometer with a x-ray source as Mg K<sub>α</sub> radiation operated at voltage of 20 kV, current of 10 mA. The computer controlled by using the AMICUS “VISION2” software.

## **4.3 Reaction study in CO hydrogenation**

### **4.3.1 Materials**

The reactant gas used for the reaction study was the carbon monoxide in hydrogen feed stream as supplied by Thai Industrial Gas Limited (TIG). The gas mixture contained 9.73 vol % CO in H<sub>2</sub> (22 CC/min). The total flow rate was 30 CC/min with the H<sub>2</sub>/CO ratio of 10/1. Ultra high purity hydrogen (50 CC/min) and high purity argon (8 CC/min) manufactured by Thai Industrial Gas Limited (TIG) were used for reduction and balanced flow rate

### **4.3.2 Apparatus**

Flow diagram of CO hydrogenation system is shown in Figure 4.1. The system consists of a reactor, an automatic temperature controller, an electrical furnace and a gas controlling system.

#### **4.3.2.1 Reactor**

The reactor was made from a stainless steel tube (O.D. 3/8"). Two sampling points were provided above and below the catalyst bed. Catalyst was placed between two quartz wool layers

#### **4.3.2.2 Automation Temperature Controller**

This unit consisted of a magnetic switch connected to a variable voltage transformer and a solid-state relay temperature controller model no. SS2425DZ connected to a thermocouple. Reactor temperature was measured at the bottom of the catalyst bed in the reactor. The temperature control set point is adjustable within the range of 0-800°C at the maximum voltage output of 220 volt.

#### 4.3.2.3 Electrical Furnace

The furnace supplied heat to the reactor for CO hydrogenation. The reactor could be operated from temperature up to 800°C at the maximum voltage of 220 volt.

#### 4.3.2.4 Gas Controlling System

Reactant for the system was each equipped with a pressure regulator and an on-off valve and the gas flow rates were adjusted by using metering valves.

#### 4.3.2.5 Gas Chromatography

The composition of hydrocarbons in the product stream was analyzed by a Shimadzu GC14B (VZ10) gas chromatograph equipped with a flame ionization detector. A Shimadzu GC8A (molecular sieve 5A) gas chromatography equipped with a thermal conductivity detector was used to analyze CO and H<sub>2</sub> in the feed and product streams. The operating conditions for each instrument are shown in the Table 4.2.

**Table 4.2** Operating condition for gas chromatograph.

Gas Chromatograph	SHIMADZU GC-8A	SHIMADZU GC-14B
Detector	TCD	FID
Column	Molecular sieve 5A	VZ10
- Column material	SUS	-
- Length	2 m	-
- Outer diameter	4 mm	-
- Inner diameter	3 mm	-
- Mesh range	60/80	60/80
- Maximum temperature	350 °C	80 °C
Carrier gas	He (99.999%)	H <sub>2</sub> (99.999%)
Carrier gas flow	40 cc/min	-
Column gas	He (99.999%)	Air, H <sub>2</sub>
Column gas flow	40 cc/min	-
Column temperature		
- initial (°C)	60	70
- final (°C)	60	70
Injector temperature (°C)	100	100
Detector temperature (°C)	100	150
Current (mA)	80	-
Analysed gas	Ar, CO, H <sub>2</sub>	Hydrocarbon C <sub>1</sub> -C <sub>4</sub>

### 4.3.3 Procedures

1. Using 0.05 g of catalyst packed in the middle of the stainless steel microreactor, which is located in the electrical furnace.

2. A flow rate of Ar = 8 CC/min, 9% CO in H<sub>2</sub> = 22 CC/min and H<sub>2</sub> = 50 CC/min in a fixed-bed flow reactor. A relatively high H<sub>2</sub>/CO ratio was used to minimize deactivation due to carbon deposition during reaction.

3. The catalyst sample was re-reduce *in situ* in flowing H<sub>2</sub> at 350 °C for 3 h prior to CO hydrogenation.

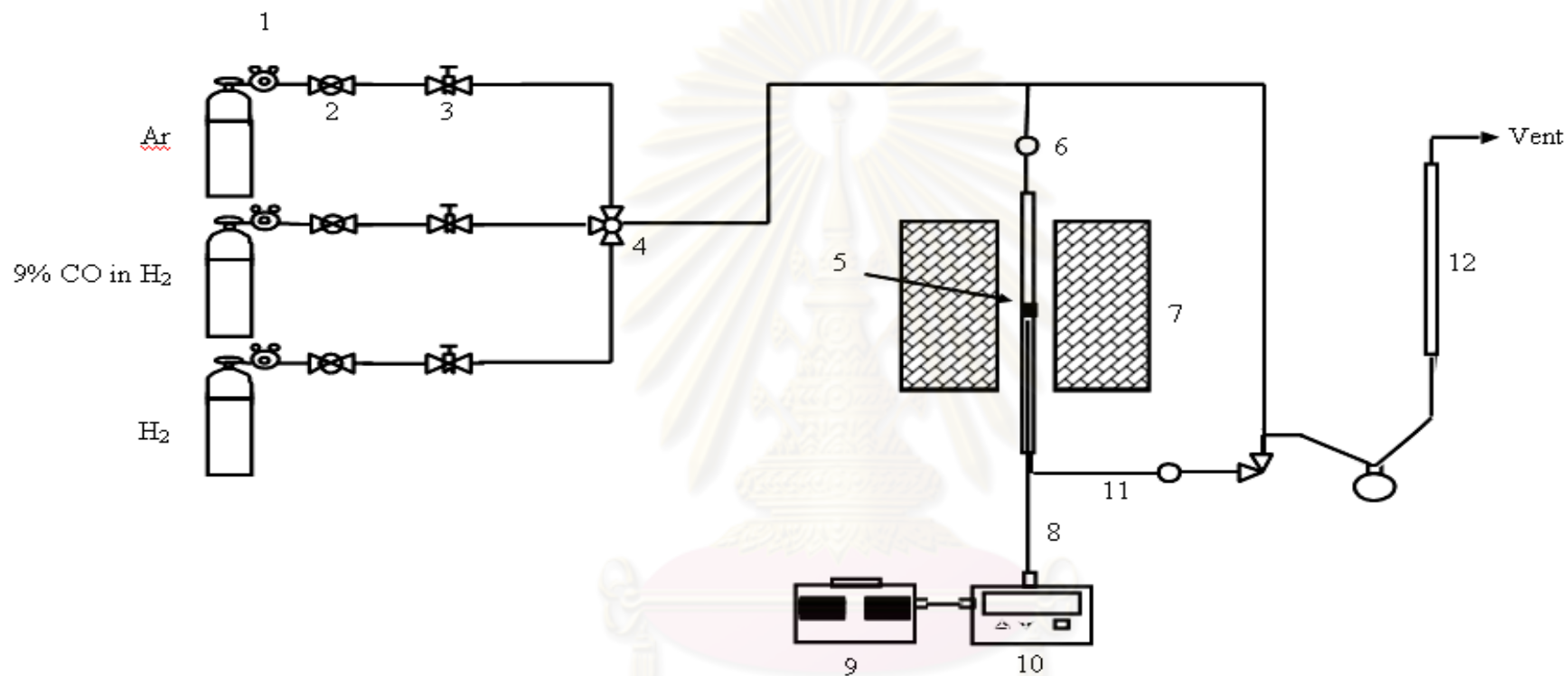
4. CO hydrogenation was carried out at 220 °C and 1 atm total pressure in flowing 9% CO in H<sub>2</sub>.

5. The effluent was analyzed using gas chromatography technique. [Thermal conductivity detector (TDC) was used for separation of carbon monoxide (CO) and methane (CH<sub>4</sub>) and flame ionization detector (FID) were used for separation of light hydrocarbon such as methane (CH<sub>4</sub>), ethane (C<sub>2</sub>H<sub>6</sub>), propane (C<sub>3</sub>H<sub>8</sub>), etc.] In all cases, steady-state was reached within 6 h.



ศูนย์วิจัยทรัพยากร  
จุฬาลงกรณ์มหาวิทยาลัย



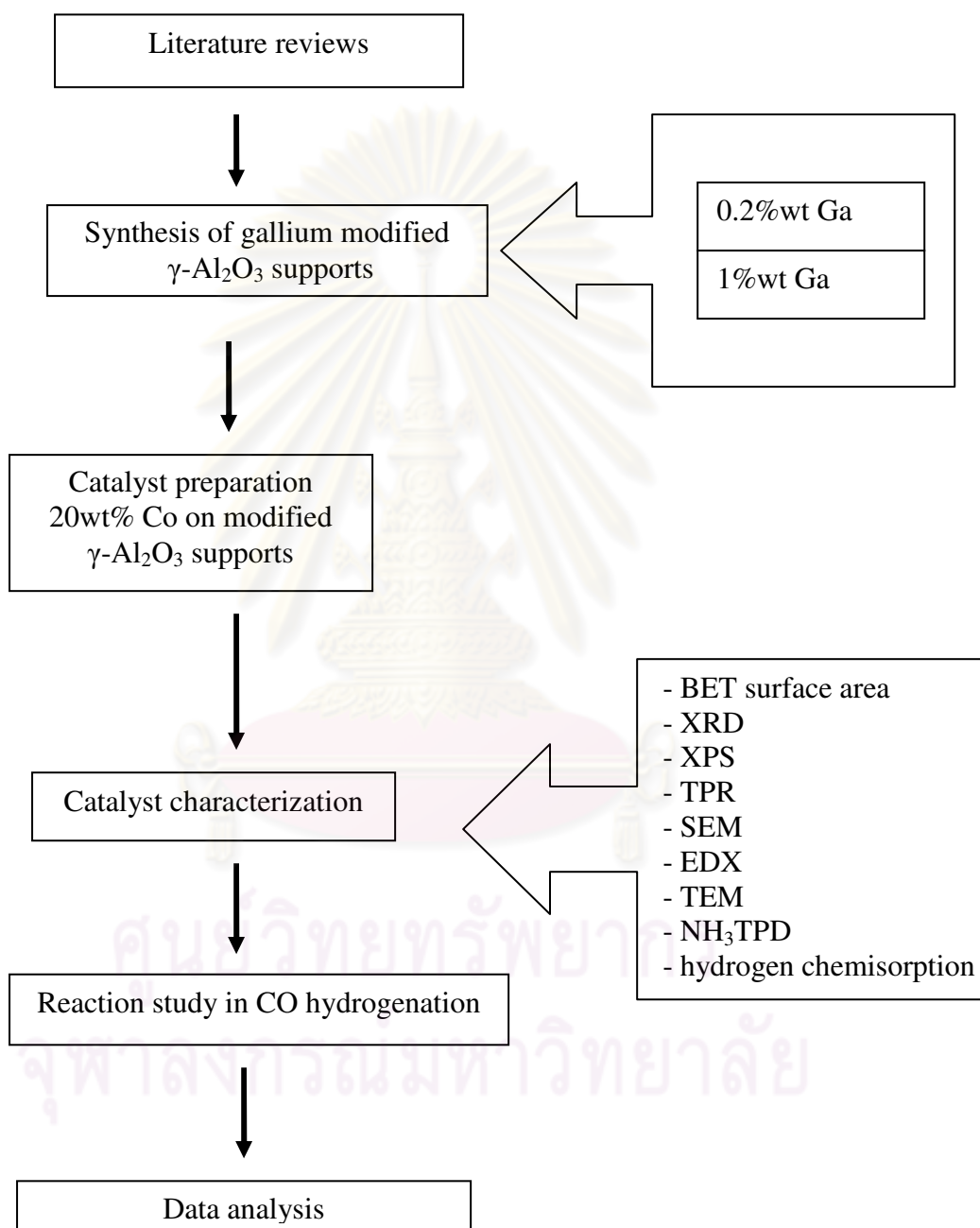


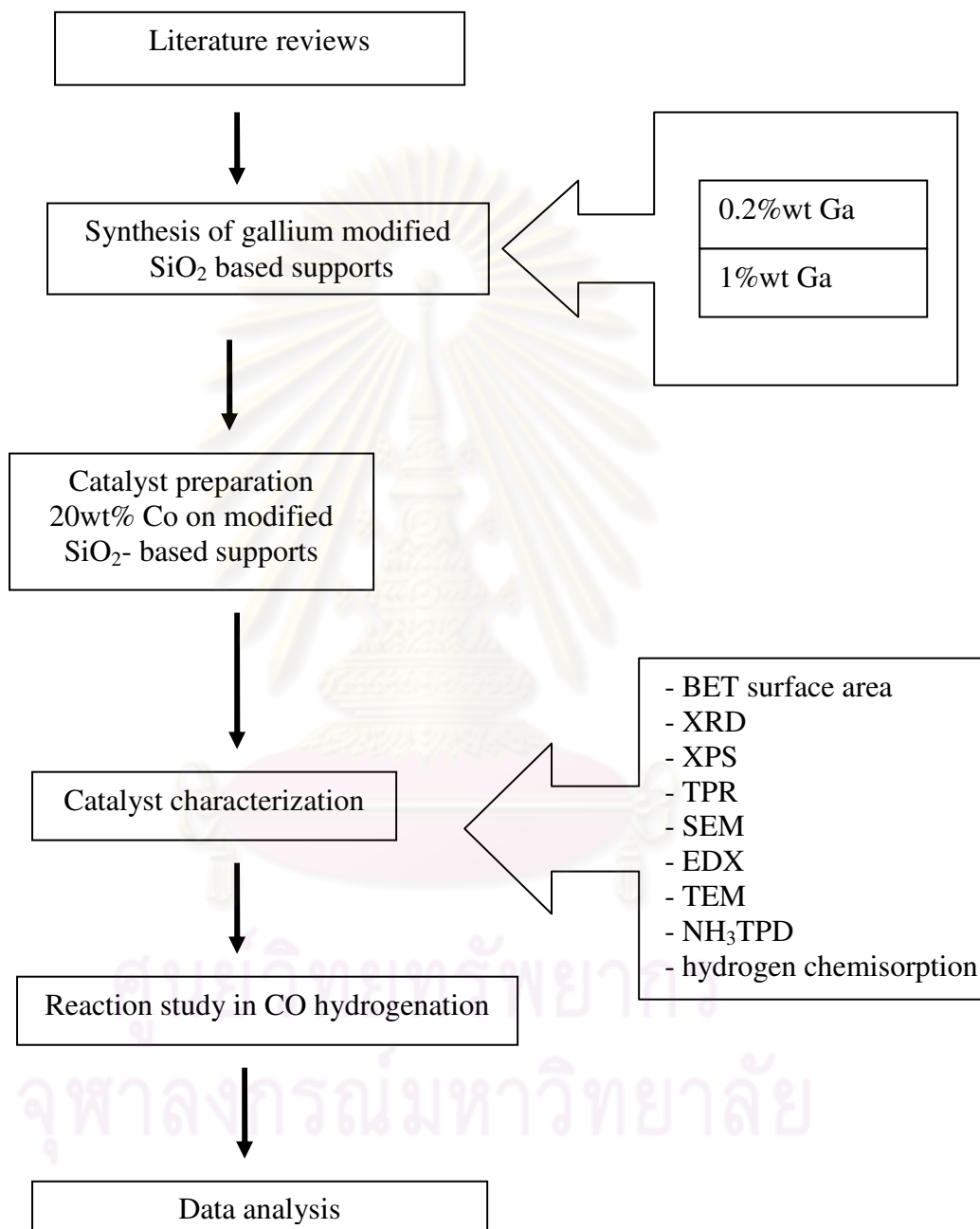
- |                                 |                            |                   |                       |
|---------------------------------|----------------------------|-------------------|-----------------------|
| 1. Pressure Regulator           | 2. On-Off Valve            | 3. Metering Valve | 4. 3-way Valve        |
| 5. Catalyst Bed                 | 6. Sampling point          | 7. Furnace        | 8. Thermocouple       |
| 9. Variable Voltage Transformer | 10. Temperature Controller | 11. Heating Line  | 12. Bubble Flow Meter |

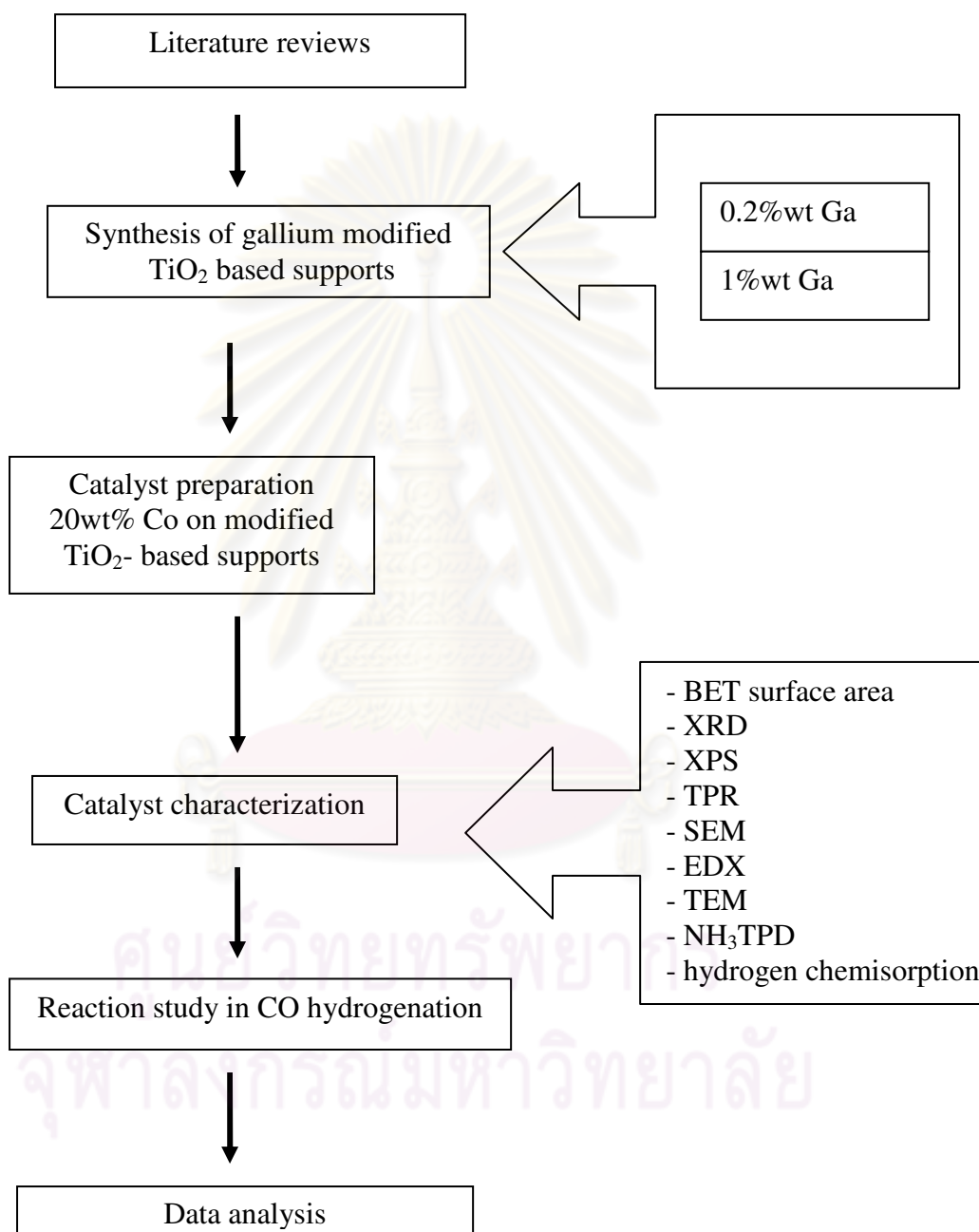
**Figure 4.1** Flow diagram of CO hydrogenation system

## RESEARCH METHODOLOGY

### Part I : Effect of Ga-modified $\gamma$ -Al<sub>2</sub>O<sub>3</sub> supports



**Part II : Effect of Ga-modified SiO<sub>2</sub> supports**

**Part III : Effect of Ga-modified TiO<sub>2</sub> supports**

## CHAPTER V

### RESULTS AND DISCUSSION

This thesis investigated effect of Ga-modified  $\text{Al}_2\text{O}_3$ ,  $\text{TiO}_2$  and  $\text{SiO}_2$  supports on characteristics and catalytic properties of supported cobalt catalyst during CO hydrogenation. In this chapter, the experimental results and discussions are described. First section described characteristics of Ga-modified  $\text{Al}_2\text{O}_3$  and  $\text{SiO}_2$ -supported Co catalysts. Second section described reduction behavior of Ga-modified  $\text{Al}_2\text{O}_3$  and  $\text{SiO}_2$ -supported Co catalysts and the last section determined catalytic activity for CO-hydrogenation over of Ga-modified  $\text{Al}_2\text{O}_3$  and  $\text{SiO}_2$ -supported Co catalysts. For Ga-modified  $\text{TiO}_2$  support Co catalysts, the results and discussions are divided in appendix A.

#### 5.1 Characteristics of Ga-modified $\text{Al}_2\text{O}_3$ and $\text{SiO}_2$ -supported Co catalyst.

##### 5.1.1 X-ray diffraction (XRD)

X-ray diffraction is used to reveal material structures because of its qualitative and nondestructive analysis. The phase identification is carried out on the basis of data from X-ray diffraction. A 20% wt of cobalt was impregnated onto Ga-modified and unmodified  $\text{Al}_2\text{O}_3$  and  $\text{SiO}_2$  supports. After calcination in air at 500 °C for 4 h, all catalysts were tested by XRD. XRD patterns for the calcined Co catalysts (with and without Ga modification) on  $\text{Al}_2\text{O}_3$  and  $\text{SiO}_2$  supports are shown in Figure 5.1. They exhibited almost identical XRD patterns. The XRD peaks of  $\text{Co}_3\text{O}_4$  were observed at 31°, 37°, 45°, 59°, and 65° (S. Rojanapipatkul and B. Jongsomjit, 2008). However, XRD peaks of  $\text{Ga}_2\text{O}_3$  were not observed in all catalyst samples. This indicated that Ga was present in a highly dispersed form.

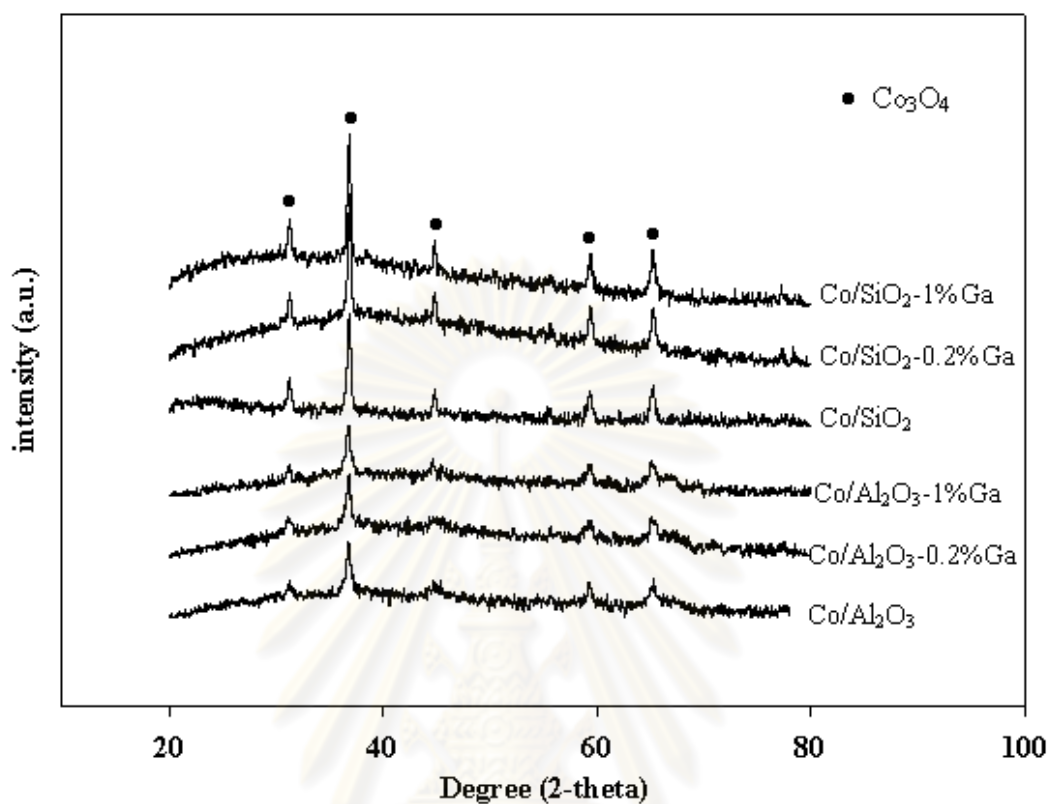


**Figure 5.1** XRD patterns for the Ga-modified and unmodified  $\text{Al}_2\text{O}_3$  and  $\text{SiO}_2$  supported cobalt catalysts.

As known, the width at half maximum of the most intense  $\text{Co}_3\text{O}_4$  peak,  $2\theta = 36.9^\circ$ , was used to calculate the  $\text{Co}_3\text{O}_4$  crystallite size. The  $\text{Co}_3\text{O}_4$  crystallite size calculated for all catalysts from the Scherrer equation are shown in Table 5.1. The crystallite size of  $\text{Co}_3\text{O}_4$  slightly increased with increased %Ga loading on  $\text{Al}_2\text{O}_3$ , but slightly decreased with increased %Ga loading on the  $\text{SiO}_2$  support.

**Table 5.1** Crystallite size of  $\text{Co}_3\text{O}_4$  from XRD of Ga-modified and unmodified  $\text{Al}_2\text{O}_3$  and  $\text{SiO}_2$  supported cobalt catalysts.

Samples	Co <sub>3</sub> O <sub>4</sub> crystallite size
	(nm) <sup>a</sup>
Co/ $\text{Al}_2\text{O}_3$	5.7
Co/ $\text{Al}_2\text{O}_3$ -0.2%Ga	7.9
Co/ $\text{Al}_2\text{O}_3$ -1%Ga	9.8
Co/ $\text{SiO}_2$	25.7
Co/ $\text{SiO}_2$ -0.2%Ga	22.5
Co/ $\text{SiO}_2$ -1%Ga	20.9

<sup>a</sup> from Scherrer's equation

### 5.1.2 N<sub>2</sub> physisorption

The BET surface area, pore size and pore volume measurement of catalysts on Ga-modified and unmodified  $\text{Al}_2\text{O}_3$  and  $\text{SiO}_2$ -supported cobalt catalyst are also shown in Table 5.2. From the result, it observed that the surface areas of the  $\text{Al}_2\text{O}_3$  supports were larger than those of  $\text{SiO}_2$  supports. This was in accordance with the smaller pore sizes of  $\text{Al}_2\text{O}_3$  than those of  $\text{SiO}_2$ . It was found that the modification of Ga on both  $\text{Al}_2\text{O}_3$  and  $\text{SiO}_2$  supports did not significantly affect the surface areas, pore size and pore volume of samples.

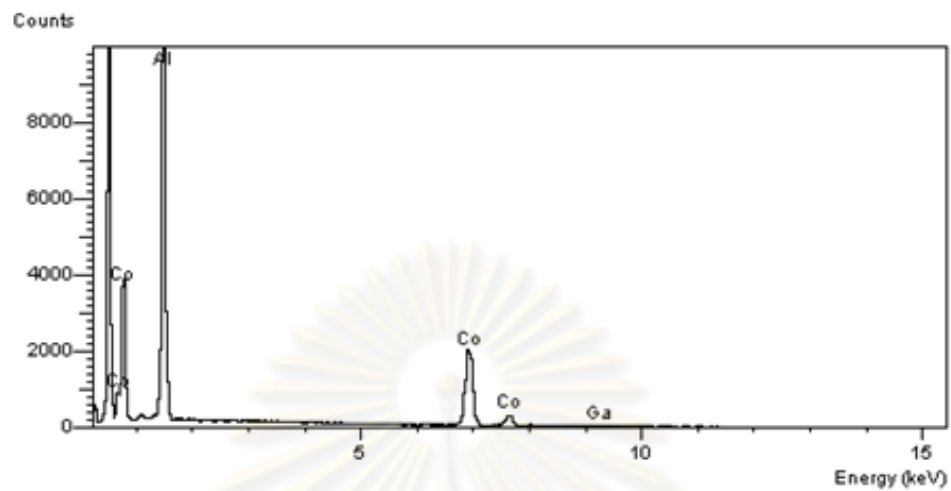
**Table 5.2** BET surface area, pore volume and pore size of Ga-modified and unmodified Al<sub>2</sub>O<sub>3</sub> and SiO<sub>2</sub> supported cobalt catalysts.

Samples	BET surface area (m <sup>2</sup> /g)	Pore size (Å)	Pore volume (cm <sup>3</sup> /g)
Co/Al <sub>2</sub> O <sub>3</sub>	111	36	0.1551
Co/Al <sub>2</sub> O <sub>3</sub> -0.2%Ga	108	37	0.1561
Co/Al <sub>2</sub> O <sub>3</sub> -1%Ga	109	36	0.1529
Co/SiO <sub>2</sub>	46	129	0.1643
Co/ SiO <sub>2</sub> -0.2%Ga	45	130	0.1481
Co/SiO <sub>2</sub> -1%Ga	47	105	0.1394

### 5.1.3 Scanning electron microscopy (SEM) and Energy dispersive X-ray spectroscopy (EDX)

The typical measurement curve for the quantitative analysis of Co/Al<sub>2</sub>O<sub>3</sub>-1%Ga and Co/SiO<sub>2</sub>-1%Ga using EDX measurement is shown in Figures 5.2 and 5.3, respectively. The amounts of elements in the various catalysts are also listed below. It can be seen that the amounts of elements in various supports varied due to the adsorption ability of each support. Results revealed that Co/Al<sub>2</sub>O<sub>3</sub>-1%Ga exhibited higher the amount of Co than Co/SiO<sub>2</sub>-1%Ga with regards to at the external surface. In addition, it was found Ga can be detected only on Al<sub>2</sub>O<sub>3</sub> support, but could not be observed on SiO<sub>2</sub>. This was probably due to Ga was dispersed more on the external surface.

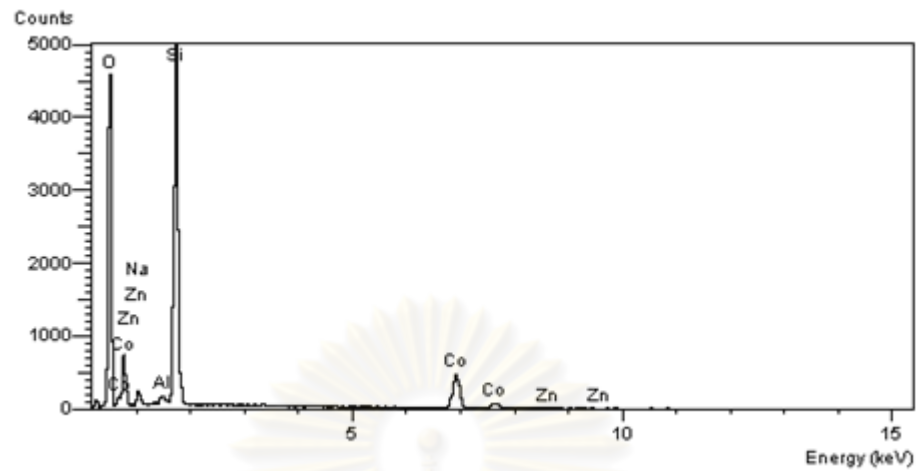




Element	Element(%)	Atomic(%)
O	57.95	75.28
Al	23.8	18.34
Co	17.32	6.11
Ga	0.92	0.28

**Figure 5.2** A typical spectrum of the Co/Al<sub>2</sub>O<sub>3</sub>-1%Ga from EDX analysis.

ศูนย์วิทยทรัพยากร  
จุฬาลงกรณ์มหาวิทยาลัย



Element	Element (%)	Atomic (%)
O	60.04	75.18
Na	2.45	2.13
Al	0.49	0.37
Si	26.12	18.63
Co	10.36	3.52
Zn	0.53	0.16

**Figure 5.3** A typical spectrum of the Co/SiO<sub>2</sub>-1%Ga from EDX analysis.

ศูนย์วิทยทรัพยากร  
จุฬาลงกรณ์มหาวิทยาลัย

Besides the content of Co and Ga in the supports, one should consider the distribution of Co and Ga in the supports. SEM and EDX were also conducted in order to study the morphologies and elemental distribution of the samples, respectively. The typical SEM micrographs along with the EDX mapping for Co/Al<sub>2</sub>O<sub>3</sub> (for Co, Al and O) and Co/SiO<sub>2</sub> (for Co, Si, and O) samples are illustrated in Figures 5.4 and 5.5 respectively. The white or light spots on the catalyst granules represent high concentrations of cobalt oxides species, where the darker areas of the granules indicate the support with no cobalt at indicating the external surface of the sample granule. It can be seen that the Co oxide species show good distribution on the surface (shown on EDX mapping) of all the samples. Apparently, SEM micrographs and EDX mapping for all samples exhibited similar trends of morphologies and elemental distributions. However for all catalyst samples with Ga modification, it can not be observed the distribution of Ga<sub>2</sub>O<sub>3</sub> or any other Ga compounds by EDX technique. This may be due only little amounts of Ga present or highly distribution of Ga as confirmed also by XRD.

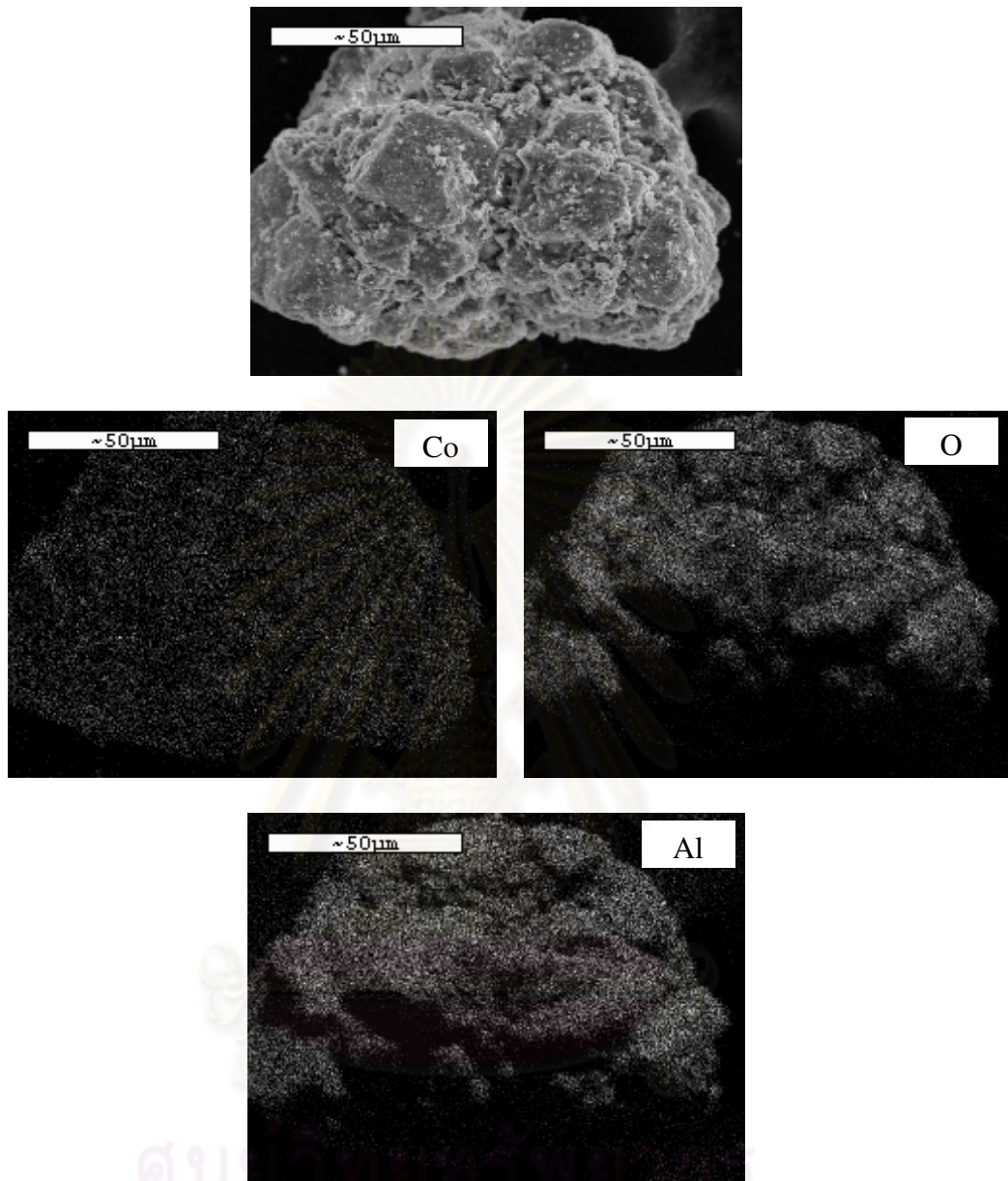


**Figure 5.4** SEM micrograph and EDX mapping of the calcined  $\text{Co}/\text{Al}_2\text{O}_3\text{-1\%Ga}$  catalysts.

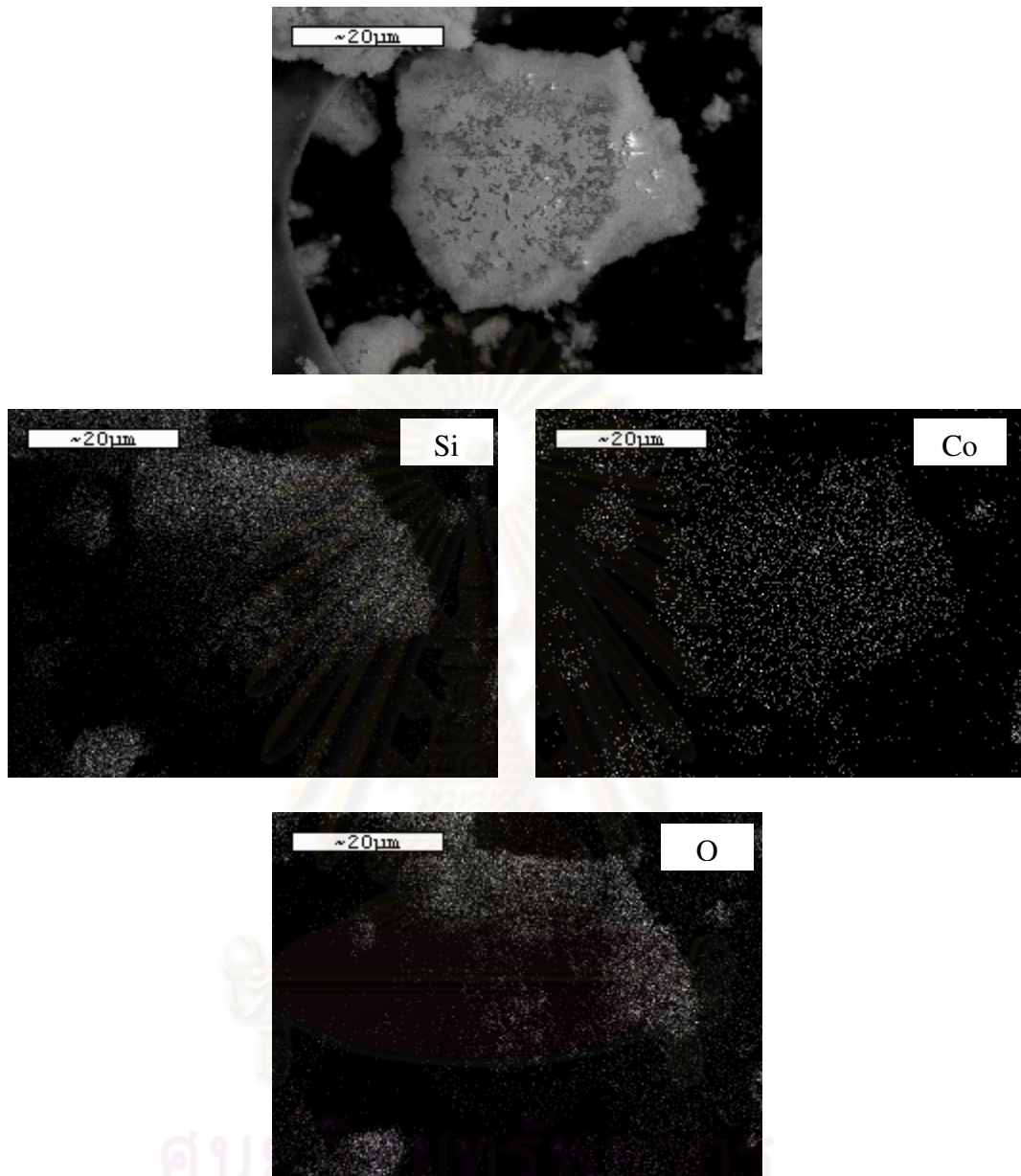


**Figure 5.5** SEM micrograph and EDX mapping of the calcined  $\text{Co/SiO}_2\text{-1\%Ga}$  catalysts.

#### 5.1.4 Transmission Electron Microscopy (TEM)

In order to determine the dispersion of cobalt oxide species and crystallite size of them, the more powerful technique, such as TEM was performed. The TEM micrographs for Co oxides species dispersed on  $\text{Al}_2\text{O}_3$  and  $\text{SiO}_2$  supports with and without Ga modification are shown in Figures 5.6 and 5.7, respectively. The dark spots represented cobalt oxide species present after calcination of samples dispersing on the support. As seen, Co oxides crystal on the  $\text{Al}_2\text{O}_3$  appeared in smaller crystal than those on  $\text{SiO}_2$ . The results were in agreement with the results obtained from XRD as shown in Table 5.1. However, considering the morphologies for the cobalt oxide species dispersed on the support, they could not differentiate between those and the supports. This was suggested that the morphologies of cobalt oxide species were essentially similar with those of the various supports indicating the more uniform of cobalt oxide species on the supports.

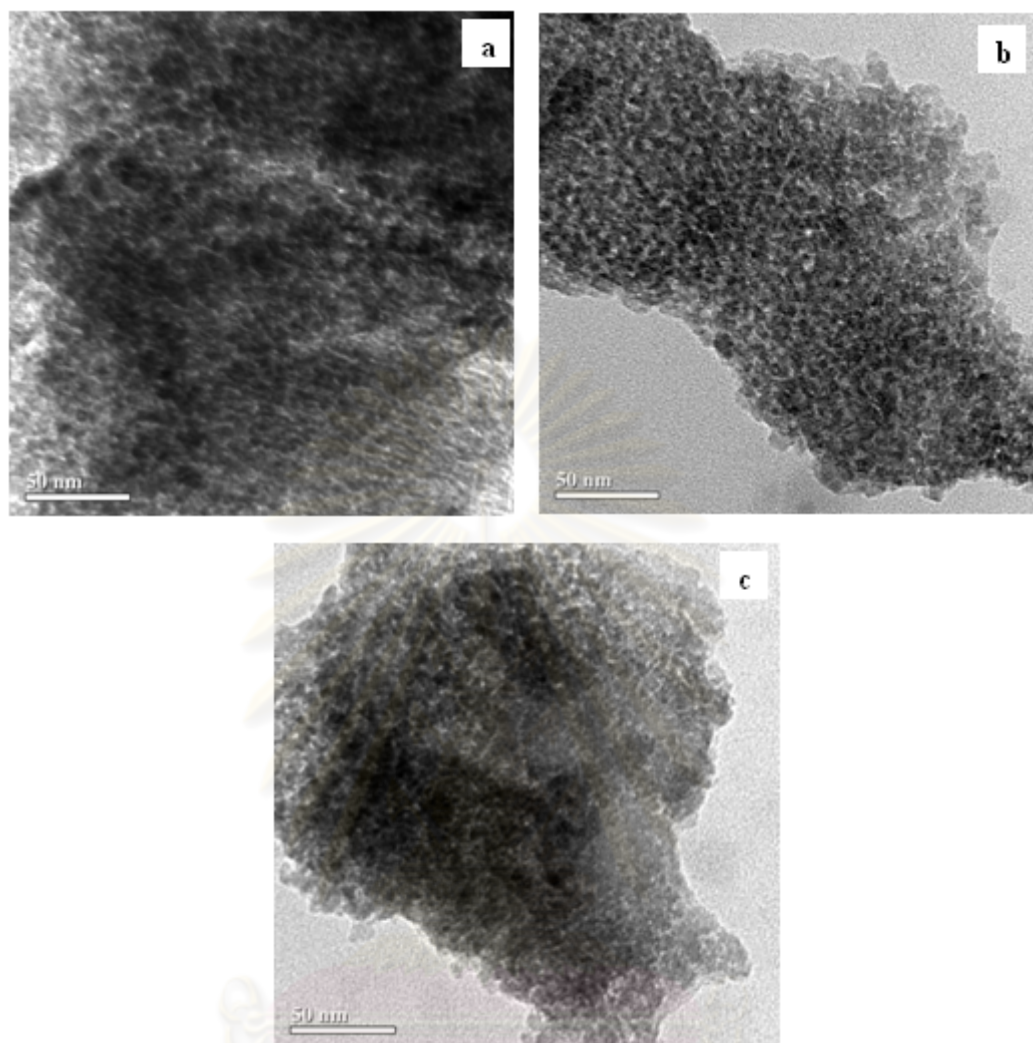


**Figure 5.6** TEM micrograph of Co supported on Ga-modified and unmodified Al<sub>2</sub>O<sub>3</sub> supported cobalt catalysts; a) Co/Al<sub>2</sub>O<sub>3</sub>, b) Co/Al<sub>2</sub>O<sub>3</sub>-0.2%Ga and c) Co/Al<sub>2</sub>O<sub>3</sub>-1%Ga.

จุฬาลงกรณ์มหาวิทยาลัย

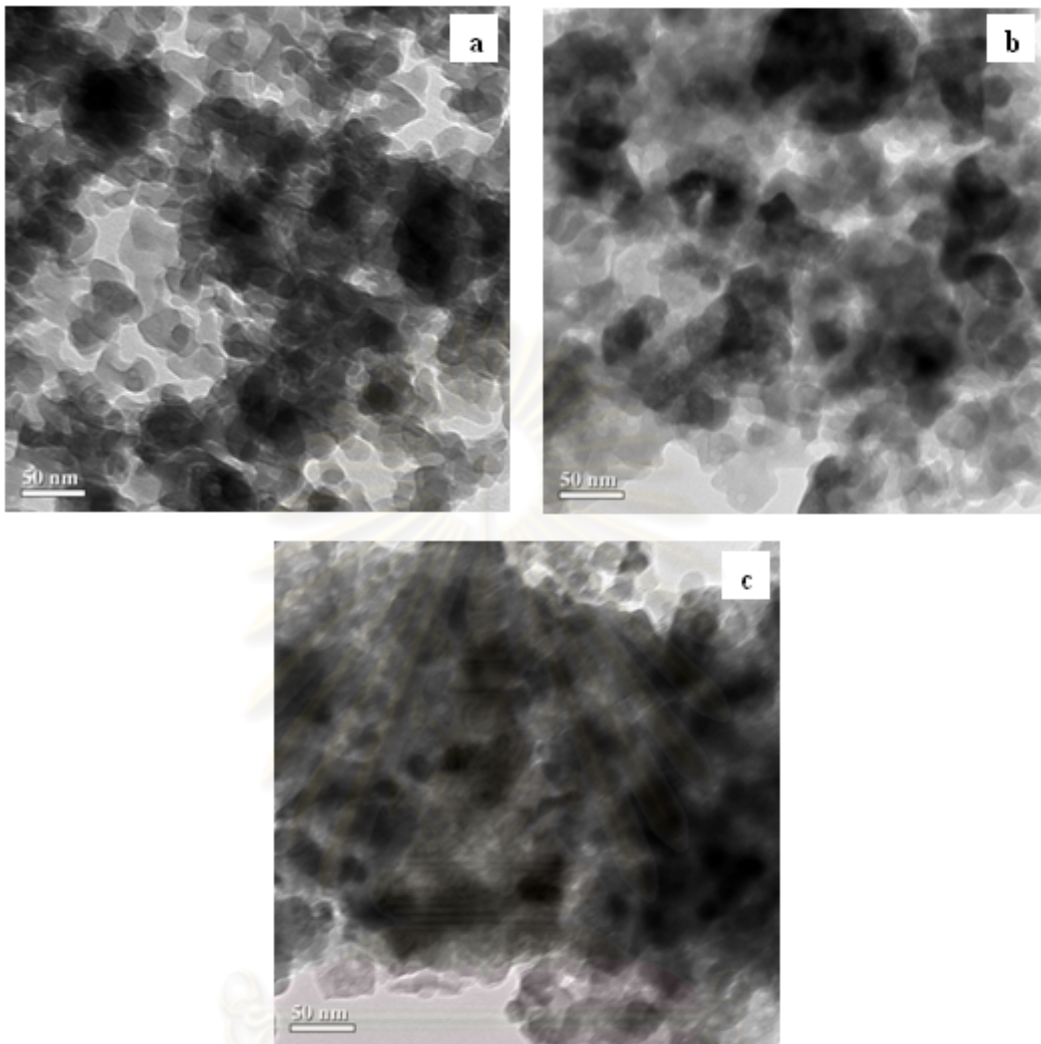


**Figure 5.7** TEM micrograph of Co supported on Ga-modified and unmodified SiO<sub>2</sub> supported cobalt catalysts; a) Co/SiO<sub>2</sub>, b) Co/SiO<sub>2</sub>-0.2%Ga and c) Co/SiO<sub>2</sub>-1%Ga.

จุฬาลงกรณ์มหาวิทยาลัย



### 5.1.5 X-ray photoelectron spectroscopy (XPS)

In order to give a better understanding on Co species present on supports, XPS was used to determine the surface compositions of the catalysts and the interaction between Ga, Co and the supports, which may result in shifts in binding energy. The deconvolution of XPS spectra of Co 2p and Ga 2p on Al<sub>2</sub>O<sub>3</sub> are shown in Figure 5.8, indicating the BE of Co 2p<sub>1/2</sub> was in the range of 795.7-796.7 eV and the BE of Co 2p<sub>3/2</sub> was in the range of 780.4-781.4 eV (Y. Okamoto *et al.*, 1975). The Ga 2p<sub>3/2</sub> BE value appeared at 1107.2-1118.2 eV (T. Mathew *et al.*, 2006). For the SiO<sub>2</sub> support, the deconvolution of XPS spectra of Co 2p and Ga 2p are shown in Figure 5.9. From the result, it indicated the BE of Co 2p<sub>1/2</sub> and Co 2p<sub>3/2</sub> with in the range of 795.2-795.6 eV and 780.3-781 eV, respectively. The BE of Ga 2p<sub>3/2</sub> was in the range of 1115.6-1118.8 eV. The surface concentrations of elements on catalysts measured by XPS are also shown in Table 5.3. It can be observed that the addition of Ga, caused the Co 2p and Ga 2p peaks to shift to higher binding energy. It was found that, the surface concentrations of Ga and Co on the Al<sub>2</sub>O<sub>3</sub> supports were larger those of SiO<sub>2</sub> supports. These results were in agreement with EDX measurement.

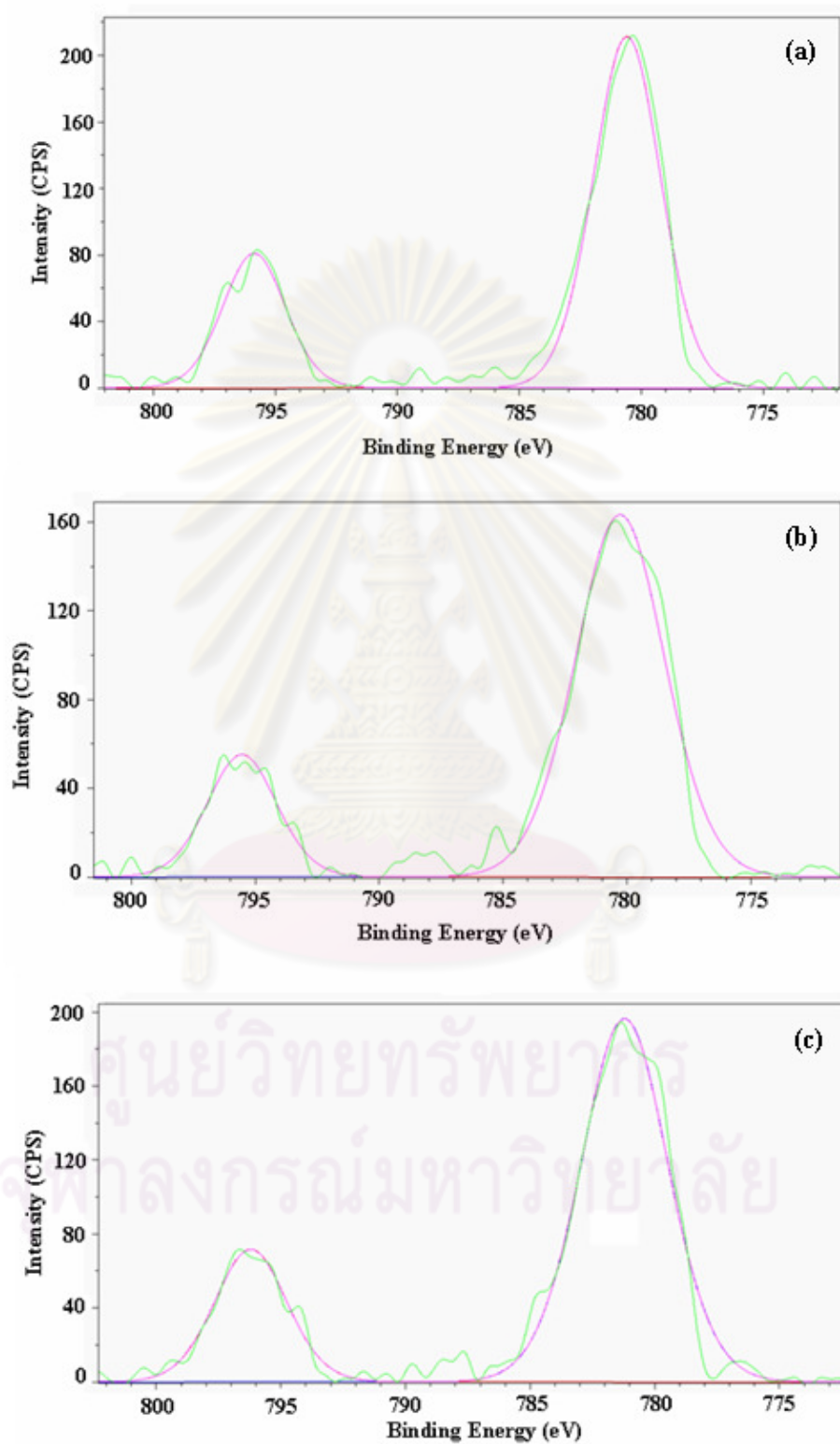


**Figure 5.8** The deconvolution of XPS spectra of Ga-modified and unmodified Al<sub>2</sub>O<sub>3</sub> supported cobalt catalysts; a) Co/Al<sub>2</sub>O<sub>3</sub>, b) Co/Al<sub>2</sub>O<sub>3</sub>-0.2%Ga and c) Co/Al<sub>2</sub>O<sub>3</sub>-1%Ga.

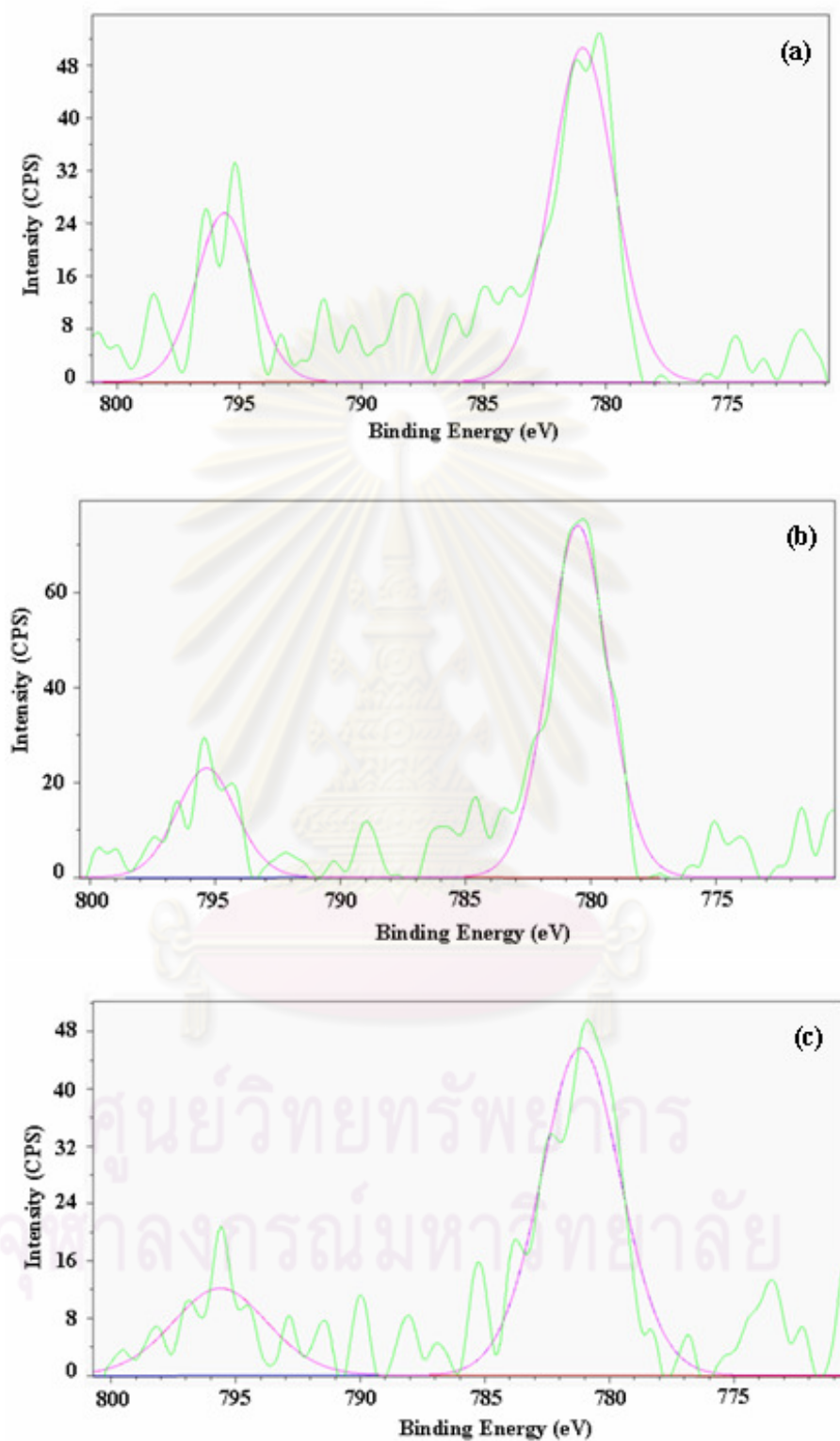


**Figure 5.9** The deconvolution of XPS spectra of Ga-modified and unmodified SiO<sub>2</sub> supported cobalt catalysts; a) Co/SiO<sub>2</sub>, b) Co/SiO<sub>2</sub>-0.2%Ga and c) Co/SiO<sub>2</sub>-1%Ga.

**Table 5.3** XPS data of Ga-modified and unmodified Al<sub>2</sub>O<sub>3</sub> and SiO<sub>2</sub> supported cobalt catalysts.

Catalysts	BE for Al 2p(eV)	BE for O 1s(eV)	BE for Si 2p(eV)	BE for Co 2p(eV)		BE for Ga 2p(eV)	Amount of element at surface(%mass)				
							Al	O	Si	Co	Ga
Co/Al <sub>2</sub> O <sub>3</sub>	75.1	531.9	-	780.4	795.7	-	28.61	51.37	-	20.01	-
Co/Al <sub>2</sub> O <sub>3</sub> -0.2%Ga	74.9	531.4	-	780.4	796.3	1107.2	41.97	43.63	-	18.99	0.11
Co/Al <sub>2</sub> O <sub>3</sub> -1%Ga	75.6	532.1	-	781.4	796.7	1118.2	26.96	50.01	-	22.02	1.02
Co/SiO <sub>2</sub>	-	532.9	103.4	780.3	795.2	-	-	53.99	43.73	2.28	-
Co/ SiO <sub>2</sub> -0.2%Ga	-	532.6	103.1	780.4	795.4	1115.6	-	52.24	44.96	2.78	0.05
Co/SiO <sub>2</sub> -1%Ga	-	532.8	103.2	781	795.6	1118.8	-	52.98	44.94	1.91	0.17

ศูนย์วิทยทรัพยากร  
จุฬาลงกรณ์มหาวิทยาลัย

### 5.1.6 NH<sub>3</sub> Temperature Programmed Desorption (NH<sub>3</sub>-TPD)

NH<sub>3</sub> temperature program desorption was a commonly used technique for the titration of surface acid sites. The strength of an acid site could be related to the corresponding desorption temperature, while the total amount of ammonia desorption after saturation coverage permits quantification of the number of acid sites at the surface (Kung *et al.*,1985). The temperature-programmed desorption profiles for the Ga-modified and unmodified Al<sub>2</sub>O<sub>3</sub> and SiO<sub>2</sub>-supported cobalt catalyst are shown in Figure 5.10. From the TPD profiles, the amounts of acid sites which are also listed in Table 5.4 were calculated from the area below curve.

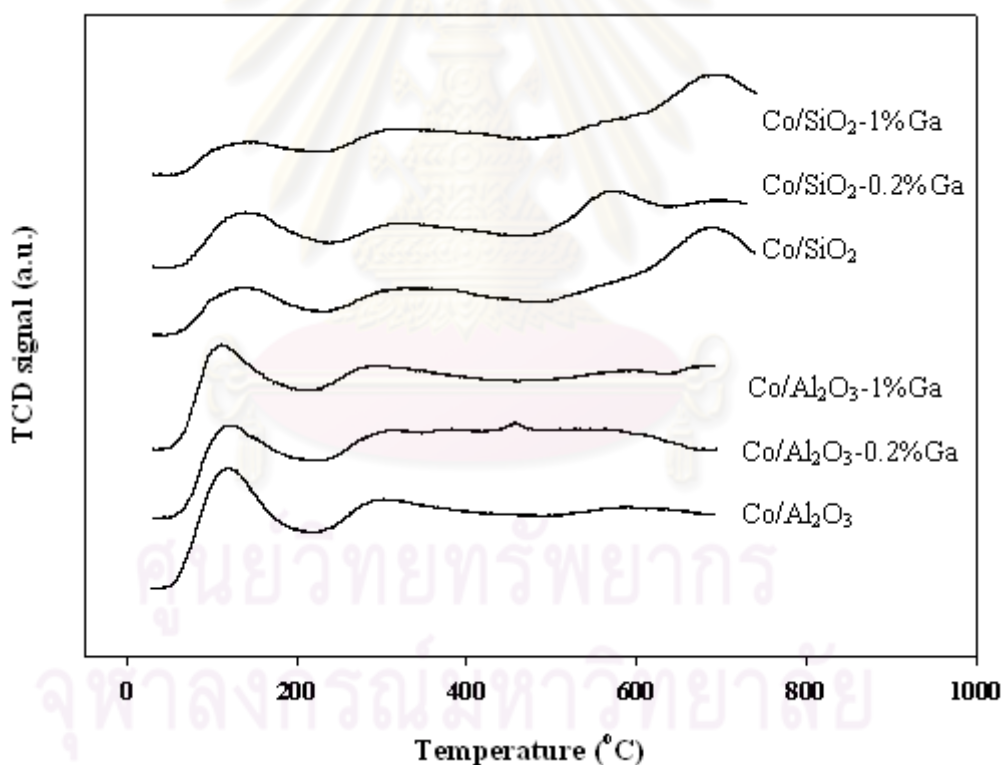


**Figure 5.10** NH<sub>3</sub>-TPD profiles of Ga-modified and unmodified Al<sub>2</sub>O<sub>3</sub> and SiO<sub>2</sub> supported cobalt catalysts.

**Table 5.4** Acidity of Ga-modified and unmodified Al<sub>2</sub>O<sub>3</sub> and SiO<sub>2</sub> supported cobalt catalysts.

Samples	Acid site ( $\mu\text{molH}^+/\text{g}$ )
Co/Al <sub>2</sub> O <sub>3</sub>	936
Co/Al <sub>2</sub> O <sub>3</sub> -0.2%Ga	892
Co/Al <sub>2</sub> O <sub>3</sub> -1%Ga	907
Co/SiO <sub>2</sub>	593
Co/ SiO <sub>2</sub> -0.2%Ga	589
Co/SiO <sub>2</sub> -1%Ga	624

The strength of an acid site could be related to the corresponding desorption temperature. From the result, it was found the Co/Al<sub>2</sub>O<sub>3</sub> had higher the amount of acid site than that of Co/SiO<sub>2</sub>. With the addition of Ga on Al<sub>2</sub>O<sub>3</sub> support, it was observed that the amount of acid site was decreased, it was suggested that the modification of Ga on Al<sub>2</sub>O<sub>3</sub> led to a decrease in the acidity of Al<sub>2</sub>O<sub>3</sub>. The results were in good agreement with those reported by Petre *et al.*, 2002. They reported that depositing Ga<sub>2</sub>O<sub>3</sub> on acidic supports led to a decrease in the acidic character of the resulting catalysts. They also revealed that the addition of Ga on Al<sub>2</sub>O<sub>3</sub> led to a decrease in the acidity of Al<sub>2</sub>O<sub>3</sub> (Petre *et al.*, 2001; Petre *et al.*, 2002). In the case of SiO<sub>2</sub> support, the amount of acid site slightly decreased with the addition of Ga 0.2%wt, but increased with Ga 1%wt addition in comparison with unmodified SiO<sub>2</sub>. Petre *et al.*, 2001 have shown that addition of Ga on SiO<sub>2</sub> led to increased in the acidic character of the resulting catalysts in comparison with the gallium-free catalyst.

### 5.1.7 Hydrogen Chemisorption

H<sub>2</sub> chemisorption was performed in order to measure the number of reduced cobalt metal surface atoms, which is related to the overall activity during CO hydrogenation. The resulted H<sub>2</sub> chemisorption is illustrated in Table 5.5.

**Table 5.5** Results of H<sub>2</sub> chemisorption Ga-modified and unmodified Al<sub>2</sub>O<sub>3</sub> and SiO<sub>2</sub> supported cobalt catalysts.

Samples	H <sub>2</sub> chemisorption (x10 <sup>18</sup> mol g cat <sup>-1</sup> )
Co/Al <sub>2</sub> O <sub>3</sub>	3.9
Co/Al <sub>2</sub> O <sub>3</sub> -0.2%Ga	9.7
Co/Al <sub>2</sub> O <sub>3</sub> -1%Ga	7.5
Co/SiO <sub>2</sub>	6.0
Co/SiO <sub>2</sub> -0.2%Ga	5.7
Co/SiO <sub>2</sub> -1%Ga	4.1

The amounts of H<sub>2</sub> adsorbed were in the range of 3.9 to 7.5 (x10<sup>18</sup> mol g cat<sup>-1</sup>) for Al<sub>2</sub>O<sub>3</sub>-support catalysts and 4.1 to 6.0 (x10<sup>18</sup> mol g cat<sup>-1</sup>) of SiO<sub>2</sub>-support catalysts. It revealed that the number of reduced cobalt metal surface atoms increased with Ga modification of Al<sub>2</sub>O<sub>3</sub>. In addition, the modification of 0.2 %Ga exhibited the highest number of active sites (9.7x10<sup>18</sup> mol g cat<sup>-1</sup>). On the other hand, the addition of Ga on the SiO<sub>2</sub> resulted in decreased number of reduced cobalt metal surface atoms. Since only Co metal has significant activity for CO hydrogenation, these results are consistent with H<sub>2</sub> chemisorption results. The corresponding trend of the CO hydrogenation rates and the H<sub>2</sub> chemisorption results was seen for all catalyst samples.

## 5.2 Reduction behavior of Ga-modified $\text{Al}_2\text{O}_3$ and $\text{SiO}_2$ -supported Co catalyst.

TPR was performed in order to determine the reduction behaviors. The TPR profiles of Co supported on  $\text{Al}_2\text{O}_3$  and  $\text{SiO}_2$  supports with and without Ga modification are shown in Figure 5.11.

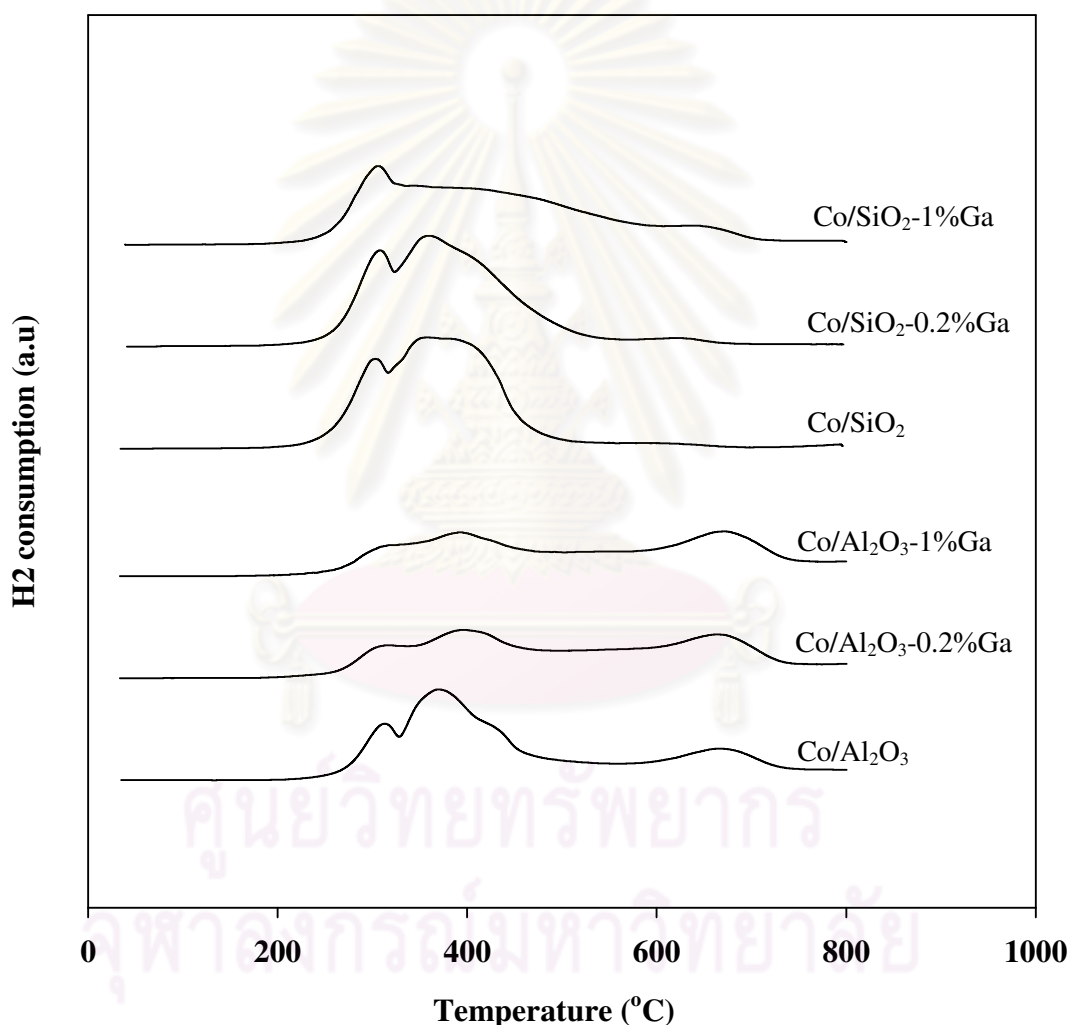


**Figure 5.11** TPR profile of Ga-modified and unmodified  $\text{Al}_2\text{O}_3$  and  $\text{SiO}_2$  supported cobalt catalysts.



The reduction temperature started at ca 200 °C and ended at ca. 800 °C. There were three major peaks for Co/Al<sub>2</sub>O<sub>3</sub> and two major peaks for Co/SiO<sub>2</sub> located at 313°C, 369°C and 665°C for Co/Al<sub>2</sub>O<sub>3</sub> and 303°C and 360°C for Co/SiO<sub>2</sub>. The first peak resulted from reduction of Co<sub>3</sub>O<sub>4</sub> to CoO, the second peak was attributed to CoO reduction into metallic cobalt and the reduction peak at high temperature (600-750°C) of Co/Al<sub>2</sub>O<sub>3</sub> was assigned to the reduction of non-stoichiometric cobalt-aluminate, which is more difficult to reduce than the reduction of Co<sub>3</sub>O<sub>4</sub> species (B. Jongsomjit., 2001). For Co/SiO<sub>2</sub>, it can be observed a broad peak at higher temperature. The TPR profile of the Al<sub>2</sub>O<sub>3</sub> and SiO<sub>2</sub> supports with Ga modification showed no reduction peak. While the addition of Ga on the Al<sub>2</sub>O<sub>3</sub>-supported Co catalyst resulted in slightly shift of the second reduction peak to higher temperature about 25°C, it indicated that the Ga modified on Al<sub>2</sub>O<sub>3</sub> support increased during reduction due to stronger interaction between cobalt and support. It was found that the modification of Ga on the Al<sub>2</sub>O<sub>3</sub> and SiO<sub>2</sub> supports apparently resulted in decreased reducibility of Co at first and second reduction peaks for Al<sub>2</sub>O<sub>3</sub> and the second reduction peak for SiO<sub>2</sub>. However, the number of reduced Co metal surface atoms can be calculated directly from the H<sub>2</sub> chemisorption results, which is more acceptable since all catalyst samples are reduced at the standard reduction condition.

### **5.3 Catalytic activity for CO-hydrogenation over Ga-modified Al<sub>2</sub>O<sub>3</sub> and SiO<sub>2</sub>-supported Co catalyst.**

In order to determine the catalytic behaviors of the Co catalysts with and without Ga modification, CO hydrogenation (H<sub>2</sub>/CO = 10/1) under methanation condition was performed to determine the overall activity and product selectivity of the samples. Hydrogenation of CO was carried out at 220 °C and 1 atm. A flow rate of H<sub>2</sub>/CO/Ar = 20/2/8 cm<sup>3</sup>/min in a fixed-bed flow reactor was used. The resulted reaction test is shown in Table 5.6.

**Table 5 .6** Reaction study of Ga-modified and unmodified Al<sub>2</sub>O<sub>3</sub> and SiO<sub>2</sub> supported cobalt catalysts.

Samples	CO conversion (%)	Rate <sup>a</sup> (x10 <sup>2</sup> gCH <sub>2</sub> /g.cat.h)		Selectivity to CH <sub>4</sub> (%)	Selectivity to C <sub>2</sub> -C <sub>4</sub> (%)
		Initial <sup>b</sup>	SS <sup>c</sup>		
Co/Al <sub>2</sub> O <sub>3</sub>	51	147	77	97	3
Co/Al <sub>2</sub> O <sub>3</sub> -0.2%Ga	90	143	135	98.9	1.1
Co/Al <sub>2</sub> O <sub>3</sub> -1%Ga	85	137	128	99.1	0.9
Co/SiO <sub>2</sub>	13	80	19	73.3	26.7
Co/ SiO <sub>2</sub> -0.2%Ga	6	19	9	70	30
Co/SiO <sub>2</sub> -1%Ga	3	14	5	66.1	33.9

<sup>a</sup> CO hydrogenation was carried out at 220 °C, 1 atm, and H<sub>2</sub>/CO/Ar = 20/2/8.

<sup>b</sup> After 5 min of reaction

<sup>c</sup> After 6 h of reaction

It indicated that the CO conversions were ranged between 51 to 90% with corresponding to the reaction rates at 77 to 138 (x10<sup>2</sup>gCH<sub>2</sub>/g.cat.h) of Co catalysts with and without Ga-modified Al<sub>2</sub>O<sub>3</sub> supports. For Co catalysts with and without Ga-modified SiO<sub>2</sub> supports, the conversions were ranged between 3 to 13% with corresponding to 5 to 19 (x10<sup>2</sup>gCH<sub>2</sub>/g.cat.h). It can be seen that the Co catalyst on Ga-modified Al<sub>2</sub>O<sub>3</sub> exhibited higher the CO conversion and reaction rate than the those of Ga-modified SiO<sub>2</sub>. It should be noted that the activities of Al<sub>2</sub>O<sub>3</sub> support were higher than those of SiO<sub>2</sub> support probably due to the higher amount of acid site on Al<sub>2</sub>O<sub>3</sub>. The results were in good agreement with those reported by Khaodee *et al.*, 2007. They reported that the catalytic performances were dependent on crystallite sizes and amount of acid–base sites. It was found that the highest catalytic activity of ZrO<sub>2</sub> appeared at the highest amount of acid sites during CO hydrogenation. Li *et al.*, 2001 have shown that the activity increased with an increase in the amount of acidic sites on the catalysts except for 35.1%Al<sub>2</sub>O<sub>3</sub>- ZrO<sub>2</sub> and Al<sub>2</sub>O<sub>3</sub> catalysts. This would suggest

that the acidic sites on the catalyst are significant for the adsorption and activation of the reactant molecular.

Based on the results, the reaction rates during methanation increased with the Ga-modified  $\text{Al}_2\text{O}_3$ . Addition of 0.2 %Ga exhibited the highest reaction rate. These results were in agreement with the results from the  $\text{H}_2$ -chemisorption as mentioned before. On contrary, the addition of Ga on  $\text{SiO}_2$  was found to decrease the reaction rate. This was basically due to decreased the number of reduced cobalt metal surface atoms with Ga modification as seen by the  $\text{H}_2$  chemisorption. Considering the selectivity of product, it was found the selectivity to methane of  $\text{Co}/\text{Al}_2\text{O}_3$  was higher than that of  $\text{Co}/\text{SiO}_2$ . On the other words, the  $\text{Co}/\text{SiO}_2$  exhibited higher amounts of long chain hydrocarbons ( $\text{C}_2\text{-C}_4$ ) than those of  $\text{Co}/\text{Al}_2\text{O}_3$ . With the addition of Ga, it showed that the selectivity to methane and  $\text{C}_2\text{-C}_4$  decreased with the Ga-modified on  $\text{Al}_2\text{O}_3$ . For  $\text{SiO}_2$ , the selectivity to methane was decreased and selectivity to  $\text{C}_2\text{-C}_4$  was increased with Ga modification. However, it was found that the Ga modification on  $\text{Al}_2\text{O}_3$  and  $\text{SiO}_2$  supports decrease the catalyst deactivation.

## CHAPTER VI

### CONCLUSIONS AND RECOMMENDATIONS

In this chapter, section 6.1 provides the conclusions obtained from the experimental results of Ga-modified  $\text{Al}_2\text{O}_3$ ,  $\text{TiO}_2$  and  $\text{SiO}_2$  supports on characteristics and catalytic properties of supported cobalt catalyst during CO hydrogenation. Additionally, recommendations for further study are given in section 6.2.

#### 6.1 Conclusions

In comparison, based on the results with regards to characteristics of  $\text{SiO}_2$  and  $\text{Al}_2\text{O}_3$ -supported cobalt catalyst, it showed that the amounts of Co obtained from EDX on the surface of  $\text{Al}_2\text{O}_3$  support were higher than those of  $\text{SiO}_2$  support. This was in agreement with the results from XPS. It was due to the pore size of  $\text{Al}_2\text{O}_3$  support was smaller than that  $\text{SiO}_2$  support. Ga modification of the  $\text{Al}_2\text{O}_3$  and  $\text{SiO}_2$  support had a significant impact on the increased number of Co active sites for  $\text{Al}_2\text{O}_3$  support, but decreased that for  $\text{SiO}_2$  support as seen by the  $\text{H}_2$  chemisorption. However, with the addition of Ga, there was no significant change in morphologies and elemental distributions of samples as seen from SEM/EDX. Based on methanation, the activity and selectivity to  $\text{CH}_4$  of  $\text{Al}_2\text{O}_3$  support was higher than that of  $\text{SiO}_2$  support. The activity was increased significantly upon Ga modification of  $\text{Al}_2\text{O}_3$ , whereas 0.2%wt of Ga exhibited the highest activity. The results were corresponding with the  $\text{H}_2$ -chemisorption, where the amounts of  $\text{H}_2$  adsorbed on the catalytic phase increased with Ga addition. On contrary, the CO conversions and reaction rates decreased with Ga addition on  $\text{SiO}_2$ . This was basically due to Ga-modified  $\text{SiO}_2$  support resulted in decreased Co reducibility and the number of Co sites active as seen by the  $\text{H}_2$  chemisorption and TPR results. However, Ga modification on  $\text{Al}_2\text{O}_3$  and  $\text{SiO}_2$  supports decrease the catalyst deactivation. In addition, the chain growth probability ( $\text{C}_2\text{--C}_4$ ) of catalyst from  $\text{SiO}_2$  was higher than that from  $\text{Al}_2\text{O}_3$ .

## 6.2 Recommendations

1. The effect of Ga modification of  $\text{TiO}_2$  without poison should be further studied.
2. The effect of acid site for carbon monoxide hydrogenation catalysts should be further investigated.
3. Besides  $\text{Al}_2\text{O}_3$ ,  $\text{SiO}_2$  and  $\text{TiO}_2$  supports, other supports such as  $\text{ZrO}_2$ , MCM-41 and etc should be further investigated with Ga modification.
4. Besides Co metal, other metals such as Ni, Pd and etc should be further investigated with Ga-modification on the supports.



ศูนย์วิจัยทรัพยากร  
จุฬาลงกรณ์มหาวิทยาลัย

## REFERENCES

- Ali, S.; Chen, B.; and Goodwin, Jr., J. G. Zr Promotion of Co/SiO<sub>2</sub> for Fischer-Tropsch Synthesis. J. Catal. 157 (1995): 35-41.
- Arean, C.O.; Mentrui, M.P.; Platero, E.E.; Xamena, F.X.L.I.; and Parra, J. B. Sol-gel method for preparing high surface area CoAl<sub>2</sub>O<sub>4</sub> and Al<sub>2</sub>O<sub>3</sub>-CoAl<sub>2</sub>O<sub>4</sub> spinels. Mater. Lett. 39 (1999): 22-27.
- Bacon, G.E. and Roberts, F.F. Neutron-diffraction studies of magnesium ferritealuminate powders. Acta. Cryst. 6 (1953): 57-62.
- Cho, W.S., and Kakihana, M. Crystallization of ceramic pigment CoAl<sub>2</sub>O<sub>4</sub> anocrystals from Co-Al metal organic precursor. J. Alloy. Compd. 287 (1999): 87-90.
- Chokkaram, S.; Srinivasan, R.; and Milburn, D. R. Conversion of 2-octanol overnickel-alumina, cobalt-alumina, and alumina catalysts. J. Mol. Catal. A-Chem. 121 (1997): 157-169.
- Das, T. K.; Jacobs, Patterson, G.; P. M.; Conner, W. A.; Li, J.; Davis, B. H. Fischer-Tropsch synthesis: characterization and catalytic properties of rhenium promoted cobalt alumina catalysts. Fuel 82 (2003): 805-815.
- Dominguez, F.; S´anchez, J.; Arteaga, G.; Choren, E. Gallia as support of Pt in benzene hydrogenation reaction. J. Mol. Catal. A-Chem. 228 (2005): 319-324.
- Edelstein, A., and Cammarata, R.C. Synthesis, Properties and Applications, Nanomaterials. Institute of physics Publishing, Bristol and Philadelphia, 1996.
- Evans, K.A.; 1993. Properties and uses of oxides and hydroxides. Downs, A. J.; Chemistry of aluminium gallium indium and thallium. 248. 1st ed. :Blackie Academic and Professional.
- Farrauto, R.J. and Bartholomew, C.H. Fundamentals of industrial catalytic processes. 1 st ed. London: Chapman & Hall, 1997.
- Feller, A.; Claeys, M.; and Steen, E. V. Cobalt Cluster Effects in Zirconium Promoted Co/SiO<sub>2</sub> Fischer-Tropsch Catalysts. J. Catal. 185 (1999): 120- 130.
- Fierro, J. L. G.; 2006. Metal Oxides: Chemistry and Applications. CRC Press : Taylor & Francis Group.
- Haddad, G. J.; Chen, B.; and Goodwin, Jr., J. G. Characterization of La<sup>3+</sup>-Promoted Co/SiO<sub>2</sub> Catalysts. J. Catal. 160(1996): 43-51.

- Haneda, M.; Joubert, E.; Menezo, J.; Duprez, D.; Barbier, J.; Bion, N.; Daturi, M.; Saussey, J.; Lavalley, J.; Hamada, H. Surface characterization of alumina-supported catalysts prepared by solgel method: Part I. Acid-base properties. Phys. Chem. Chem. Phys. 3 (2001): 1366-1370.
- Iglesia, E. Design, synthesis, and use of cobalt-based Fischer-Tropsch synthesis catalysts. Appl. Catal. A. 161 (1997): 59-78.
- Jacobs, G.; Das, T. K.; Zhang, Y.; Li, J.; Racoillet, G.; Davis, B. H. Fischer-Tropsch synthesis: support, loading, and promoter effects on the reducibility of cobalt catalysts. Appl. Catal. A. 233 (2002): 263-281.
- Jongsomjit, B.; Panpranot, J., and Goodwin, Jr., J.G. Co-support compound formation in alumina-supported cobalt catalysts. J. Catal. 204 (2001): 98-109.
- Jongsomjit, B.; Panpranot, J.; and Goodwin, Jr., J. G. Effect of zirconia-modified alumina on the properties of Co/ $\gamma$ -Al<sub>2</sub>O<sub>3</sub> catalysts. J. Catal. 215(2003): 66-77.
- Li, J., and Coville, N. J. The effect of boron on the catalyst reducibility and activity of Co/TiO<sub>2</sub> Fischer-Tropsch catalysts. Appl. Catal. A. 181 (1999): 201-208.
- Li, J.; Jacobs, G.; Das, T.; and Davis, B. H. Fischer-Tropsch synthesis: effect of water on the catalytic properties of a ruthenium promoted Co/TiO<sub>2</sub> catalyst. Appl. Catal. A. 233 (2002): 255-262.
- Li, X.; Asami, K.; Luo, M.; Michiki, K.; Tsubaki, N.; Fujimoto, K. Direct synthesis of middle iso-paraffins from synthesis gas. Catal. Today 84 (2003): 59-65.
- Li, Y.; He, D.; Yuan, Y.; Cheng, Z.; Zhu, Q. Selective formation of isobutene from CO hydrogenation over zirconium dioxide based catalysts. Energy Fuels 15 (2001): 1434-1440.
- Khaodee, W.; Jongsomjit, B.; Assabumrungrat, S.; Preserthdam, P.; Goto, S. Investigation of isosynthesis via CO hydrogenation over ZrO<sub>2</sub> and CeO<sub>2</sub> catalysts: Effects of crystallite size, phase composition and acid-base sites. Catal. Com. 8 (2007): 548-556.
- Kraum, M., and Baerns, M. Fischer-Tropsch synthesis: the influence of various cobalt compounds applied in the preparation of supported cobalt catalysts on their performance. Appl. Catal. A. 186 (1999): 189-200.
- Kung, M. C. and Kung, H. H. IR studies of NH<sub>3</sub>, Pyridine, CO, and NO adsorbed on transition metal oxides. Catal. Rev. Sci. Eng. 27 (1985): 425-460.

- Mathew, T.; Yamada, Y.; Ueda, A.; Shioyama, H.; Kobayashi, T. Metal oxide catalysts for DME steam reforming:  $\text{Ga}_2\text{O}_3$  and  $\text{Ga}_2\text{O}_3\text{-Al}_2\text{O}_3$  catalysts with and without copper. Appl. Catal. A 286 (2005): 11–22.
- Mathew, T.; Yamada, Y.; Ueda, A.; Shioyama, H.; Kobayashi, T.; Gopinath, C. S. Effect of support on the activity of  $\text{Ga}_2\text{O}_3$  species for steam reforming of dimethyl ether. Appl. Catal. A, 300 (2006): 58-66.
- Maunula, T.; Kintaichi, Y.; Haneda, M.; Hamada, H. Preparation and reaction mechanistic characterization of sol–gel indium/alumina catalysts developed for  $\text{NO}_x$  reduction by propene in lean conditions. Catal. Lett. 61 (1999): 121-130.
- Mimani, T. Instant synthesis of nanoscale spinel aluminates. J. Alloy. Compd. 315 (2001): 123-128.
- Okamoto, Y.; Nakano, H.; Imanaka, T.; Teranishi, S. X-ray photoelectron spectroscopic Studies of catalysts supported cobalt catalysts. Bulletin of the chemical society of Japan 48 (1975): 1163-1168.
- Othmer, K. Encyclopedia of chemical technology. Vol 6. 4<sup>th</sup> ed. New york: A Wiley Interscience Publication, John Wiley&Son, 1991.
- Panpranot, J.; Goodwin, Jr, J. G.; and Sayari, A. CO Hydrogenation on Ru-Promoted Co/MCM-41 Catalysts. J. Catal. 211 (2002): 530–539.
- Petre, A. L.; Auroux, A.; Gervasini, A.; Caldararu, M.; Ionescu, N. I. Calorimetric characterization of surface reactivity of supported  $\text{Ga}_2\text{O}_3$  catalyst. J. Therm. Anal. Calorim. 64 (2001): 253-260.
- Petre, A.L.; Perdigon-Melon, J.A.; Gervasini, A.; Auroux, A. Acid-base properties of alumina-supported  $\text{M}_2\text{O}_3$  (M=B, Ga, In) Catalysts. Top. Catal. 19 (2002): 271-281.
- Pradyot Patnaik, Ph.D. Handbook of inorganic chemicals. New York: McGraw-Hill, 2002.
- Riva, R.; Miessner, H.; Vitali, R.; Piero, G. D. Metal–support interaction in Co/ $\text{SiO}_2$  and Co/ $\text{TiO}_2$ . Appl. Catal. A, 196 (2000): 111–123.
- Rohr, F.; Lindvag, O.A.; Holmen, A.; Blekkan, E.A. Fischer–Tropsch synthesis over cobalt catalysts supported on zirconia-modified alumina. Catal. Today, 58 (2000): 247–254.



- Rojanapipatkul, S., and Jongsomjit, B. Synthesis of cobalt on cobalt-aluminate via solvothermal method and its catalytic properties for carbon monoxide hydrogenation. *Catal. Com.* 10 (2008): 232-236.
- Schanke, D.; Vada, S.; Blekkan, E. A.; Hilmen, A. M.; Hoff, A.; Holmen, A. Study of Pt-promoted cobalt CO hydrogenation catalysts. *J. Catal.* 156 (1995): 85-95.
- Shimizu, K.; Satsuma, A.; and Hattori, T. Selective catalytic reduction of NO by hydrocarbons on Ga<sub>2</sub>O<sub>3</sub>/Al<sub>2</sub>O<sub>3</sub> catalysts. *Appl. Catal. B.* 16 (1998): 319-326.
- Sun, S.; Tsubaki, N.; and Fujimoto, K. The reaction performances and characterization of Fischer–Tropsch synthesis Co/SiO<sub>2</sub> catalysts prepared from mixed cobalt salts. *Appl. Catal. A.* 202 (2000): 121–131.
- Takahashi, M.; Inoue, N.; Nakatani, T.; Takeguchi, T.; Iwamoto, S.; Watanabe, T.; Inoue, M. Selective catalytic reduction of NO with methane on  $\gamma$ -Ga<sub>2</sub>O<sub>3</sub>-Al<sub>2</sub>O<sub>3</sub> solid solutions prepared by the glycothermal method. *Appl. Catal. B* 65 (2006): 142–149.
- Takahashi, M.; Nakatani, T.; Iwamoto, S.; Watanabe, T.; Inoue, M. Performance of solvothermally prepared Ga<sub>2</sub>O<sub>3</sub>-Al<sub>2</sub>O<sub>3</sub> catalysts for SCR of NO with methane. *Appl. Catal. B* 70 (2007): 73–79.
- Voß, M.; Borgmann, D.; and Wedler, G. Characterization of Alumina, Silica, and Titania Supported Cobalt Catalysts. *J. Catal.* 212 (2002): 10–21.
- Wittayakhun, J.; Krisdanurak, N.; 2004. Catalysis: Fundamentals and Applications, 1<sup>st</sup> ed., Thammasart university publishing
- Young, R.S. COBALT: Its Chemistry, Metallurgy, and Uses. New York: Reinhold Publishing Corporation, 1960.
- Zhang, Y.; Wei, D.; Hammache, S.; Goodwin, Jr., J. G. Effect of Water Vapor on the reduction of Ru-Promoted Co/Al<sub>2</sub>O<sub>3</sub>. *J. Catal.* 188 (1999): 281–290.



**APPENDICES**

ศูนย์วิทยทรัพยากร  
จุฬาลงกรณ์มหาวิทยาลัย

## APPENDIX A

### EFFECT OF GA-MODIFIED TiO<sub>2</sub> SUPPORT ON CHARACTERISTICS AND CATALYTIC PROPERTIES OF SUPPORTED COBALT CATALYST

XRD patterns for the calcined Co catalysts (with and without Ga modification) on TiO<sub>2</sub> supports are shown in Figure 1.

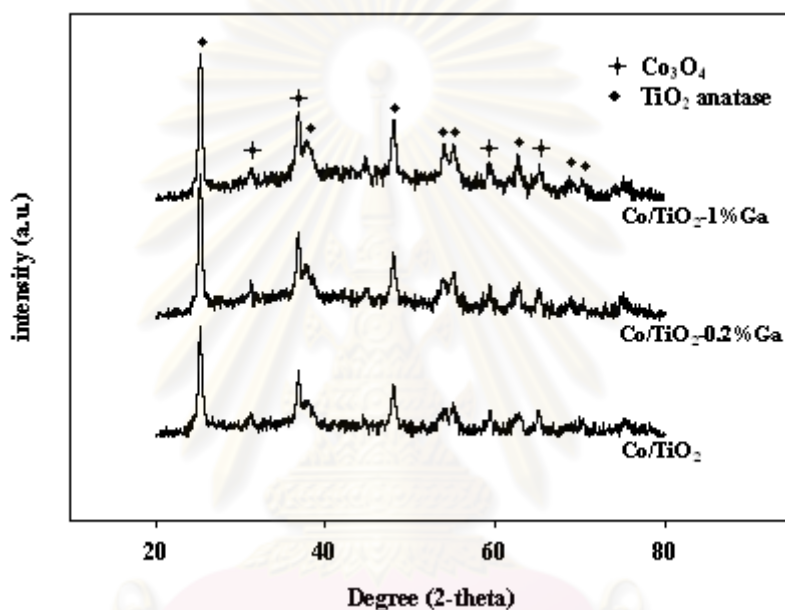


**Figure A.1** XRD patterns of Ga-modified and unmodified TiO<sub>2</sub> supported cobalt catalysts.

It showed that all catalysts exhibited mainly two XRD patterns including (i) the patterns for TiO<sub>2</sub> support in anatase phase (26°, 37°, 48°, 55°, 56°, 62°, 69°, 71° and 75°) and (ii) the patterns for Co<sub>3</sub>O<sub>4</sub> formed after calcination (31°, 36°, 59 and 65°). The Co<sub>3</sub>O<sub>4</sub> crystallite size calculated for all catalysts from the Scherrer equation are shown in Table A.1. The crystallite sizes of Co<sub>3</sub>O<sub>4</sub> were ranged from 17.1-10.6 nm. It was found that, the crystallite size of Co<sub>3</sub>O<sub>4</sub> slightly decreased when %Ga loading increased on TiO<sub>2</sub>.

**Table A.1** The average crystallite sizes of Ga-modified TiO<sub>2</sub> supported cobalt catalysts.

sample	Co <sub>3</sub> O <sub>4</sub> crystallite size (nm) <sup>a</sup>
Co/TiO <sub>2</sub>	17.1
Co/TiO <sub>2</sub> -0.2%Ga	16.7
Co/TiO <sub>2</sub> -1%Ga	10.6

<sup>a</sup> from Scherrer's equation

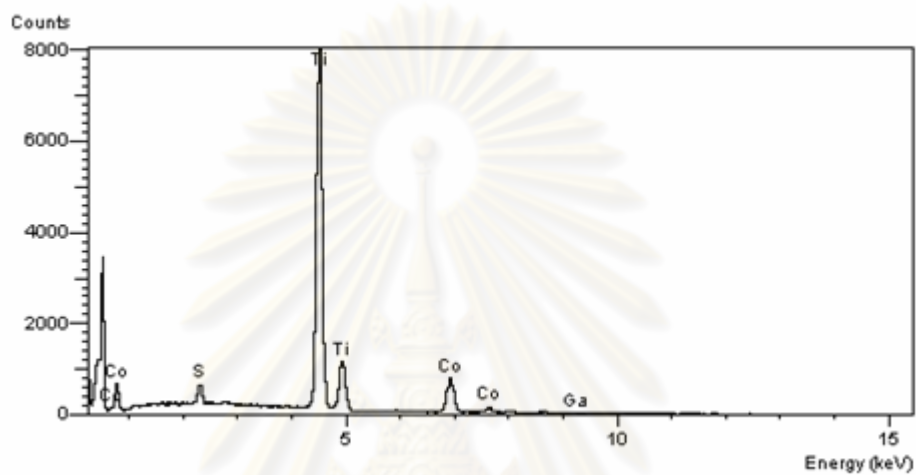
Table A.2 summarizes the physical properties of 20 wt% cobalt on Ga-modified supported cobalt catalyst. From the result, it was found that the modification of Ga on the TiO<sub>2</sub> supports did not affect significantly the surface areas, pore size and pore volume of the resulting samples.

**Table A.2** BET surface area, pore size and pore volume of Ga-modified TiO<sub>2</sub> supported cobalt catalysts.

sample	BET surface area (m <sup>2</sup> /g)	Pore size (Å)	Pore volume (cm <sup>3</sup> /g)
Co/TiO <sub>2</sub>	55	107	0.1859
Co/ TiO <sub>2</sub> -0.2%Ga	53	107	0.1894
Co/TiO <sub>2</sub> -1%Ga	55	101	0.1855

The typical measurement curve for the quantitative analysis of Co/TiO<sub>2</sub>-1%Ga using EDX is shown in Figures A.2. The amounts of elements in the various catalysts are also listed below. It was found that the amounts of Co and Ga on the surface of TiO<sub>2</sub> support was less than the Al<sub>2</sub>O<sub>3</sub> support (from Figure 5.2), properly due to the pore size of TiO<sub>2</sub> support was larger pore size than Al<sub>2</sub>O<sub>3</sub> support (from Table 5.2). Besides the content of Co and Ga in the supports, one should consider the distribution of Co and Ga in the supports. SEM and EDX were also conducted in order to study

the morphologies and elemental distribution of the samples, respectively. The typical SEM micrographs along with the EDX mapping for Co/TiO<sub>2</sub> (for Co, Ti, O and S) samples are illustrated in Figures A.3. It can be seen that the distribution of Co was well on the surface of the support.



Element	Element(%)	Atomic(%)
O	56.37	79.9
S	0.86	0.61
Ti	34.59	16.38
Co	7.68	2.96
Ga	0.5	0.16

**Figure A.2.** A typical spectrum of the Co/TiO<sub>2</sub>-1%Ga from EDX analysis.

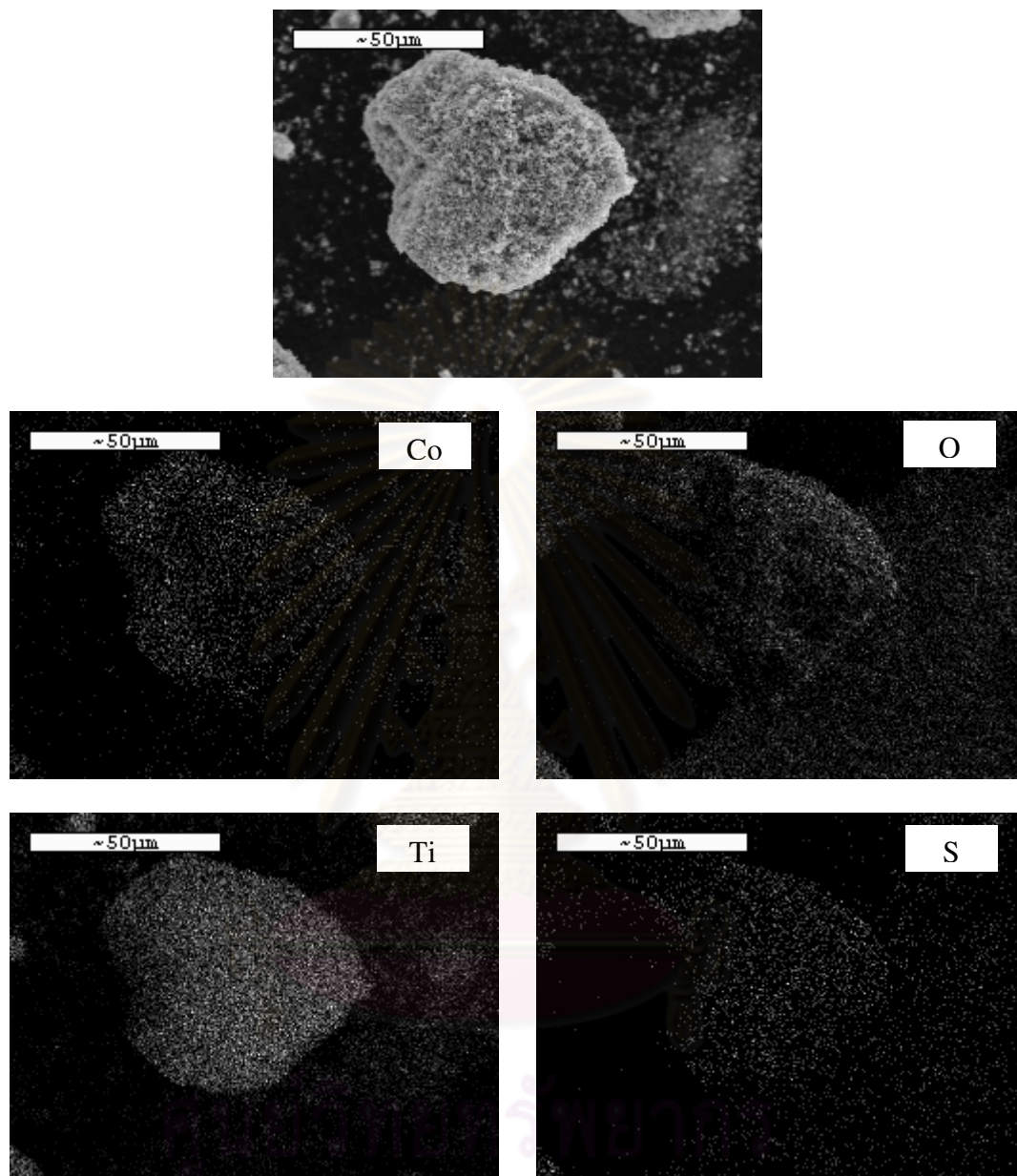


**Figure A.3** SEM micrograph and EDX mapping of the calcined Co/TiO<sub>2</sub>-1%Ga catalysts.

In order to determine the dispersion and crystallite size of Co oxides species dispersed on the supports employed, the high resolution TEM was used. The TEM micrographs Ga-modified and unmodified  $\text{TiO}_2$  supported cobalt catalyst are shown in Figure A.4. The dark spots represented the cobalt species dispersing on the catalyst granule. However, considering the morphologies for the cobalt oxide species ( $\text{Co}_3\text{O}_4$ ) dispersed on the support, they could not be differentiated between those and the supports. It was suggested that the morphologies of cobalt oxide species were essentially similar for all  $\text{TiO}_2$  supports.

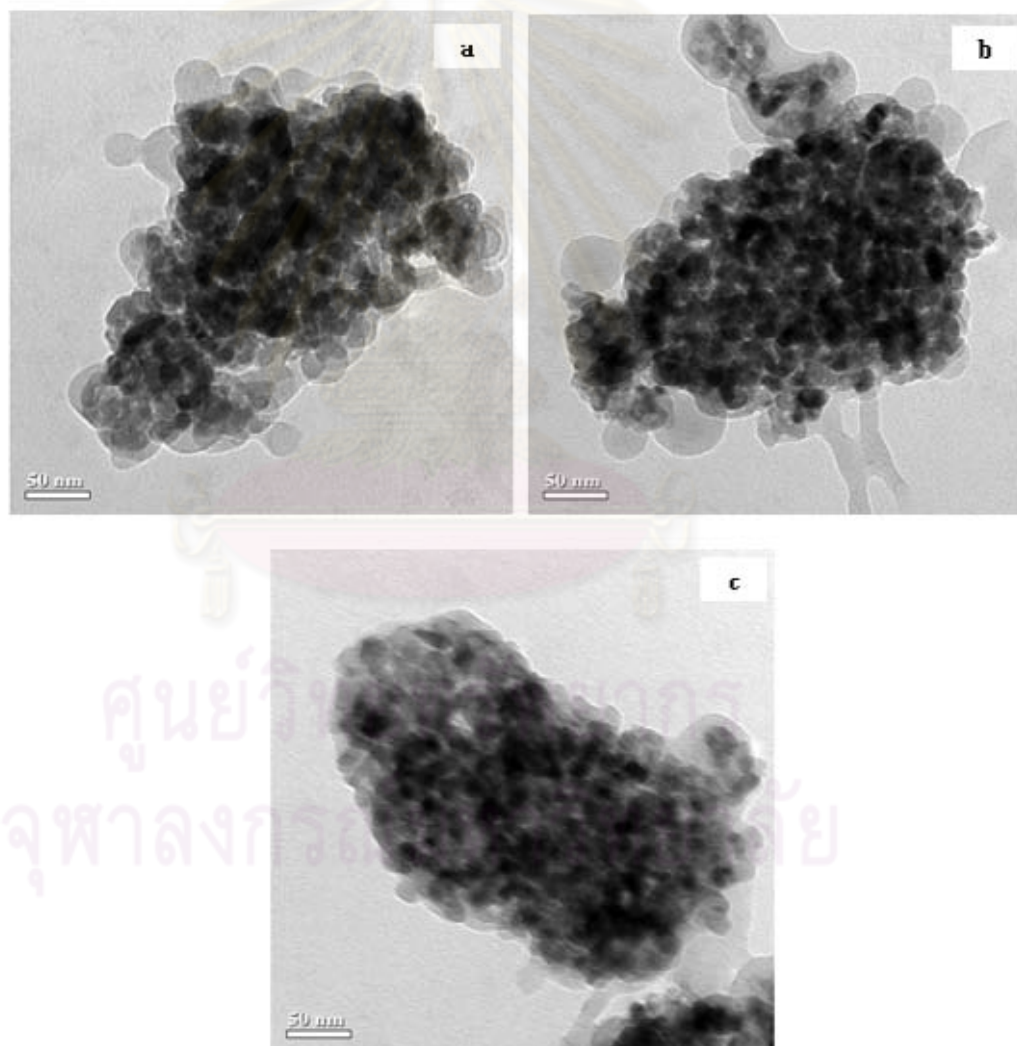


**Figure A.4** TEM micrograph of Co supported on Ga-modified and unmodified  $\text{TiO}_2$  supported cobalt catalysts; a)  $\text{Co}/\text{TiO}_2$ , b)  $\text{Co}/\text{TiO}_2\text{-}0.2\%\text{Ga}$ , c)  $\text{Co}/\text{TiO}_2\text{-}1\%\text{Ga}$ .

In order to give a better understanding on species present on supports, XPS is used to determine the surface compositions of the catalysts and the interaction between Ga, Co and the supports. A typical XPS profile of Co 2p and Ga 2p on Al<sub>2</sub>O<sub>3</sub> are shown in Figure A.5, indicating the BE of Co 2p<sub>1/2</sub> in the range of 796-796.8 eV, BE of Co 2p<sub>3/2</sub> in the range of 780.3-781.4 eV[19]. and the Ga 2p<sub>3/2</sub> BE value that appeared at 1112.1-1117.6 eV[20]. The surface concentrations of element on catalysts measured by XPS are also shown in Table A.3. Addition Ga, the Ga 2p peak shifts to higher binding energy but not affect significantly the binding energy of Co 2p peaks.



ศูนย์วิทยทรัพยากร  
จุฬาลงกรณ์มหาวิทยาลัย



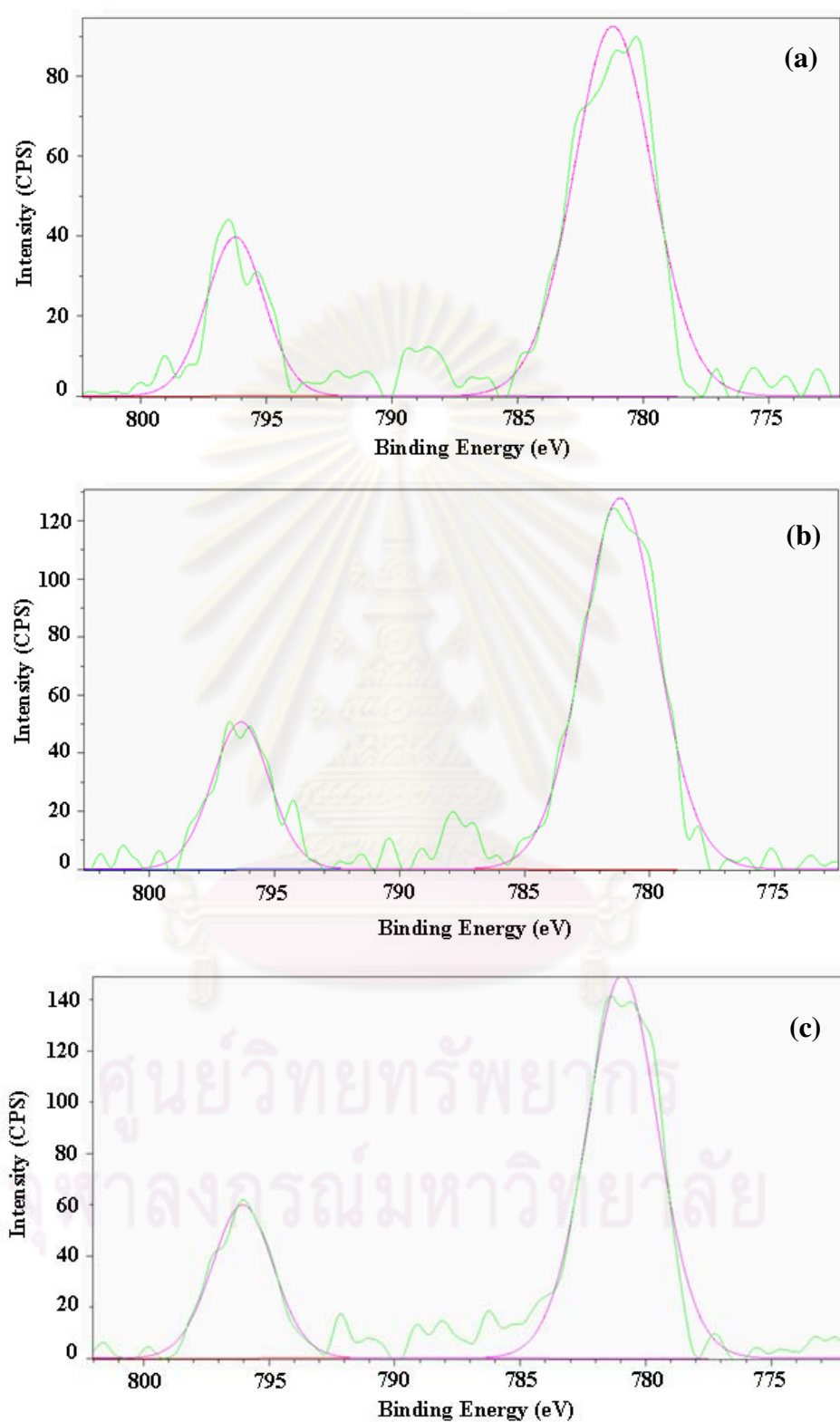


**Figure A.5** The deconvolution of XPS spectra of Ga-modified and unmodified TiO<sub>2</sub> supported cobalt catalysts; a) Co/TiO<sub>2</sub>, b) Co/TiO<sub>2</sub>-0.2%Ga and c) Co/TiO<sub>2</sub>-1%Ga.

**Table A.3** XPS data of Ga-modified TiO<sub>2</sub> supported cobalt catalysts.

Catalysts	BE for Co 2p(eV)		BE for Ti 2p(eV)		BE for O 1s(eV)	BE for Ga 2p(eV)	BE for S 2p(eV)	Amount of element at surface(%mass)				
								Co	Ti	O	Ga	S
Co/TiO <sub>2</sub>	780.3	796.5	459.6	465.3	531	-	169.1	12.07	31.97	55.06	-	0.9
Co/ TiO <sub>2</sub> -0.2%Ga	781.4	796.8	459.5	465	531.1	1112.1	168.4	12.39	33.74	52.56	0.2	1.1
Co/ TiO <sub>2</sub> -1%Ga	781.4	796	459.3	465.1	530.6	1117.6	169.3	12.12	34.01	51.33	1.49	1.05

ศูนย์วิทยทรัพยากร  
จุฬาลงกรณ์มหาวิทยาลัย

The acid properties of the catalysts were measured by NH<sub>3</sub>-TPD. The NH<sub>3</sub>-TPD profiles are shown in Figure A.6 and the TPR profiles of Co supported on TiO<sub>2</sub> supports with and without Ga modification are shown in Figure A.7.

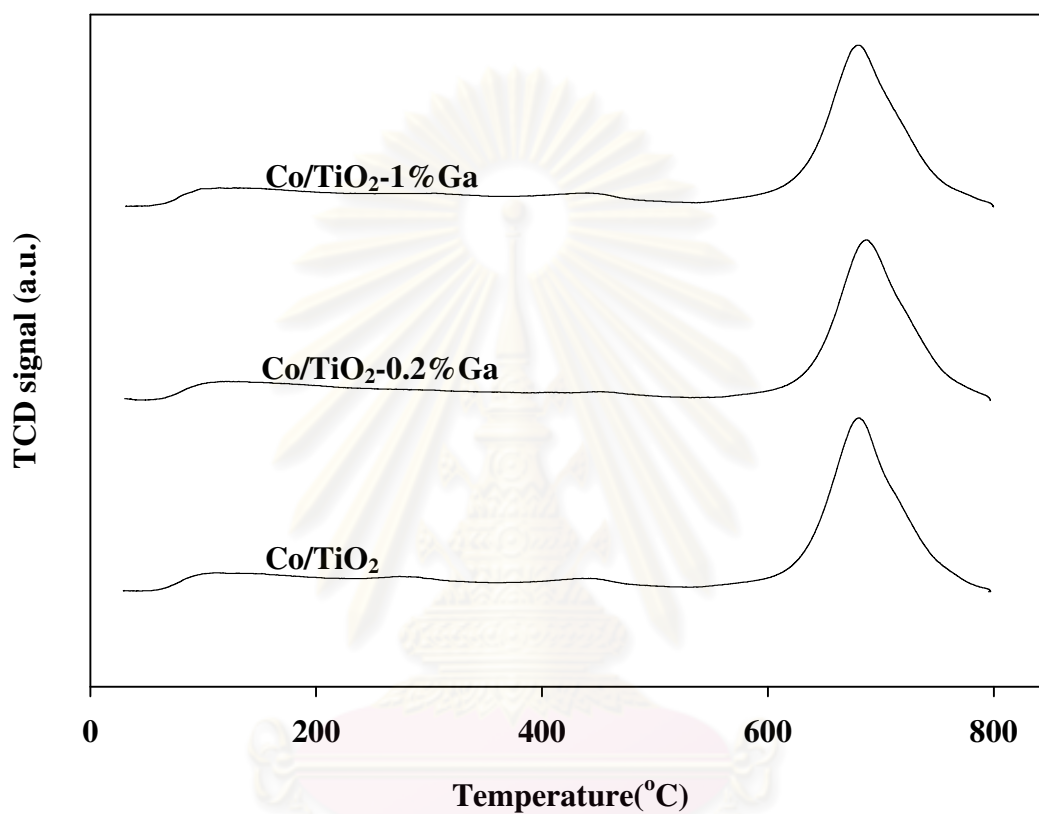


**Figure A.6** NH<sub>3</sub>-TPD profiles of Ga-modified TiO<sub>2</sub> supported cobalt catalysts.

ศูนย์วิทยทรัพยากร  
จุฬาลงกรณ์มหาวิทยาลัย

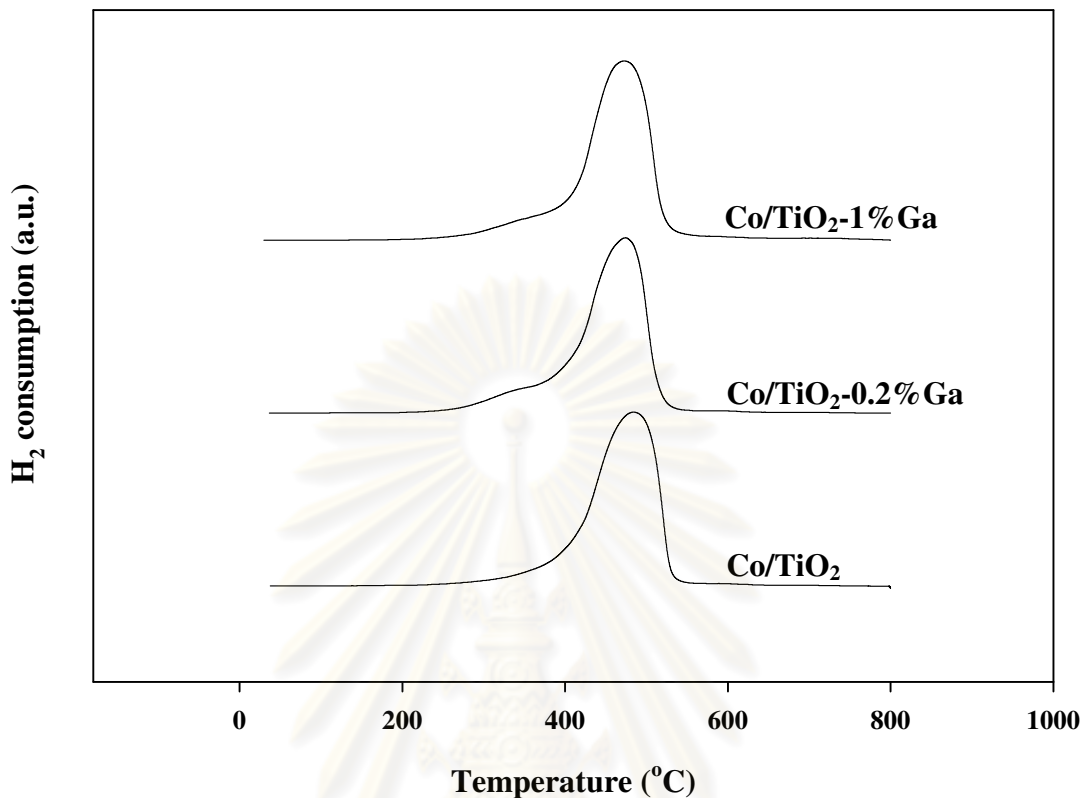


**Figure A.7** TPR profile of Ga-modified and unmodified TiO<sub>2</sub> supported cobalt catalysts.

From the result, it was found that the modification of Ga on the TiO<sub>2</sub> supports did not affect significantly the amount of acid site and reduction peak of the resulting samples.

In order to determine the catalytic behaviors of the Co catalysts with and without Ga modification, CO hydrogenation ( $H_2/CO = 10/1$ ) under methanation condition was performed to determine the overall activity and product selectivity of the samples. Hydrogenation of CO was carried out at 220 °C and 1 atm. A flow rate of  $H_2/CO/Ar = 20/2/8 \text{ cm}^3/\text{min}$  in a fixed-bed flow reactor was used. The resulted reaction test is shown in Table A.4.

**Table A.4** Reaction study of Ga-modified and unmodified TiO<sub>2</sub> supported cobalt catalysts.

Catalyst	CO conversion (%) <sup>a</sup>		
	initial <sup>b</sup>	30 min	SS <sup>c</sup>
Co/TiO <sub>2</sub>	71.24	2.37	0
Co/TiO <sub>2</sub> -0.2%Ga	95.56	2.88	0
Co/TiO <sub>2</sub> -1%Ga	69.86	2.66	0

<sup>a</sup> CO hydrogenation was carried out at 220 °C, 1 atm, and H<sub>2</sub>/CO/Ar = 20/2/8.

<sup>b</sup> After 5 min of reaction.

<sup>c</sup> After 3 h of reaction.

From the resulted, it was found that the activity of Ga-modified and unmodified TiO<sub>2</sub> supported cobalt catalysts were decreased dramatically at 30 min of reaction. It probably due to it observed sulphur on the surface of catalysts. It indicated that, poisoning of the catalyst samples with sulphur lead to a significant decrease of the CO conversion. The results were in good agreement with those reported by Giorgio *et al.*,2007. They reported that the effect of sulphur poisoning (in the range 0-2000 ppm) on the characteristics and catalytic performances in the Fisher-Tropsch synthesis (FTS), they was found that that the addition of sulphur determined progressive decreased of the catalyst activity, measured in term of CO conversion.

ศูนย์วิทยทรัพยากร  
จุฬาลงกรณ์มหาวิทยาลัย

## APPENDIX B

### CALCULATION FOR CATALYST PREPARATION

#### Calulation of support composition (Ga-modified supports(Al<sub>2</sub>O<sub>3</sub>, SiO<sub>2</sub> and TiO<sub>2</sub>))

Preparation of Ga-modified support (Al<sub>2</sub>O<sub>3</sub>, SiO<sub>2</sub> and TiO<sub>2</sub>) support with various ratios of Ga to support (0.2 and 1%wtGa) by incipient wetness impregnation method are shown as follows:

- Reagent:
- Gallium (III) nitrate hydrate (Ga(NO<sub>3</sub>)<sub>3</sub>)  
Molecular weight = 255.7 g/mol  
Gallium (Ga), Atomic weight = 69.7 g/mol
  - Support :
    - Al<sub>2</sub>O<sub>3</sub>
    - SiO<sub>2</sub>
    - TiO<sub>2</sub>

- For 0.2%wt of Ga is shown as follow:

Based on 100 g of catalyst used, the composition of the catalyst will be as follows:

$$\begin{aligned}\text{Gallium} &= 0.2 \text{ g} \\ \text{Al}_2\text{O}_3 &= 100 - 0.2 = 99.8 \text{ g}\end{aligned}$$

For 1 g of support (Al<sub>2</sub>O<sub>3</sub>)

$$\text{Cobalt required} = 1 \times \frac{0.2}{99.8} = 0.002 \text{ g}$$

Gallium 0.002 g was prepared from Gallium (III) nitrate hydrate

$$\begin{aligned}\text{Gallium (III) nitrate hydrate required} &= \frac{0.002}{69.7} \times 255.7 \\ &= 0.0073 \text{ g}\end{aligned}$$

- For 1%wt of Ga is shown as follow:

Based on 100 g of catalyst used, the composition of the catalyst will be as follows:

$$\begin{aligned} \text{Gallium} &= 1 \text{ g} \\ \text{Al}_2\text{O}_3 &= 100 - 1 = 99 \text{ g} \end{aligned}$$

For 1 g of support ( $\text{Al}_2\text{O}_3$ )

$$\text{Cobalt required} = 1 \times \frac{1}{99} = 0.0101 \text{ g}$$

Gallium 0.0101 g was prepared from Gallium (III) nitrate hydrate

$$\begin{aligned} \text{Gallium (III) nitrate hydrate required} &= \frac{0.0101}{69.7} \times 255.7 \\ &= 0.0370 \text{ g} \end{aligned}$$

Since the pore volume of Ga-modified  $\text{Al}_2\text{O}_3$  support is 0.4 ml/g. Thus, the total volume of impregnation solution which must be used is 0.4 ml for alumina by the requirement of incipient wetness impregnation method, the de-ionized water is added until equal pore volume for dissolve gallium (III) nitrate hydrate.

### **Calculation of cobalt loading**

Preparations of 20%wtCo/ $\text{Al}_2\text{O}_3$  by the incipient wetness impregnation method are shown as follows:

Reagent: - Cobalt (II) nitrate hexahydrate ( $\text{Co}(\text{NO}_3)_2 \cdot 6\text{H}_2\text{O}$ )

Molecular weight = 291.03 g/mol

Cobalt (Co), Atomic weight = 58.933 g/mol

- Support: -  $\text{Al}_2\text{O}_3$  and Ga-modified  $\text{Al}_2\text{O}_3$

-  $\text{SiO}_2$  and Ga-modified  $\text{SiO}_2$

-  $\text{TiO}_2$  and Ga-modified  $\text{TiO}_2$

Based on 100 g of catalyst used, the composition of the catalyst will be as follows:

$$\begin{aligned} \text{Cobalt} &= 20 \text{ g} \\ \text{Al}_2\text{O}_3 &= 100 - 20 = 80 \text{ g} \end{aligned}$$

For 1 g of support ( $\text{Al}_2\text{O}_3$ )

$$\text{Cobalt required} = 1 \times \frac{20}{80} = 0.25 \text{ g}$$

Cobalt 0.25 g was prepared from Cobalt (II) nitrate hexahydrate

$$\begin{aligned} \text{Cobalt (II) nitrate hexahydrate required} &= \frac{0.25}{58.933} \times 291.03 \\ &= 1.234 \text{ g} \end{aligned}$$

Since the pore volume of  $\text{Al}_2\text{O}_3$  support is 1 ml/g. Thus, the total volume of impregnation solution which must be used is 1 ml for  $\text{Al}_2\text{O}_3$  by the requirement of incipient wetness impregnation method, the de-ionized water is added until equal pore volume for dissolve cobalt (II) nitrate hexahydrate.

ศูนย์วิทยทรัพยากร  
จุฬาลงกรณ์มหาวิทยาลัย



## APPENDIX C

### CALCULATION OF THE CRYSTALLITE SIZE

#### Calculation of the crystallite size by Debye-Scherrer equation

The crystallite size was calculated from the half-height width of the highest intensity diffraction peak of XRD patterns of transition alumina.

From Scherrer equation:

$$D = \frac{K\lambda}{\beta \cos \theta} \quad (\text{C.1})$$

where  $D$  = Crystallite size, Å

$K$  = Crystallite-shape factor = 0.9

$\lambda$  = X-ray wavelength, 1.5418 Å for  $\text{CuK}\alpha$

$\theta$  = Observed peak angle, degree

$\beta$  = X-ray diffraction broadening, radian

The X-ray diffraction broadening ( $\beta$ ) is the pure width of a powder diffraction free from all broadening due to the experimental equipment.  $\alpha$ -Alumina is used as a standard sample to observe the instrumental broadening since its crystallite size is larger than 2000 Å. The X-ray diffraction broadening ( $\beta$ ) can be obtained by using Warren's formula.

From Warren's formula:

$$\beta = \sqrt{B_M^2 - B_S^2} \quad (\text{C.2})$$

where  $B_M$  = The measured peak width in radians at half peak height.

$B_S$  = The corresponding width of the standard material.

**Example:** Calculation of the crystallite size of  $\gamma\text{-Al}_2\text{O}_3$

$$\begin{aligned} \text{The half-height width of peak} &= 1.87^\circ \text{ (from the figure C.1)} \\ &= (1.87 \times \pi) / 180 \\ &= 0.0326 \text{ radian} \end{aligned}$$

The corresponding half-height width of peak of  $\alpha$ -alumina (from the  $B_s$  value at the  $2\theta$  of  $67.44^\circ$  in figure C.2) = 0.0057 radian

$$\begin{aligned} \text{The pure width, } \beta &= \sqrt{B_M^2 - B_S^2} \\ &= \sqrt{0.0326^2 - 0.0057^2} \\ &= 0.032 \text{ radian} \end{aligned}$$

Scherrer equation:

$$\beta = 0.032 \text{ radian}$$

$$2\theta = 66.98^\circ$$

$$\theta = 33.49^\circ$$

$$\lambda = 1.5418 \text{ \AA}$$

$$\text{The crystallite size} = \frac{0.9 \times 1.5418}{0.032 \cos 33.49}$$

$$= 51.99 \text{ \AA}$$

$$= 5.2 \text{ nm}$$

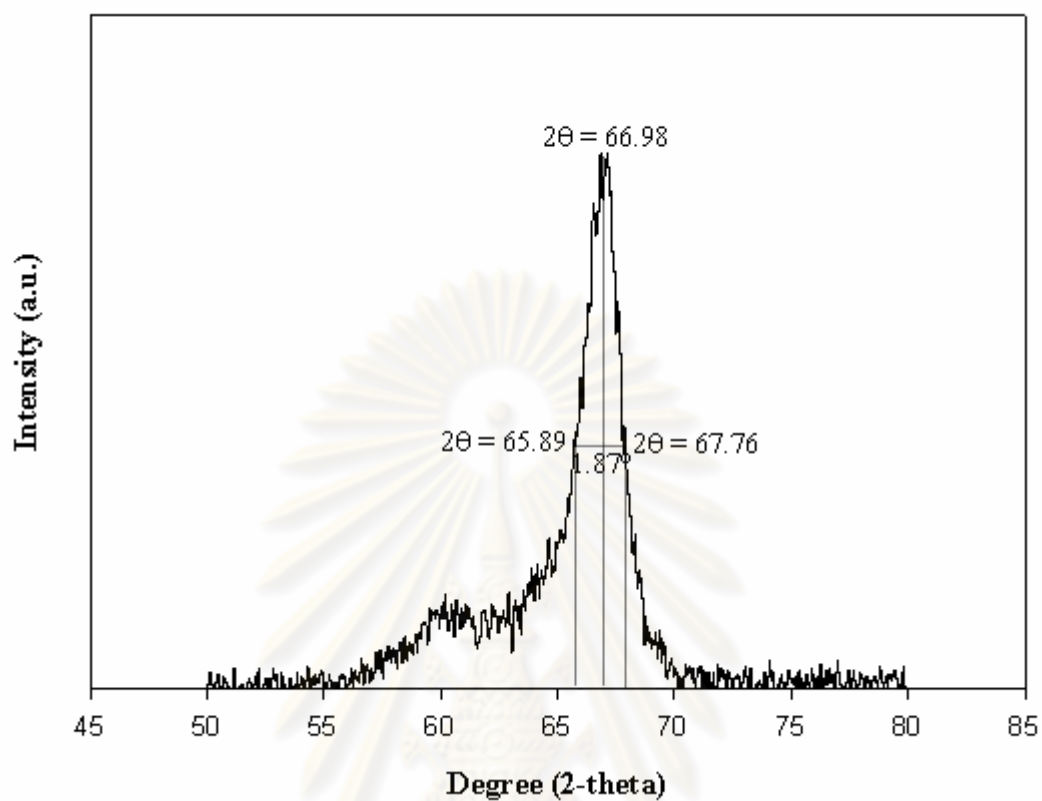


**Figure C.1** The measured peak of  $\gamma$ - $\text{Al}_2\text{O}_3$  to calculate the crystallite size.

ศูนย์วิทยทรัพยากร  
จุฬาลงกรณ์มหาวิทยาลัย

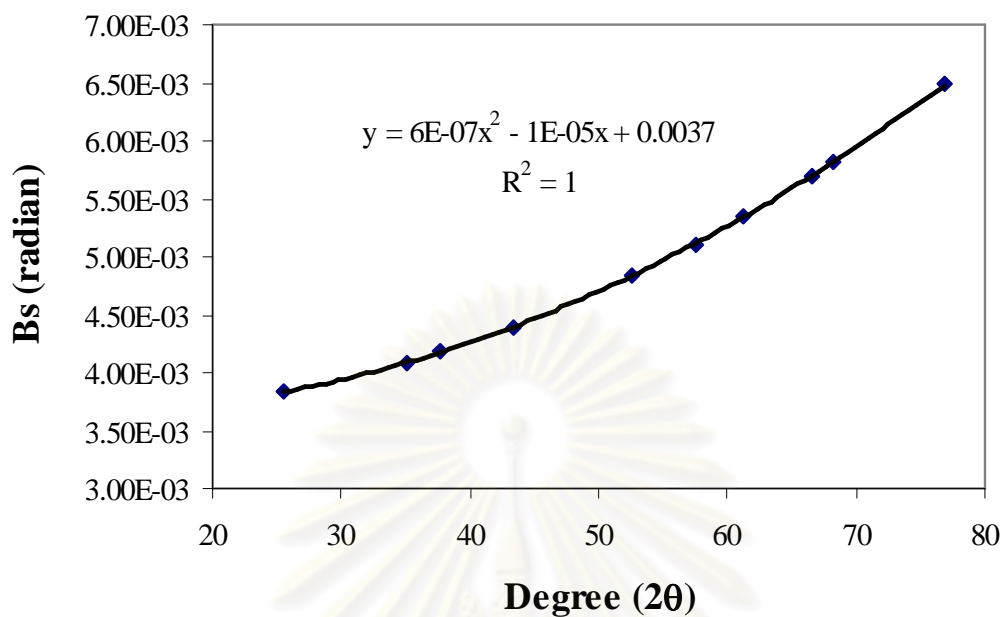


**Figure C.2** The plot indicating the value of line broadening due to the equipment. The data were obtained by using  $\alpha$ -alumina as standard

ศูนย์วิทยทรัพยากร  
จุฬาลงกรณ์มหาวิทยาลัย

## APPENDIX D

### CALCULATION OF THE ACIDITY

#### Calculation of total acid sites

For example, Co/Al<sub>2</sub>O<sub>3</sub>, total acid sites is calculated from the following step.

#### 1. Conversion of total peak area to total peak volume

Conversion factor from Micromeritics Chemisorp 2750 is equal to 77.57016 ml/area unit. Therefore, total peak volume is derived from

$$\begin{aligned}\text{Total peak volume} &= 77.57016 \times \text{total peak area} \\ &= 77.57016 \times 0.1971 \\ &= 15.2891 \text{ ml}\end{aligned}$$

#### 2. Calculation for adsorbed volume of 15% NH<sub>3</sub>

$$\begin{aligned}\text{Adsorbed volume of 15\% NH}_3 &= 0.15 \times \text{total area peak} \\ &= 0.15 \times 15.2891 \text{ ml} \\ &= 2.2934 \text{ ml}\end{aligned}$$

#### 3. Total acid sites are calculated from the following equation

$$\text{Total acid sites} = \frac{(\text{Adsorbed volume, ml}) \times 101.325 \text{ Pa}}{\left(8.314 \times 10^{-3} \frac{\text{Pa} \cdot \text{ml}}{\text{K} \cdot \mu\text{mol}}\right) \times 298 \text{ K} \times (\text{weight of catalyst, g})}$$

For Co/Al<sub>2</sub>O<sub>3</sub> sample, 0.1003 g of this one was measured, therefore

$$\begin{aligned}\text{Total acid sites} &= \frac{2.2933 \text{ ml} \times 101.325 \text{ Pa}}{\left(8.314 \times 10^{-3} \frac{\text{Pa} \cdot \text{ml}}{\text{K} \cdot \mu\text{mol}}\right) \times 298 \text{ K} \times 0.1003 \text{ g}} \\ &= 935 \mu\text{mol H}^+/\text{g}\end{aligned}$$



ศูนย์วิทยทรัพยากร  
จุฬาลงกรณ์มหาวิทยาลัย

## APPENDIX E

### CALCULATION FOR TOTAL H<sub>2</sub> CHEMISORPTION

Calculation of the total H<sub>2</sub> chemisorption and metal dispersion of the catalyst, a stoichiometry of H/Co = 1, measured by H<sub>2</sub> chemisorption is as follows:

Let the weight of catalyst used	=	W	g
Integral area of H <sub>2</sub> peak after adsorption	=	A	unit
Integral area of 45 μl of standard H <sub>2</sub> peak	=	B	unit
Amounts of H <sub>2</sub> adsorbed on catalyst	=	B-A	unit
Volume of H <sub>2</sub> adsorbed on catalyst	=	$45 \times [(B - A) / B]$	μl
Volume of 1 mole of H <sub>2</sub> at 100°C	=	28.038	μl
Mole of H <sub>2</sub> adsorbed on catalyst	=	$[(B - A) / B] \times [45 / 28.038]$	mole
Total H <sub>2</sub> chemisorption	=	$[(B - A) / B] \times [45 / 28.038] \times [1 / W]$	mole/g of catalyst
	=	N	mole/g of catalyst

ศูนย์วิทยทรัพยากร  
จุฬาลงกรณ์มหาวิทยาลัย

## APPENDIX F

### CALIBRATION CURVES

This appendix showed the calibration curves for calculation of composition of reactant and products in CO hydrogenation reaction. The reactant is CO and the main product is methane. The other products are linear hydrocarbons of heavier molecular weight that are C<sub>2</sub>-C<sub>4</sub> such as ethane, ethylene, propane, propylene and butane.

The thermal conductivity detector, gas chromatography Shimadzu model 8A was used to analyze the concentration of CO by using Molecular sieve 5A column.

The VZ10 column are used with a gas chromatography equipped with a flame ionization detector, Shimadzu model 14B, to analyze the concentration of products including of methane, ethane, ethylene, propane, propylene and butane. Conditions uses in both GC are illustrated in Table C.1.

Mole of reagent in y-axis and area reported by gas chromatography in x-axis are exhibited in the curves. The calibration curves of CO, methane, ethane, ethylene, propane, propylene and butane are illustrated in the following figures.

ศูนย์วิทยทรัพยากร  
จุฬาลงกรณ์มหาวิทยาลัย



**Table F.1** Conditions use in Shimadzu modal GC-8A and GC-14B.

Parameters	Condition	
	Shimadzu GC-8A	Shimadzu GC-14B
Width	5	5
Slope	50	50
Drift	0	0
Min. area	10	10
T.DBL	0	0
Stop time	50	60
Atten	0	0
Speed	2	2
Method	41	41
Format	1	1
SPL.WT	100	100
IS.WT	1	1

ศูนย์วิทยทรัพยากร  
จุฬาลงกรณ์มหาวิทยาลัย

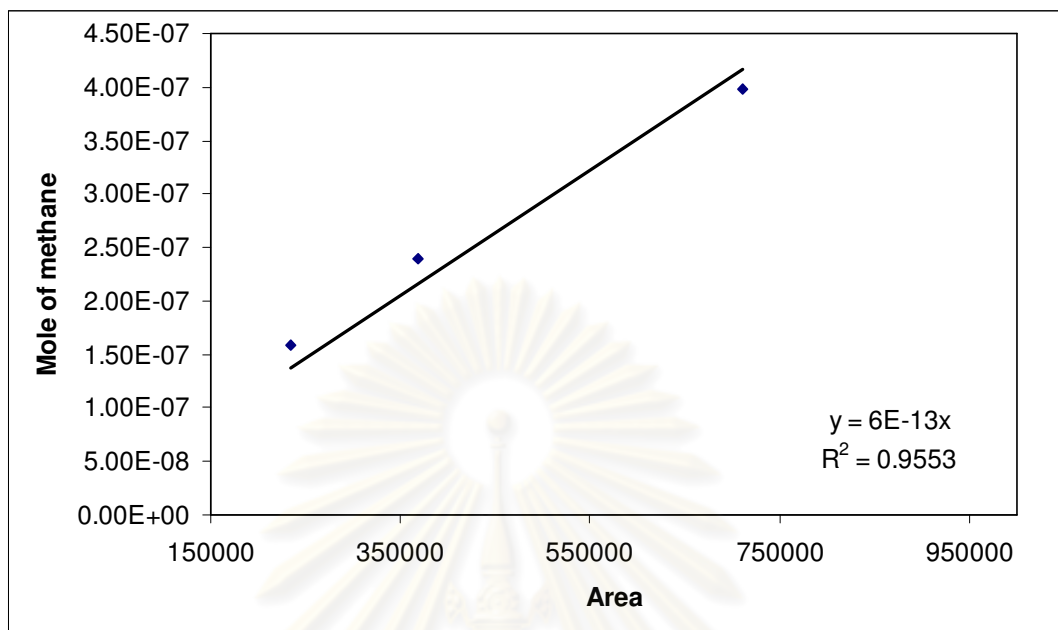


**Figure F.1** The calibration curve of methane.

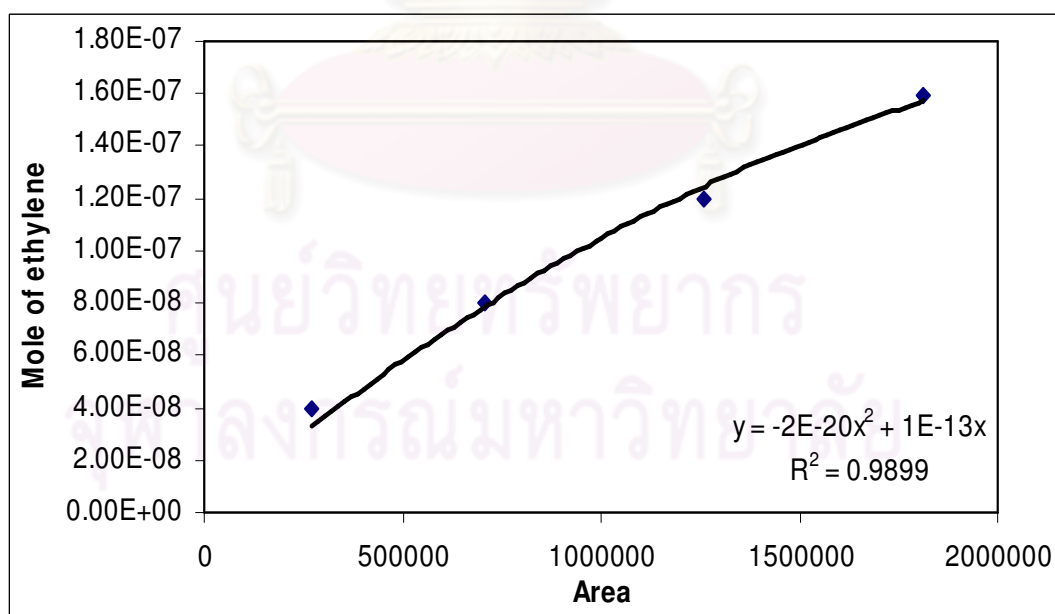


**Figure F.2** The calibration curve of ethylene.

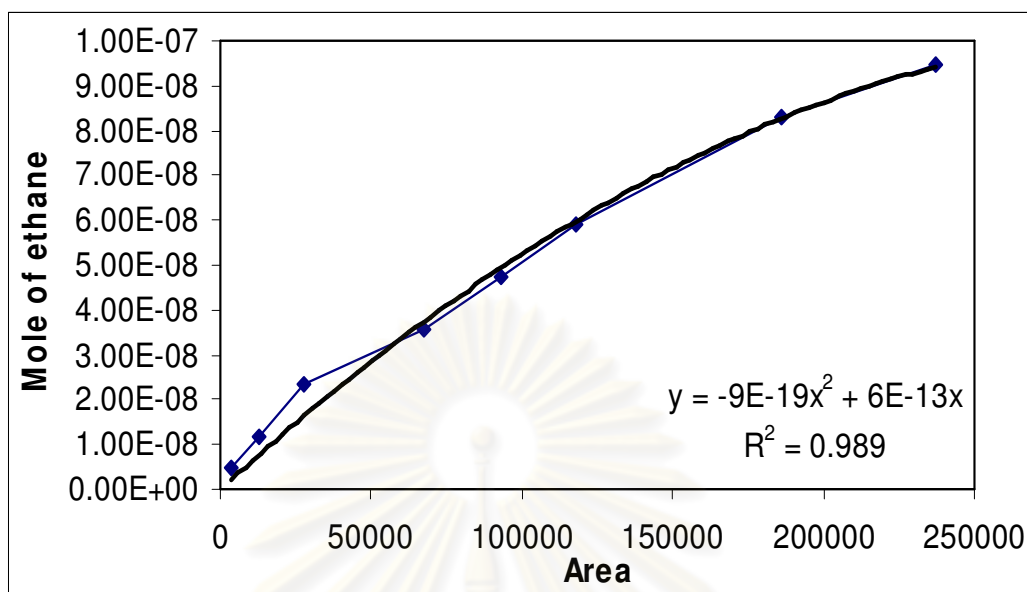


Figure F.3 The calibration curve of ethane.

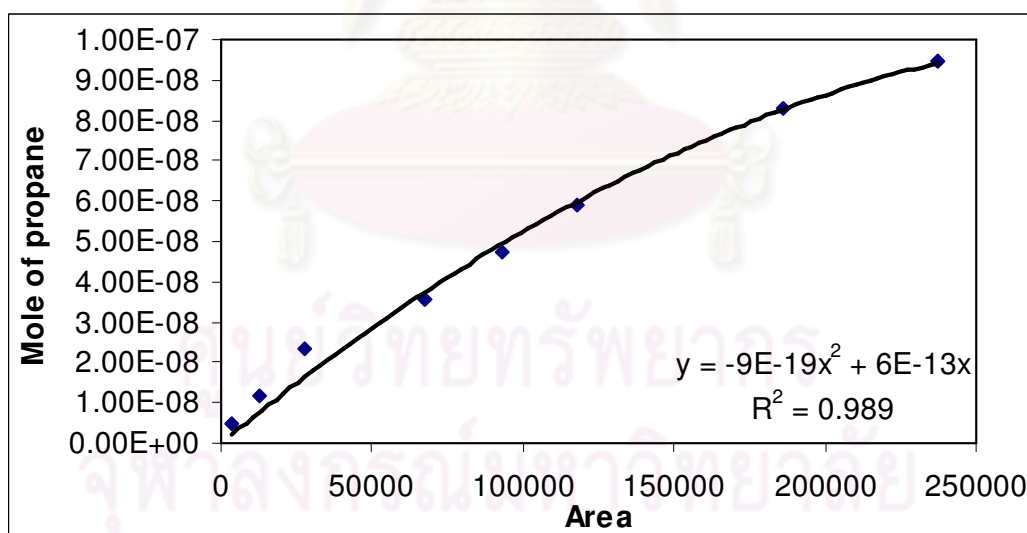


Figure F.4 The calibration curve of propane.

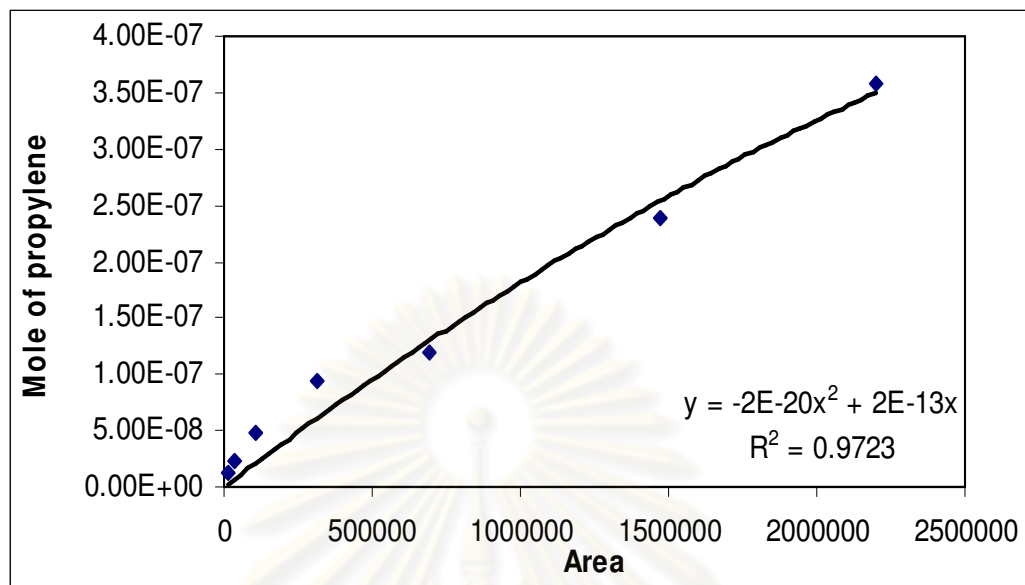


Figure F.5 The calibration curve of propylene.

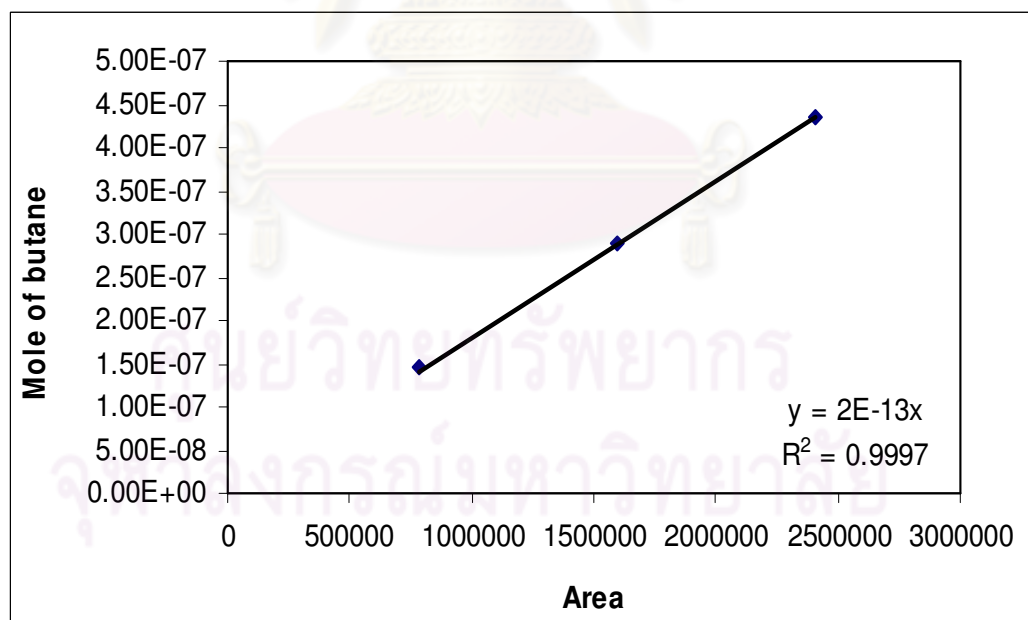
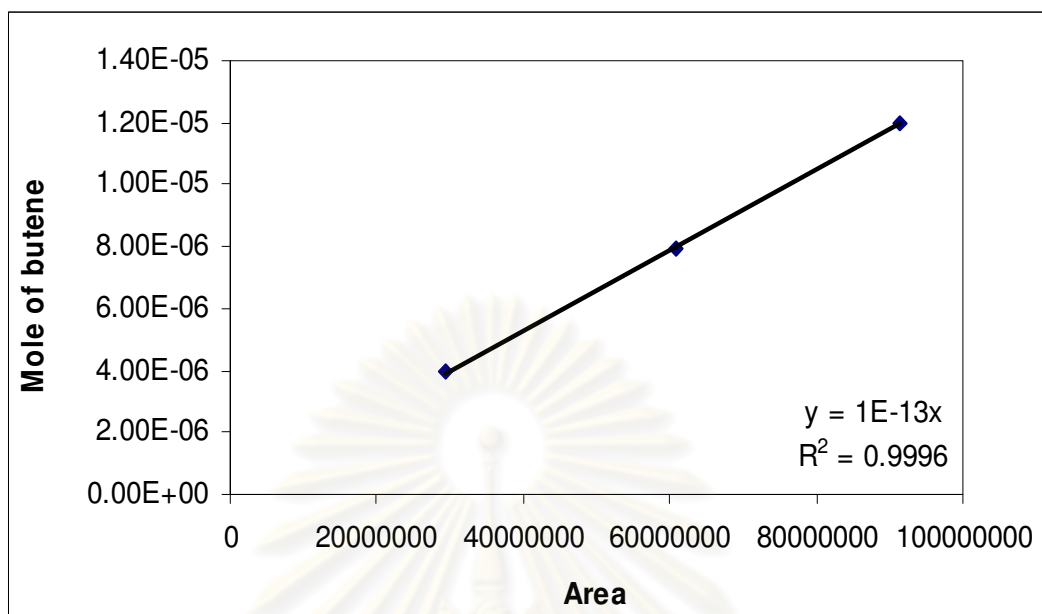
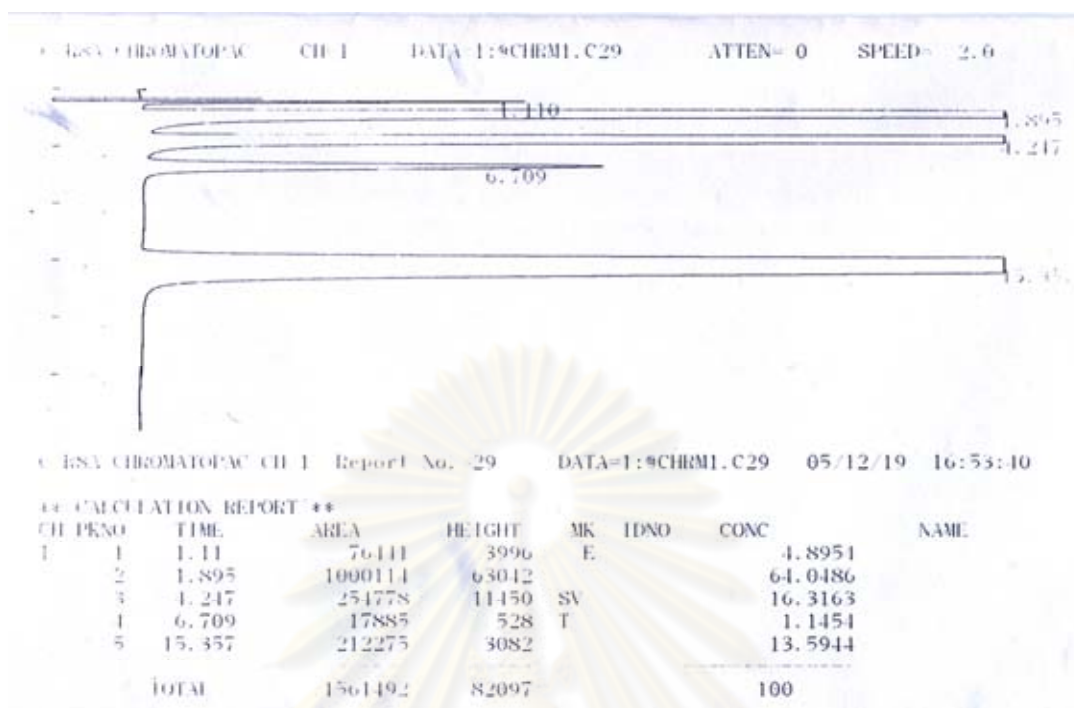


Figure F.6 The calibration curve of butane.



**Figure F.7** The calibration curve of butylene.

ศูนย์วิทยทรัพยากร  
จุฬาลงกรณ์มหาวิทยาลัย



**Figure F.8** The chromatograms of catalyst sample from thermal conductivity detector, gas chromatography Shimadzu model 8A (Molecular sieve 5A column).

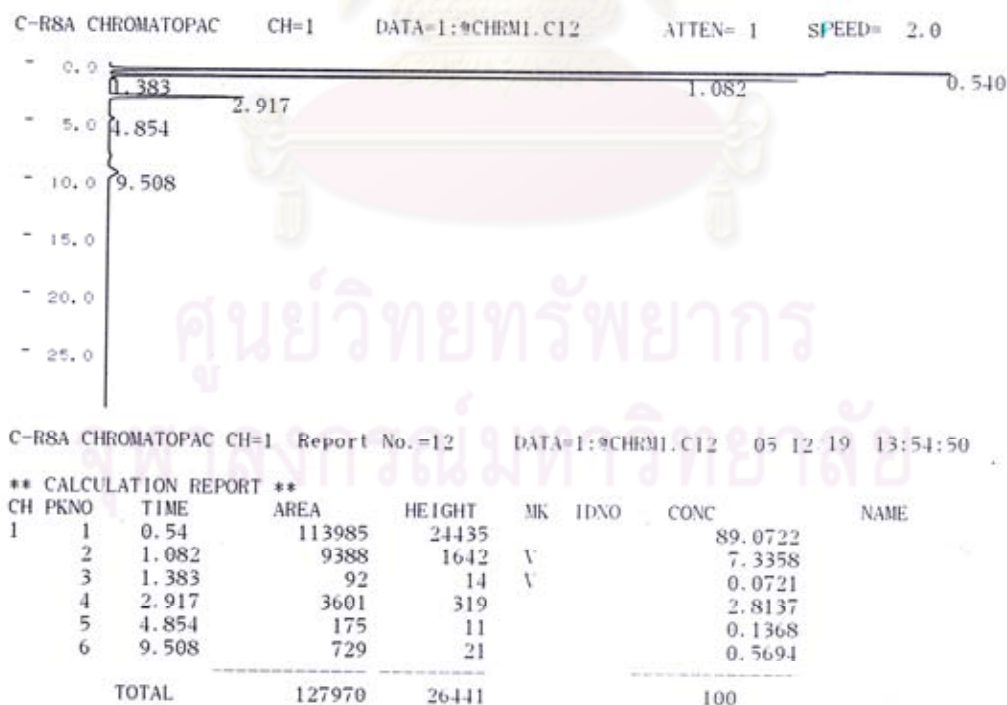


**Figure F.9** The chromatograms of catalyst sample from flame ionization detector, gas chromatography Shimadzu model 14B (VZ10 column).

## APPENDIX G

### CALCULATION OF CO CONVERSION, REACTION RATE AND SELECTIVITY

The catalyst performance for the CO hydrogenation was evaluated in term of activity for CO conversion, reaction rate and selectivity.

CO conversion is defined as moles of CO converted with respect to CO in feed:

$$\text{CO conversion (\%)} = \frac{100 \times [\text{mole of CO in feed} - \text{mole of CO in product}]}{\text{mole of CO in feed}} \quad (\text{i})$$

Reaction rate was calculated from CO conversion that is as follows:

Let the weight of catalyst used	=	W	g
Flow rate of CO	=	2	cc/min
Reaction time	=	60	min
Weight of CH <sub>2</sub>	=	14	g
Volume of 1 mole of gas at 1 atm	=	22400	cc

$$\text{Reaction rate (g CH}_2\text{/g of catalyst.h)} = \frac{\% \text{ conversion of CO} \times 60 \times 14 \times 2}{W \times 22400} \quad (\text{ii})$$

Selectivity of product is defined as mole of product (B) formed with respect to mole of CO converted:

$$\text{Selectivity of B (\%)} = 100 \times [\text{mole of B formed} / \text{mole of total products}] \quad (\text{iii})$$

Where B is product, mole of B can be measured employing the calibration curve of products such as methane, ethane, ethylene, propane, propylene and butane

$$\text{mole of CH}_4 = (\text{area of CH}_4 \text{ peak from integrator plot on GC-14B}) \times 8 \times 10^{12} \quad (\text{iv})$$

## APPENDIX H

### LIST OF PUBLICATIONS

- **Proceeding**

Orapin Chokpaisan and Bunjerd Jongsomjit, “A study of methanation over Co/Al<sub>2</sub>O<sub>3</sub> Ga catalysts”, Proceeding of the 18<sup>th</sup> Thailand Chemical Engineering and Applied Chemistry Conference, Phattaya Thailand, Oct., 2008.

- **International Paper**

Orapin Chokpaisan and Bunjerd Jongsomjit, “Characteristics of Ga-modified SiO<sub>2</sub>- and Al<sub>2</sub>O<sub>3</sub>-supported cobalt catalyst over methanation”, view be submitted to Catalysis Communications.



ศูนย์วิทยทรัพยากร  
จุฬาลงกรณ์มหาวิทยาลัย



## VITA

Miss Orapin Chokpaisan was born on 2<sup>nd</sup> July 1984, in Phatthalung, Thailand. She finished high school from Princess Chulabhorn's College, Trang, in 2003, and received her Bachelor degree of Chemical Engineering from Faculty of Engineering, Prince of Songkla University, Songkla, Thailand, in March 2007. She continued her Master's study at the department of Chemical Engineering, Faculty of Engineering, Chulalongkorn University in 2007.



ศูนย์วิทยทรัพยากร  
จุฬาลงกรณ์มหาวิทยาลัย